



**ANALYZING THE VIABILITY OF PHOTOVOLTAIC PAVEMENT SYSTEMS:
QUANTIFYING CLIMATE IMPACTS ON POTENTIAL POWER AND THE
RISKS OF IMPLEMENTATION**

THESIS

John H. Nussbaum, Capt, USAF

AFIT-ENV-MS-17-M-206

**DEPARTMENT OF THE AIR FORCE
AIR UNIVERSITY**

AIR FORCE INSTITUTE OF TECHNOLOGY

Wright-Patterson Air Force Base, Ohio

DISTRIBUTION UNLIMITED

The views expressed in this thesis are those of the author and do not reflect the official policy or position of the United States Air Force, Department of Defense, or the United States Government. This material is declared a work of the United States Government and is not subject to copyright protection in the United States.

AFIT-ENV-MS-17-M-206

**ANALYZING THE VIABILITY OF PHOTOVOLTAIC PAVEMENT SYSTEMS:
QUANTIFYING CLIMATE IMPACTS ON POTENTIAL POWER AND THE
RISKS OF IMPLEMENTATION**

THESIS

Presented to the Faculty

Department of Engineering Management

Graduate School of Engineering and Management

Air Force Institute of technology

Air University

Air Education and Training Command

In Fulfillment of the Requirements for the

Degree of Master of Science in Engineering Management

John H. Nussbaum, MSc, EIT

Captain, USAF

10 February 2017

DISTRIBUTION UNLIMITED

**ANALYZING THE VIABILITY OF PHOTOVOLTAIC PAVEMENT SYSTEMS:
QUANTIFYING CLIMATE IMPACTS ON POTENTIAL POWER AND THE
RISKS OF IMPLEMENTATION**

John H. Nussbaum, MSc, EIT

Captain, USAF

Approved:

_____ Ronald A. Coutu, Jr., PhD., Marquette University (Co-Chairman)	_____ Date
_____ Capt Robert A. Lake, PhD., USAF (Co-Chairman)	_____ Date
_____ Col Paul Cotelleso, PhD., USAF (Member)	_____ Date
_____ Alfred E. Thal, Jr., PhD USAF (Member)	_____ Date

Abstract

Three global manufacturers of photovoltaic pavement systems have garnered both interest and ire of technical communities who see potential but are concerned about implementation. Solar Roadways, Incorporated out of Sandpoint, Idaho is the sole U.S. manufacturer. Consisting of hexagonal pavers with a sandwich construction of tempered glass and polymer fill, the paver units are self-heating and contain multi-colored light emitting diodes (LEDs) as well as an integrated drainage system in their final construction. Existing research has documented how qualitative analysis identified test standards required to find the implement this technology without changing airfield pavement design methodologies. Additionally, at over four times the space efficiency, concerns regarding the reduction in per-square-inch performance efficiency are absolved.

In this research, statistical analysis is used to develop the Global Photovoltaic Power Potential Laboratory (GP3L). This study establishes a theoretical potential for photovoltaics across the United States Air Force (USAF) as well as enhances the understanding of the correlation with ambient temperature and quantifies a possible correlation between ambient humidity to the performance of photovoltaics. The GP3L system allows for logistical regressions, based on a modified Koppen-Geiger Climate Classification System, as well as linear regressions based on ambient conditions.

Lastly, it proposes a methodology of quantifying subjectively established risk to the installation mission caused by implementing photovoltaic pavement systems. This methodology also identifies the quantity of various pavements which can be replaced based on the Mission Dependency Index (MDI) of 26 different Category Codes (CATCODE) of pavements while maintaining acceptable levels of risk.

This work is dedicated to the USAF Civil Engineer Community. May we never accept that "it's as good as it gets."

Acknowledgments

Scott and Julie Brusaw (Solar Roadways, Inc.), Sten de Wit (SolaRoad), Eric Weaver (FHWA Office of Infrastructure R&D), Brian Smyers (AFRL/RQVV), and Capt David Simpson (AFIT/CEC) who all provided information on the existing products on the market, pavement standards, and access to resources for analysis.

Dr. Ed White (AFIT/ENC) who shaped the statistics, design of experiments, and ultimately enabled the GP3L concept to exist.

Dr. Alfred Thal (AFIT/ENV) and Maj Tod Laurvick (AFIT/ENG) conducted technical reviews and ensured the analysis within the document was sound as there was such a broad spectrum of content within this line of research.

Mrs. Robbyn Turner (AFIT/ENE), Maj Monica Nussbaum, and Mrs. Dona Nussbaum who conducted grammar and formatting reviews because we all know Engineers struggle to write.

Col Paul Cotelleso (AU Det 1/CC) and Capt Robert Lake (AFIT/ENG) who found funding and supported the immediate needs of this line of research so that we could take advantage of initial momentum.

Ben Wallace (WBI), Mike White (WBI), Robert Beakler (WBI) from Tech Edge Works who allotted manufacturing space, equipment, and materials as well as motivating curiosity to build all 40 test systems.

Capt Bill Kaval (AFIT/ENG) and 1Lt Andrew Jones (AFIT/ENG) who designed the hardware and wrote the code for the test system used in GP3L while simultaneously completing their own graduate studies, I'm eternally in their debt.

John H. Nussbaum

Table of Contents

	Page
Abstract.....	iv
Acknowledgments.....	vi
Table of Contents.....	vii
List of Figures.....	ix
List of Tables.....	xii
List of Equations.....	xiv
I. Introduction.....	1
Problem Statement.....	3
Research Questions.....	5
Research Focus.....	5
II. Literature Review.....	7
General Issue.....	7
Market Conditions for Photovoltaic Pavements.....	10
Application of Existing Pavement Design Methods to Photovoltaic Pavements.....	12
Research Question 1: Horizontal Photovoltaic Performance Modeling.....	17
Characterizing Temperature Effects.....	17
Characterizing Humidity Effects.....	24
Foundations for Research.....	28
Research Question 2: Risk Modeling of Photovoltaic Pavement Systems.....	30
Foundations for Research.....	31
III. Methodology.....	32
Research Question 1: Photovoltaic Performance Modeling.....	33
Site Selection.....	33
Test System Design.....	35
Research Question 2: Risk Modeling of Photovoltaic Pavement Systems.....	37
Conclusion.....	38
IV. Analysis and Results.....	40
Research Question 1: Photovoltaic Performance Modeling.....	40
Research Question 2: Risk Modeling of Photovoltaic Pavement Systems.....	65
Conclusion.....	75

V. Conclusions and Recommendations	77
Research Question 1: Photovoltaic Performance Modeling	77
Research Question 2: Risk Modeling of Photovoltaic Pavement Systems	79
Significance of Research.....	80
Recommendations for Future Research	81
Summary	81
Appendix A – GP3L Test System Physical Design.....	83
Test System Hardware Design	83
Test System Structure Design	85
Appendix B – GP3L Test System Coding	88
Test System Software Design	88
Photovoltaic Panel Monitoring Code	89
Code to Communicate with RockBlock Iridium Satellite Link	108
Interface between PV Monitoring Code and RockBlock Communications Code.....	120
Appendix C – GP3L Test System Users Guidance	123
Operations Manual	123
Appendix D – Test System Beta Testing Results	125
Appendix E – Test Standard Heuristics	129
References.....	138
Vitae.....	143

List of Figures

	Page
Figure 1. Current photovoltaic pavement systems on the market [9, 42, 43] [9] [42] [43]	6
Figure 2. Energy Consumption Breakdowns within the Federal Government, DoD, and USAF [4]	7
Figure 3. Renewable Energy Goals and Projections [4]	8
Figure 4. Screen capture of YouTube video of the Operation AURORA [5]	8
Figure 5. Equation 12-1 from UFC 3-260-02 Unreinforced Rigid Overlay Thickness [17]	13
Figure 6. Screen capture of FAARFIELD Software Package Overlay Design Window [44].....	14
Figure 7. Comparison of five published models and a concept model excluding Temperature (Tc) [7]	17
Figure 8. Published efficiency (η) and temperature (β) coefficients since 1977 [21]	19
Figure 9. Published power efficiency equations as a function of temperature since 1977 [21].....	20
Figure 10. Published total array power equations as a function of temperature since 1979 [21].....	21
Figure 11. SNL published research showing the non-linearity of the Temperature- Irradiance relationship [22].....	22
Figure 12. Relationship between ambient humidity and irradiance [25].....	24
Figure 14. Diagram equating Air Mass to Zenith Angle. NOTE: climactic conditions are specified [28]	26

Figure 13. Diagrams clarifying how humidity can change apparent Air Mass [29].....	26
Figure 16. Comparison of the probability densities of Clearness Index measured at AM1.5 versus AM3 [29].....	27
Figure 15. Comparison of the probability densities of Clearness Index by the minute versus by the hour [29]	27
Figure 17. Atmospheric Absorption Spectrum of Irradiance [30].....	29
Figure 18. Correlation Analysis of 1,763 Installation Latitudes and Longitudes as created by the JMP Software Package	33
Figure 19. Histogram of all latitudes with a bin size of 1 degree as created by the JMP Software Package and ANOVA bins shown	41
Figure 20. Histogram of all longitudes with a bin size of 1 degree as created by the JMP Software Package and ANOVA bins shown	42
Figure 21. ANOVA for Latitude Bins of all USAF Installations evaluated by the JMP Software Package.....	44
Figure 22. ANOVA for Longitude Bins of all USAF Installations evaluated by the JMP Software Package.....	45
Figure 23. Chart of Latitude and Longitude ANOVA Bins and subsequent 25 Regions Labeled produced by JMP Software Package	47
Figure 24. Aircraft Operations Mission Pavement Failure Impact Scale	72
Figure 25. Non-Aircraft Operations Mission Pavement Failure Impact Scale	74
Figure 26. Node Chip diagram with component functions identified	83
Figure 27. Base Chip diagram with component functions identified	84
Figure 28. “Omega” Test System	85

Figure 29. “Omega” Internal Components	86
Figure 30. Basic setup for a GP3L Test System (second panel not shown)	87
Figure 31. GP3L Test System Daily Status Message Code.....	89
Figure 32. Power over Time from “Omega” test system.....	125
Figure 33. Declining Power Comparison to Ambient Humidity and Ambient Temperature.....	126
Figure 34. Multivariate Analysis of Cleaned Omega Test Data.....	127
Figure 35. Fit Model of Cleaned Omega Test Data.....	128
Figure 36. Three-Point Loading Fixture specified in C78 and D7264 [19] [18][34, 17]	129
Figure 36. Specimen mounting and loading configuration for C273M-16 [40].....	131
Figure 38. Specimen mounting and loading diagram from D4027-98(2011) [34].....	132
Figure 39. Test specimen specifications for D4027-98(2011) [34].....	132
Figure 40. Three-Rail shear testing apparatus and mounting diagram for D4255-15a [37]	135
Figure 41. Modified SR3 paver for attachment of the Three-Rail Shear Test apparatus [37].....	136

List of Tables

	Page
Table 1. Comparison of Regional Mean Lat/Long to Nearest Installation Lat/Long	48
Table 2. Comparison of Regional Mean Lat/Long to Selected Installation Lat/Long.....	49
Table 3. Pareto Analysis of Installations per Region.....	50
Table 4. Uninvestigated Köppen-Geiger Climate Classification Types	51
Table 5. Pareto Analysis of All Possible USAF Installation Climate Classifications	52
Table 6. Pareto Analysis of All USAF Installation Main Climate/Precipitation Classifications.....	53
Table 7. Pareto Analysis of All USAF Installation Precipitation/Temperature Classifications.....	54
Table 8. Climate Classifications of Lat/Long Based Test Sites.....	55
Table 9. Alignment of Lat/Long Test Sites to Pareto Analysis of Main Climate/Precipitation Climate Classifications.....	56
Table 10. Alignment of Lat/Long Test Sites to Pareto Analysis of Precipitation/Temperature Climate Classifications	56
Table 11. Options for Additional Climate Based Test Sites for Main Climate/Precipitation Effects Analysis for Top 90% of Pareto Analysis from Table 9	57
Table 12. Options for Additional Climate Based Test Sites for Precipitation/Temperature Effects Analysis for Top 90% of Pareto Analysis from Table 10	58
Table 13. Climate Classifications of the Final Selection of Test Sites	60
Table 14. Installation-to-Region versus Test Site-to-Region Pareto Analyses.....	61

Table 15. Comparison of Main Climate/Precipitation Classification Pareto Analyses of All Installations versus Final Test Site Selection	62
Table 16. Comparison of Precipitation/Temperature Classification Pareto Analysis of All Installations versus Final Test Site Selection	62
Table 17. Comparison of Köppen-Geiger Climate Classification Pareto Analysis of All Installations versus Final Test Site Selection	64
Table 18. Pareto Analysis of All CATCODES of Pavements Considered Eligible for Replacement with Photovoltaic Pavement Systems	66
Table 19. Table of CATCODEs and Corresponding MDIs.....	68
Table 20. Aircraft Operation Missions Pavement Failure Impact Conceptual Rules.....	71
Table 21. Non-Aircraft Operation Missions Pavement Failure Impact Conceptual Rules	73
Table 22. Comparison of Procedures for ASTM Test Standard C1026 and C1645 [35] [36][35, 36]	133

List of Equations

	Page
Equation 1. Pavement Thickness over Stabilized Base	15
Equation 2. Non-bonded Rigid Pavement Overlay Thickness over Rigid Pavement.....	16

ANALYZING THE VIABILITY OF PHOTOVOLTAIC PAVEMENT SYSTEMS: A STUDY IN STRUCTURAL TESTING METHODS, MEASURING POTENTIAL POWER, AND QUANTIFYING THE RISKS OF IMPLEMENTATION

I. Introduction

Energy security is a relatively new concept. The Department of Defense (DoD) has expressed a significant and growing interest in methodologies to ensure that its installations retain energy despite threats in a growingly hostile world climate. The best way to ensure energy is available when needed is to own production of it. The DoD is pushing renewable energy systems to this effect, but traditional methods come with inherent problems.

Photovoltaic systems typically require large fields for arrays of solar panels which are most commonly owned by private companies who sell the power back to the installation. These Public-Public/Public-Private partnerships afford some level of energy security to installations, but are not owned by the DoD and so risk still remains. Additionally, they come with maintenance tails which must be accounted for either through contracts or personnel and they eliminate operating space which is a concern should that space ever be needed for future requirements.

Wind generating systems are not feasible to be installed in the overwhelming majority of United States Air Force (USAF) installations. They represent an obstruction to airfield operations. They may be able to be installed in remote and isolated sites, but do not generate a reliable enough energy source when constructed in remote, isolated, single installation systems.

Renewable Energy systems, though, do represent a method of providing energy security as they are much more difficult to attack through cyber-attacks and represent a lower threat should they be attacked conventionally. Additionally, as there's no "supply chain" for renewable energy systems, they're less expensive and cumbersome to operate freeing up manpower for primary, effects-generating portions of the mission. For this reason, identifying any method of capitalizing on renewable energy systems on every installation to maximize its effect is a very valuable objective to the DoD.

The objective of this research is to identify if photovoltaic pavements represent a great enough benefit to continue research into them. The Department of Transportation has been funding research into their development in the United States market while both the Netherlands and France are actively pursuing their own methodologies. Considering the massive volume of pavements on DoD installations, for which analysis was completed on USAF installations, this represents a massive potential power plant which could prove to provide total energy autonomy to certain installations.

However, with each new technology comes risk. Product development of these systems is not yet complete. Beta testing is proving merit, case studies are elaborating on the potential of the concept, and initial analysis has identified how to implement the technology while minimizing the effect on pavement design methodologies, especially for airfields.

What remains a question is how much potential photovoltaics have across the USAF which covers an extremely broad span of potential locations and climates. Additionally, implementation of this system represents risk as it could fail in a number of

ways. Analysis and quantification of that risk is critical to ensure it is minimized due to the no-fail nature of USAF mission sets.

In opening the door to this concept, initial research seeks to establish lines of effort for continued research. While some are done in partnership with the industry manufacturers, others are done independently to establish the potential behind the concepts for USAF applications. In all, the goal of this research is to analyze the viability for continued research into one method of providing energy security through renewable energy systems such as photovoltaic pavement systems.

Problem Statement

To evaluate a photovoltaic pavement's ability to replace traditional pavements, its performance characteristics must be identified in a manner allowing existing design methodologies to be applied to the non-standard material makeup of these products. Existing pavement structural standards have been designed and evolved specifically to evaluate traditional, homogeneous pavement materials. Application of the glass/polymer/metallic materials in photovoltaic pavement systems required a radical and controversial rethinking of pavement design standards. However, test standards that account for materialistic differences while still evaluating the systems for the characteristics necessary to equate the performance of the system to traditional pavement structures have been identified through heuristic-based qualitative analysis. This adhered to the Civil Engineer Flight Plan requirements to use standardized design methods across the enterprise despite the application of new technologies by eliminating the need to create a new design method for a new pavement material [1]. Therefore, the design

method, or the “how,” of photovoltaic pavement systems is not a major concern. What is in need of further analysis is “where” these non-optimally oriented systems might be of most efficiency and “why” these should be considered over traditional photovoltaic arrays.

Models are used to identify how much power can be produced at specific locations to effectively size and determine the potential cost-benefit of photovoltaic pavement systems. Current models vary in their accuracy, based on multiple factors. One factor requiring extensive empirical data, which must be measured across a global spectrum, are the effects of climate on various photovoltaic technologies; each of which will respond uniquely to changes in temperature and humidity. The National Renewable Energy Laboratory maintains Typical Meteorological Year (TMY) datasets, the most current of which is the third edition, or “TMY3,” for the United States, as well as limited international locations [2]. The data includes temperature and humidity, as well as several other meteorological variables measured specifically for photovoltaic research. Despite having this information, the NREL’s “PVWatts” model requires assumptions regarding the losses caused by soiling, shading, snow, light-induced degradation, and age [3]. Data are still lacking for climate types outside the United States and the specific impacts of meteorological conditions on photovoltaic panels.

Unique to traditional photovoltaic power plant arrays, pavement-replacing systems must serve more purposes than simply producing power. Therefore, the risk in implementing this emerging, disruptive technology is greater than traditional arrays and must be balanced with the potential benefit. A positive present worth may not negate the risks associated with their installation. While the total benefit depends on the power

produced, as well as the summation of any secondary characteristics of the individual systems, characterizing the risk of implementing the technologies can be modeled uniformly. Risk characterization must take into account the mission of the installation, the types of pavements being replaced, impacts to mission execution should the pavements fail, and the quantity of pavement replaced because total system failure represents an entirely different level of risk than partial pavement system failure.

For the purposes of this research, U.S.-manufactured photovoltaic pavement systems will be prioritized for analysis. Additionally, it is known that some of the data regarding pavements and locations of USAF installations are not completely accurate. These inaccuracies are partially due to security concerns with releasing the specific locations and quantities of some assets.

Research Questions

The core questions which this research seeks to answer:

1. Where does data need to be gathered to better quantify the impacts of ambient temperature and humidity to improve current models, which estimate the climatological impacts on photovoltaic system performance?
2. How can the risk to the generalized USAF mission sets be quantified to allow for risk/benefit analysis for the implementation of photovoltaic technologies on USAF installations?

Research Focus

The focus of this research is determining the viability of photovoltaic pavement systems, with deference given to US-manufactured systems, specifically for

implementation on USAF installations. SRI is the sole US manufacturer of a photovoltaic pavement system. The SR3 system, shown on the top left of Figure 1 with its international competition, the SolaRoad and Wattway systems, has the greatest secondary and tertiary benefits and is the simplest to implement in complicated arrangements given its modular nature. The remainder of this document will break each chapter into sub-sections, based on each of the research questions, to prevent confusion regarding the specific content being discussed.



Figure 1. Current photovoltaic pavement systems on the market [9, 42, 43] [9] [42] [43]

II. Literature Review

General Issue

Emerging photovoltaic pavement system technologies have the potential to provide energy security, autonomy, and decentralized power production which represents a more stable, reliable, and defensible source of power. This is of critical interest specifically for USAF installations not just because most installations do not have large plots of land for the construction of traditional photovoltaic power plant arrays, but also because the USAF is the single largest consumer of energy in the Department of Defense (DoD), as shown in Figure 2. Due to DoD requirements to increase renewable energy production to 25% of consumption by 2025, as shown in Figure 3, finding new ways of producing power on installations without disrupting the mission is a priority [4]. At many locations where it was previously unfeasible, this disruptive technology fits niche requirements like those represented by the microgrids desired on USAF installations.

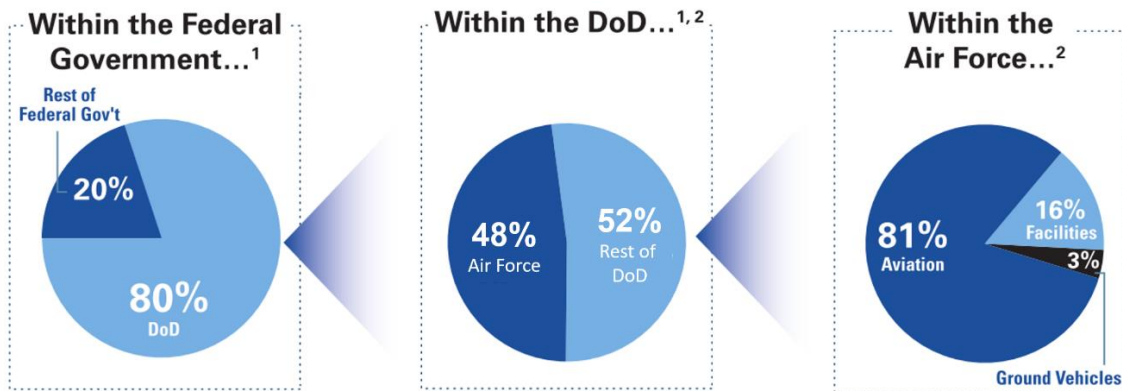


Figure 2. Energy Consumption Breakdowns within the Federal Government, DoD, and USAF [4]

Renewable Power Goal Under 10 U.S. Code 2911

Renewable Energy Electricity Requirements (MWh)

	FY13	FY14	FY15	FY16	FY17
RE goals	13%	14%	15%	16%	17%
RE electricity required (MWh)	1,179,155	1,257,161	1,333,488	1,408,164	1,481,212

Mechanisms to Reach RE Goals (MWh)

	FY13	FY14	FY15	FY16	FY17
On-base RE (carried fwd)	446,261	552,142	723,357	1,363,230	1,830,971
ECIP/SRM/ARRA (new on-base)	9,916	32,018	6,341	11,083	6,246
PPA RE (new on-base)	95,966	127,151	376,251	141,299	77,614
EUL RE (new on-base)	0	12,045	257,281	315,360	0
Commercial Bundled RE Purchase	54,899	54,899	54,899	169,899	169,899
Totals	607,041	778,256	1,418,129	2,000,870	2,084,730

EUL = Enhanced Use Lease, ECIP = Energy Conservation Investment Program, PPA = Power Purchase Agreement, SRM = Sustainment Restoration & Modernization

Figure 3. Renewable Energy Goals and Projections [4]

Additionally, the Department of Homeland Security (DHS) conducted an experiment titled Operation AURORA which was broadcast by CNN in 2007. It proved that traditional alternating current or mechanically-based power production methods can be destroyed by cybersecurity threats, as shown in Figure 4 [5]. Photovoltaic pavements cannot be destroyed by cybersecurity threats in this manner, rendering them more secure.



Figure 4. Screen capture of YouTube video of the Operation AURORA [5]

However, given the emerging nature of photovoltaic pavements, continued testing must be accomplished on them to ensure that they meet all specifications for pavements. Test standards for pavement systems have long been based on homogenous mixtures of either Asphaltic Concrete Cement (ACC), also known as “rigid” pavements, or Portland Concrete Cement (PCC), also known as “flexible” pavements. These test standards are not intended for the materials in photovoltaic pavement systems, though. However, existing research has documented how qualitative analysis of test standards based on heuristics developed from traditional methods can identify critical metrics [6]. Most importantly, this research allowed for implementation of new materials and technologies, such as the glass/polymer/metal construction of photovoltaic pavement systems, to be implemented using current, standard design methodologies which is a priority of the USAF Civil Engineer community [1].

However, enhanced models must be developed to evaluate photovoltaic pavement system performance and further determine their capability to meet a broader spectrum of applications than traditional photovoltaic arrays. Research at Sandia National Laboratories has shown that the five most commonly used models to predict photovoltaic performance include up to 30 variables each which account the effects of various losses [7]. The data for environmental losses, such as soiling and shading, is typically entered as a percent loss purely based on user estimates and are only included in a few of the models [7]. This contributes to a margin of error anywhere from $\pm 1\%$ to $\pm 11\%$ for these models, based on analysis of known products using crystalline silicone technology; unknown products vary up to $\pm 14\%$ and non-crystalline silicone technologies need additional study before results are published [7].

The volume and types of pavement replaced by these systems at each USAF installation is of significant importance for decision-makers as it is a risk-based decision. USAF leadership must consider the effects on unique mission requirements, availability of various pavement types, and the ability to generate and store power to ascertain how much pavement to replace and if there is a reasonably positive return on the investment. Mission requirements will determine the magnitude of power required as well as the risk. Additionally, various types of pavement will result in varying levels of structural risk. Photovoltaic power is only produced during daylight hours and is impacted both by changing weather patterns and seasonal cycles, so storage is critical for nighttime operations and will have to be developed to create the desired microgrids.

Market Conditions for Photovoltaic Pavements

Photovoltaic pavement systems are a relatively new and disruptive technology. There are a number of naysayers who can be found with a simple Google search who believe that the concept is improbable if not impossible to apply in the real world. The most effective argument against them is that a horizontally inclined photovoltaic panel under a very thick pane of tempered structural glass will never be as efficient as a panel inclined towards the sun under a thin layer of glass. Most of the remaining arguments, such as the idea that glass is not strong enough to use as a pavement surface, are based on misinformation or misunderstandings of standards and material science. Structural testing and vetting of the product, as well as several test beds, have been thoroughly executed though continued study is necessary to completely vet the most current models of the various products [8].

Currently, the only US manufacturer of photovoltaic pavements is Solar Roadways, Incorporated (SRI), out of Sandpoint, Idaho. This organization received Small Business Innovation Research (SBIR) Phase I funding in August 2009, Phase II in July 2011, and Phase IIB in November of 2015, for their SR3 paver unit [9]. Phase IIB required testing including freeze-thaw cycling, moisture conditioning, shear testing, and advanced loading [9]. The Research Civil Engineer for the Federal Highway Administration (FHWA) stated that FHWA typically uses AASHTO standards for testing, but that ASTM standards may also be applicable.

AASHTO guidance referenced how 23 CFR 637 dictated that each State Transportation Department (STD) must establish an FHWA-accredited Central Laboratory to ensure that materials used on the federal highway system meet quality standards [10]. The material testing and standards outlined by the Transportation Curriculum Coordination Council (TC3), the “technical service program” with AASHTO, identified that rigid pavement sampling and testing included ASTM standards [11]. Additionally, the AASHTO Pavement Management Guide also detailed multiple ASTM standards for pavement system maintenance and asset management [12]. The aforementioned qualitative analysis relied on the ASTM library of standards to identify those providing the metrics required by these governing bodies of pavement design [6]. This was not only completed for the previously mentioned requirement for the Modulus of Elasticity, but also for shear strength, freeze/thaw cycling, and moisture conditioning. Since test standards have been identified, evaluation of the products is enabled. These specific metrics, required by the SBIR Phase IIB funding, are of significant concern due to known issues with SR2 to soften introducing shear failure in high temperature areas as

well as potentially delamination concerns similar to that which occurred to the SolaRoad test bed in Amsterdam due to freeze/thaw cycling and moisture ingress [8, 9] [8] [9].

The argument about inch-for-inch efficiency may be true, but it does not account for many other aspects of this technology that make it a competitive concept within the industry. Secondly, emerging research is beginning to identify that horizontally inclined panels may be more efficient in overcast conditions due to their ability to absorb a broader angle of indirect irradiance [9]. Though limited research is available, at this time, to fully analyze this pavement-replacing method of using photovoltaics, as it has only appeared as a concept within the last decade, the research which has been done has identified the methods to determine if photovoltaic pavements can be used to replace standard pavement surfaces.

Application of Existing Pavement Design Methods to Photovoltaic Pavements

As stated above, the pavement design method need not be changed as existing research has identified that these materialistically unique systems can be implemented through existing design methods by using heuristically vetted standards identified through qualitative analysis [6]. Rigid pavement is generally defined as pavement that provides resistance to bending and distributes surface loads over a large area of their foundation relative to the load footprint [13]. Flexible pavement is generally defined as a structure that relies on internal shear strength and particulate interlock for stability while transferring loads to subgrade material using cementing agents, generally bituminous in nature [14]. Based on these definitions, photovoltaic pavement systems are more closely

aligned with the definition of a rigid pavement, as they are generally non-flexible and are not made of aggregate bound by bituminous or other materials.

Specifically for airfields, current rigid pavement overlay design methods require the use of a singular metric, the Modulus of Elasticity (also known as a Flexural Modulus). This is the single variable required for a material to be used as an airfield pavement. This is confirmed by referencing both Unified Facilities Criteria (UFC) 3-260-02 as shown in Figure 5, which specifies airfield pavement design for the DoD. This figure shows the equation for unreinforced rigid overlays. In it, a substitution for the variables regarding the overlay with the characteristics of the photovoltaic pavement can be made to assess the thickness of the base concrete pavement. Additionally, the FAARFIELD software package, mandated by the Federal Aviation Administration (FAA) as shown in Figure 6 also mandates solely the Modulus of Elasticity of the rigid overlay to design the subsequent layered pavement system. Use of the UFCs was mandated by the DoD in 2002 [15]. Both UFC 3-260-02 and UFC 3-250-01FA identify the locations for various pavement types, both rigid and flexible, and how to design them [16] [17][16, 17].

$$h_o = \sqrt[1.4]{h_d^{1.4} - \left[\left(\sqrt[3]{\frac{E_b}{E_c}} \right) h_b \right]^{1.4}} \quad (12-1)$$

where

h_o = thickness of plain concrete overlay, millimeters (inches)

h_d = design thickness of equivalent single slab placed directly on foundation, millimeters (inches)

E_b = modulus of elasticity of base MPa (psi)

E_c = modulus of elasticity of concrete, usually taken as 27,575 MPa (4×10^6 psi)

h_b = thickness of stabilized layer or lean concrete base, millimeters (inches)

Figure 5. Equation 12-1 from UFC 3-260-02 Unreinforced Rigid Overlay Thickness [17]

For airfield pavements, UFC 3-260-02 requires the use of ASTM Test Standard C78 to evaluate the flexural modulus, the only variable required for design, of traditional concrete [17]. ASTM Active Test Standard D7264/D7264M-15 was identified based on the heuristical analysis as a satisfactory alternative that is materialistically specific to photovoltaic pavement systems. This test standard identified the “strength, stiffness, and load/deflection behavior...of polymer matrix composite materials” using the same test apparatus as C78 [18] [19] [18, 19]. Additionally, the standard stated that the procedure may be used to “determine flexural properties of structures,” which allows testing the laminated structure of glass and polymer representative of the photovoltaic pavement systems such as the SR3 product [18]. The data produced through this test standard included the Modulus of Elasticity for the test specimen.

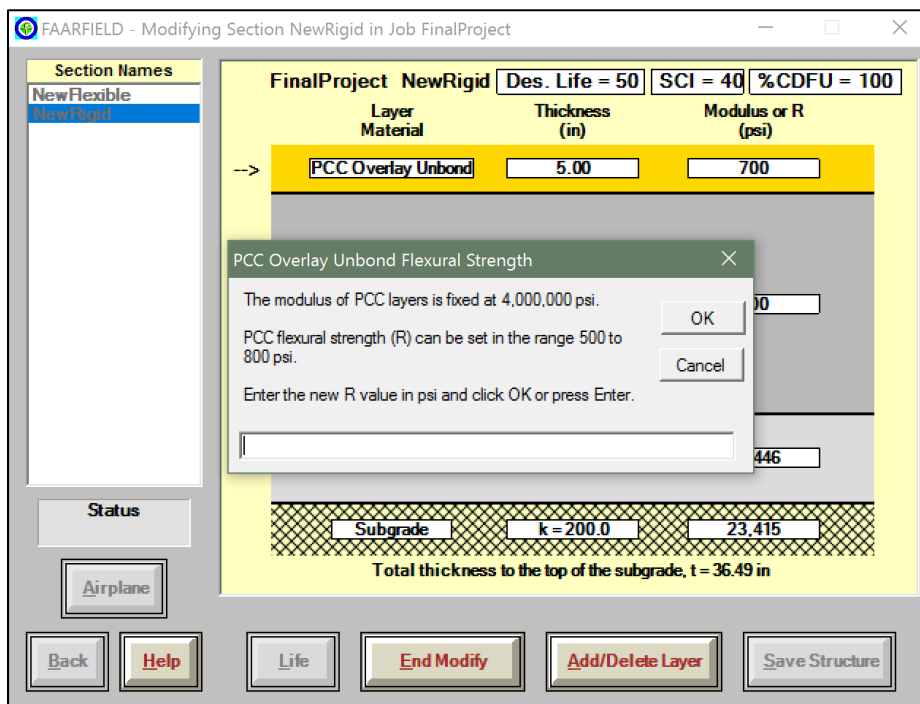


Figure 6. Screen capture of FAARFIELD Software Package Overlay Design Window [44]

While the FAARFIELD software package is the standard for airfields across the United States, DoD airfield pavement design still uses equations and hand calculations. As these systems are considered to be non-bonded overlays, the equation variables must be clarified to enable their use since the current variable definitions are based on traditional rigid pavements. Specifically, Equation 1, which is Equation 12-1 from UFC 3-260-02, calculates pavement thickness with a given Modulus of Elasticity over a stabilized base [17]. Equation 2, which is Equation 17-3 from UFC 3-260-02, calculates the thickness of a non-bonded rigid overlay over an existing pavement [17]. These variable definition modifications do not change the intent of the equations, but provide clarity regarding what each variable within the equation means, as previous published versions referred only to “overlay” or “base” layers.

$$h_o = \sqrt[1.4]{h_d^{1.4} - \left[\left(\sqrt[3]{\frac{E_b}{E_c}} \right) h_b \right]^{1.4}} \quad (1) [17]$$

h_o = pavement thickness (h_d or h_e)

h_d = design thickness if full cross section were made of in situ stabilized base as identified in the design curves in UFC 3-260-02, Chapter 12

E_b = Modulus of Elasticity of the stabilized base

E_c = Modulus of Elasticity of the pavement (SR3 paver for h_d or existing concrete for h_e for Eqn (2))

h_b = thickness of stabilized base

$$h_o = \sqrt{h_d^2 - C \left(\frac{h_d}{h_e} * h_E \right)^2} \quad (2) [17]$$

h_o = new overlay thickness (SR3 paver thickness)

h_d = pavement thickness if full cross section were made of material with empirically determined flexural strength of the overlay (if SR3 paver placed directly on subgrade, how thick would it have to be)

h_e = pavement thickness if full cross section were made of material with the measured flexural strength of the underlay (if existing pavement were thickened to meet design requirements, how thick would it have to be)

h_E = existing underlay thickness

C = Condition Coefficient of Existing Pavements (reference UFC 3-260-02, Chapter 17, Paragraph 5.b.)

This completed the identification of the required variables for pavement design, methods of ascertaining those variables for the SR3 product, and how to apply them to current design methodologies. Therefore, the “how” is answered as we have identified the methodology to implement this materially unique structure using existing pavement design methods. We are left with the “where” and the “why” to answer.

Research Question 1: Horizontal Photovoltaic Performance Modeling

Characterizing Temperature Effects

A study was completed on four radiation models, three module performance models, an inverter model, and the PVWATTS and PVMod models, which compared their predicted performance to empirical data [7]. When a temperature coefficient was included in the models, accuracy across the board was improved between 2.1% and 10.4% [7]. The most accurate of these models was an internal model called “PVMod,” which was developed at Sandia National Laboratories (SNL) and is available in the Solar Advisor Model (SAM) software package, with an accuracy of 1.9% to 3.2% modeled-to-measured, as shown in Figure 7 [7]. The mathematical equation for this model does not appear to be available as it is an internal model published only in the software of SAM; however, the SNL model is available with guidance on how to use it and is the second most accurate model. This model includes four temperature coefficients--whereas most models only use two, which means the SNL model is more flexible for various technologies and ambient conditions [20].

Solar Advisor Model							
	No Tc	Eff. + TC	Five Para.	SNL Mod	PV Mod	PV Watts	
kW	1.1	12.3%	7.2%	9.1%	5.4%	3.2%	10.2%
1.11	7.5%	4.7%	6.5%	2.4%	2.6%	9.6%	
2.3	11.8%	4.7%	8.5%	3.6%	1.9%	9.6%	

Table 2. Comparison of Modeled to Measured Array Output (Modeled ÷ Measured – 1)

Figure 7. Comparison of five published models and a concept model excluding Temperature (Tc) [7]

However, module operating temperature may be calculated accurately using existing algorithms, so it can be predicted based on ambient conditions including irradiance, wind speed, mounting system, and ambient temperature [20]. Additionally, techniques are available to determine the diffuse components of irradiance, and testing validated that these calculated figures did not reduce the SNL model's accuracy [20]. However, the accuracy of these models depends on the accuracy of the information coming from predictive algorithms for system characteristics which, in turn, depends on having accurate ambient condition data and exposure-based degradation data [20]. Failure to incorporate this information decreased model accuracy by up to 18% [20].

Reviewing several decades of photovoltaic research has determined that the study of power efficiency factors for photovoltaic technologies has yet to be fully realized. Some of this is due to the fact that the models were established based on a geographically limited range of sites which only allows quantification of a specific climate type. Other variance is likely due to differing photovoltaic systems. Of the 21 analyzed studies publishing temperature coefficients and module electrical efficiency coefficients during the last several decades, there have been five coefficients published for Mono-Si panels, one for Poly-Si, 17 for PV/T systems, two for a-Si, one for UTC/PV systems, and an overall average set of factors published by SNL, as shown in Figure 8 [21]. Separately, 19 studies published 24 different functions to evaluate PV array efficiency as a function of temperature, as shown in Figure 9. Amongst these models, 14 call for ambient temperature. Additionally, 27 studies have published 28 functions for PV array power as a function of temperature (two teams published the same function making for 29 total published functions), as shown in Figure 10, of which 14 also call for ambient

temperature [21]. One possible cause of this variance is that data collection and photovoltaic cell technologies have changed and improved greatly since 1977, though a modern update of these figures has not been provided nor were these established based on globally evaluated empirical data.

Table 1
Evans–Florschuetz PV efficiency correlation coefficients $\eta_T = \eta_{T_{ref}} [1 - \beta_{ref} (T - T_{ref})]$.

T_{ref} (°C)	$\eta_{T_{ref}}$	β_{ref} (°C ⁻¹)	Comments	References
25	0.15	0.0041	Mono-Si	Evans and Florschuetz (1977)
28	0.117 (average) (0.104–0.124)	0.0038 (average) (0.0032–0.0046)	Average of Sandia and commercial cells	OTA (1978)
25	0.11	0.003	Mono-Si	Truncellito and Sattolo (1979)
25	0.13	0.0041	PV/T system	Mertens (1979)
		0.005		Barra and Coiante (1993)
20	0.10	0.004	PV/T system	Prakash (1994)
25	0.10	0.0041	PV/T system	Garg and Agarwal (1995)
				Agarwal and Garg (1994)
				Garg et al. (1994)
20	0.125	0.004	PV/T system	Hegazy (2000)
25		0.0026	a-Si	Yamawaki et al. (2001)
25	0.13	0.004	Mono-Si	RETScreen (2001)
	0.11	0.004	Poly-Si	
	0.05	0.0011	a-Si	
25	0.178	0.00375	PV/T system	Nagano et al. (2003)
25		0.005	Mono-Si	Tobias et al. (2003)
25	0.12	0.0045	Mono-Si	Chow (2003)
25	0.097	0.0045	PV/T system	Zondag et al. (2003)
25		0.0045	PV/T system	Radziemska (2003)
25	0.0968	0.0045		Bakker et al. (2005)
		0.005	UTC/PV system	Naveed et al. (2006)
25	0.09	0.0045	PV/T system	Tiwari and Sodha (2006a)
25	0.12	0.0045	PV/T system	Tiwari and Sodha (2006b)
25		0.0045 c-Si	PV/T system	Zondag (2007)
		0.0020 a-Si		
25	0.12	0.0045	PV/T system	Tiwari and Sodha (2007)
25	0.12	0.0045	PV/T system	Assoa et al. (2007)
25	0.127	0.0063	PV/T system	Tonui and Tripanagnostopoulos (2007a)
25	0.127 unglazed	0.006	PV/T system	Tonui and Tripanagnostopoulos (2007b)
	0.117 glazed			
25		0.0054	PV/T system	Othman et al. (2007)

Notes:

- At $T_{ref} = 25$ °C, average $\eta_{ref} \approx 0.12$ and average $\beta_{ref} \approx 0.0045$ °C⁻¹.
- The same correlation has been adopted in Hart and Raghuraman (1982), Cox and Raghuraman (1985), Sharan and Kandpal (1987), and Sharan et al. (1987), although no numerical values are given for the parameters.

Figure 8. Published efficiency (η) and temperature (β) coefficients since 1977 [21]

Table 2
PV array efficiency as a function of temperature.

Correlation	Comments	Ref.
$\eta_T = \eta_{T_{ref}} [1 - \beta_{ref}(T - T_{ref})]$	$T_{ref} = 25^\circ\text{C}$, $\eta_{T_{ref}} = 0.15$, $\beta_{ref} = 0.0041^\circ\text{C}^{-1}$, c-Si, T in $^\circ\text{C}$	Evans and Florschuetz (1977)
$\eta_{PV} = \eta_{ref} - \mu(T_c - T_{ref})$	μ = overall cell temperature coefficient	Bazilian and Prasad (2002)
$\eta = \eta_a - c(\bar{T} - T_a)$	\bar{T} = mean solar cell temp, η_a = efficiency at T_a , c = temperature coefficient	Bergene and Løvrik (1995)
$\eta = \eta_{25} + b(T_c - 25)$	$b = b(G_T)$, T in $^\circ\text{C}$	Durisch et al. (1996)
$\eta(G_T, T_c) = \eta(G_T, 25^\circ\text{C})[1 + c_3(T_c - 25)]$	$c_3 = -0.5$ (% loss per $^\circ\text{C}$) for c-Si, $-0.02, \dots, -0.41$ for thin film cells	Mohring et al. (2004)
$\eta_T = \eta_0 - K(T^{1/4} - T_0^{1/4})$	$T_0 = 273\text{ K}$, $K = 22.4$	Ravindra and Srivastava (1979/80)
$\eta_a = \eta_n \times k_\gamma \times k_\theta \times k_x \times k_\lambda$ with $k_\gamma = 1 - \gamma(T_c - 25)/100$	k_γ = power temperature coefficient, $k_j, j = \theta, \alpha, \lambda$ optical, absorption, spectrum correction factors	Aste et al. (2008)
$\eta = \eta_{T_{ref}} \left[1 - \beta_{ref}(T_a - T_{ref}) - \frac{\beta_{ref}\tau\alpha G_T}{nU_L} \right]$ $\bar{\eta} = \eta_{T_{ref}} \left[1 - \beta_{ref}(T_a - T_{ref}) - \frac{\beta_{ref}(T_c - T_{ref})}{nU_L} \right]$	5% low predictions, $\beta_{ref} \sim 0.004^\circ\text{C}^{-1}$, $\eta_{T_{ref}} = 0.15$, $T_{ref} = 0^\circ\text{C}$ $\bar{\eta}$ = monthly average efficiency, V = dimensionless, $\beta_{ref} \sim 0.004^\circ\text{C}^{-1}$	Siegel et al. (1981) Siegel et al. (1981)
$\eta_i = \eta_{T_{ref}} [1 - \beta_{ref}(T_{c,i} - T_{ref}) + \gamma \log_{10} I_i]$	η_i = hourly efficiency, I_i = incident hourly insol, $\beta_{ref} \sim 0.0045^\circ\text{C}^{-1}$, $\gamma \sim 0.12$	Evans (1981) and Cristofari et al. (2006)
$\eta = \eta_{T_{ref}} [1 - \beta_{ref}(T_c - T_{ref}) + \gamma \log_{10} G_T]$	η = instantaneous efficiency, $\beta_{ref} = 0.0044^\circ\text{C}^{-1}$, $\eta_{T_{ref}} = 0.125$, $T_{ref} = 25^\circ\text{C}$	Notton et al. (2005)
$\bar{\eta} = \eta_{T_{ref}} \{1 - \beta_{ref}[(T_c - T_a) - (T_a - \bar{T}_a) - (\bar{T}_a - T_{ref})] + \gamma \log_{10} I\}$ $\eta = \eta_{ref} [1 - a_1(T_c - T_{ref}) + a_2 \ln(G_T/1000)]$	$\bar{\eta}$ = monthly average efficiency, $\beta_{ref} \sim 0.0045^\circ\text{C}^{-1}$, $\gamma \sim 0.12$ For Si $a_1 = 0.005$, $a_2 = 0.052$, omitting the \ln term slightly overestimates η	Evans (1981) Anis et al. (1983)
$\eta(XG_T, T) = \eta(G_T, T_{ref}) [1 - \beta_{ref}(T - T_0)] \left(1 + \frac{k_8 T}{q} \frac{\ln X}{V_{oc}(G_T, T_0)}\right)$	X = concentration factor, for $X = 1$ it reduces to Eq. (2)	Lasnier and Ang (1990)
$\eta = \eta_{ref} \left\{ 1 - \beta \left[T_a - T_{ref} + (T_{NOCT} - T_a) \frac{G_T}{G_{NOCT}} \right] \right\}$	The T_c expression from Kou et al. (1998) is introduced into the η expression in Evans and Florschuetz (1977)	-
$\eta = \eta_{ref} \left\{ 1 - \beta \left[T_a - T_{ref} + \left(\frac{9.5}{5.7+3.8I_w} \right) (T_{NOCT} - T_a) \frac{G_T}{G_{NOCT}} \right] \right\}$	The T_c expression from Duffie and Beckman (2006) is introduced into the η expression in Evans and Florschuetz (1977)	-
$\eta = \eta_{ref} \left[1 - 0.9\beta \frac{G_T}{G_{T,NOCT}} (T_{c,NOCT} - T_{a,NOCT}) - \beta(T_a - T_{ref}) \right]$ $\eta_{nom} = -0.05T_{surface} + 13.75$ $\eta_{meas} = -0.053T_{back} + 12.62$ $\eta = a_0 + a_1 \frac{T_c(\Delta T) - T_\infty}{T_\infty} + a_2 \frac{G_T - G_{ref}}{G_{ref}}$	Assumes $\eta \approx 0.9(\tau\alpha)$ $T_{surface} = 1.06T_{back} + 22.6$ Nominal vs measured values $A_k, k = 0, 1$ and 2 are empirical constants, T_∞ is the indoor ambient temperature	Hove (2000) Yamaguchi et al. (2003) Zhu et al. (2004)
$\eta_{MPP}(G_T, T) = \eta_{MPP}(G_T, 25^\circ\text{C})(1 + \alpha(T - 25))\eta_{MPP}(G_T, 25^\circ\text{C})$ $= a_1 + a_2 G_T + a_3 \ln(G_T)$	$a_1 - a_3$ device specific parameters, MPP tracking system	Beyer et al. (2004)
$\eta = \eta_{NOCT} [1 - MPTC(T_{NOCT} - T_c)]$ $\eta = a + b \frac{T_{in} - T_a}{G_T}$	$MPTC$ = maximum power temperature coefficient ^a PV/T collector. PV cover: 100% $\rightarrow a = 0.123$, $b = -0.464$ 50% $\rightarrow a = 0.121$, $b = -0.450$	Perlman et al. (2005) Chow et al. (2006)
$\eta = 0.94 - 0.0043 \left[\bar{T}_a + \frac{\bar{G}_T}{(22.4+8.7\bar{V}_w)} - 25 \right] \pm 2.6\%$	Overbars denote daily averages. $\bar{G}_T = \text{Wh/m}^2$ received/length of day (h) \bar{V}_w in m/s	CLEFS CEA (2004)

Notes:

- In Bücher (1997): PRT factor temperature effect on PV performance.
 - In Oshiro et al. (1997): KPT cell temperature factor.
 - In Jardim et al. (2008): NOCT-corrected efficiency.
- ^a With $MPTC = -0.5\%$ loss per $^\circ\text{C}$, the efficiency is $\eta = 11.523 - 0.0512T_c$.

Figure 9. Published power efficiency equations as a function of temperature since 1977 [21]

Table 3
PV array power as a function of temperature $P = \eta_c AG_T$.

Correlation	Comments	References
$P = \eta_{T_{ref}} AG_T (\tau \alpha) [1 - \beta_{ref} (T_p - T_{ref})]$	T_p = plate temperature, $\eta_{T_{ref}} = 0.118$ at 45 °C – air coll, $\eta_{T_{ref}} = 0.108$ at 28 °C – water coll	Hendrie (1979)
$P_{T_c} = \eta_{ref} AG_T K_f [1 + \alpha(T_c - 25)]$	$T_{ref} = 25$ °C, $\eta_{T_{ref}} = 0.13$, $\alpha = -0.004$ °C ⁻¹ , K_f factor for rest, frame installation, T_c in °C	Nishioka et al. (2003)
$P = \eta_c AG_T \tau_g p [1 - \beta_{ref} (T_c - 25)]$	p = packing factor, T_c in °C, τ_g = glazing transmissivity	Chow et al. (2006)
$P = \eta_{T_{ref}} AG_T [1 - 0.0045(T_c - 298.15)]$	$\eta_{T_{ref}} = 0.14$, T_c in K	Jie et al. (2007a)
$P = \eta_{T_{ref}} AG_T \tau_{pv} [1 - 0.0045(T_c - 25)]$	$\eta_{T_{ref}} = 0.14$, T_c in °C, τ_{pv} = pv cell glazing transmittance	Jie et al. (2007b)
$P = \eta_{T_{ref}} AG_T [1 - \beta_{ref} (T_c - T_{ref}) + \gamma \log_{10} G_T]$	$\beta_{ref} = 0.0044$ °C ⁻¹ for pc-Si, γ is usually taken as 0	Cristofari et al. (2006)
$P_T = P_{ref} [1 - \beta_{ref} (T - T_{ref})]$	$\beta_{ref} = 0.004$ – 0.006 °C ⁻¹ , T in °C, T_{ref} = reference temperature	Buresch (1983)
Same as above	$\beta_{ref} = 0.004$	Twidell and Weir (1986)
$P(T) = P(25)[1 - \gamma(T - 25)]$	$\gamma = 0.0053$ °C ⁻¹ for c-Si range: 0.004 – 0.006 °C ⁻¹	Parretta et al. (1998)
$P_T = P_{25}[1 - 0.0026(T - 25)]$	a-Si, T in °C, power degrades to $0.82P_{init}$	Yamawaki et al. (2001)
$P_T = P_{25} + \frac{dP}{dT} (T - 25)$	$\frac{dP}{dT} = -0.00407$, -0.00535 , Si space cells, T in °C	Osterwald (1986)
$P(T) \approx G_T [\eta_0 - c(T - T_a)]$	η_0 = efficiency at T_a , c = temperature dependence factor	Bergene and Løvvik (1995)
$P_{max} = P_{max,ref} [1 - Df(T_c - 25)]$	Df = “deficiency factor” = 0.005 °C ⁻¹	Al-Sabounchi (1998)
$P_{max} = P_{max,ref} \frac{G_T}{G_{T,ref}} [1 + \gamma(T_c - T_{ref})]$	γ = temperature factor for power, $\gamma = -0.0035$ (range -0.005 °C ⁻¹ to -0.003 °C ⁻¹), T_c in °C	Menicucci and Fernandez (1988)
$P_{max} = P_{max,ref} \frac{G_T}{G_{T,ref}} [1 + \gamma(T_c - 25)]$	$\gamma = -0.0035$ (range -0.005 °C ⁻¹ to -0.003 °C ⁻¹) T_c in °C	Fuentes et al. (2007)
$P_{max} = P_{max,ref} \frac{G_T}{1000} [1 + \gamma(T_c - T_{ref})]$	γ = temperature factor for power, $T_{ref} = 25$ °C, used in PVFORM	Marion (2002)
$P_{mp,T} = I_{mp,T} [1 - \alpha(T - T_r)] [V_{mp,T} - \beta V_{mp}^{STC} (T - T_r)]$	STC refers to ASTM standard conditions (1000 W/m ² , AMI = 1.5, $T_r = 25$ °C)	King et al. (1997)
$P_{max} = P_{max,ref} \frac{G_T}{G_{T,ref}} [1 + \alpha(T - T_{ref})] [1 + \beta_{ref} (T - T_{ref})]$	Adapted from the MER model ^a . Coefficient δ evaluated at actual conditions	Kroposki et al. (2000)
$\left[1 + \delta(T) \ln \left(\frac{G_T}{G_{T,ref}} \right) \right]$		
$P = P_0 [1 + (\alpha - \beta_{ref}) \Delta T]$	α : 0.0005 °C ⁻¹ , β : 0.005 °C ⁻¹	Patel. (1999)
$P = (\alpha T_c + \beta) G_T$	α = temperature coefficient, β = calibration constant	Yang et al. (2000)
$P = -4.0 + 0.053 G_T + 0.13 T_c - 0.00026 G_T T_c$	MPPTTracked 100 kWp system	Risser and Fuentes (1983)
$P = -0.4905 + 0.05089 G_T + 0.00753 T_c - 0.000289 G_T T_a$	MPPTTracked 100 kWp system	Risser and Fuentes (1983)
$P_T = -8.6415 + 0.076128 G_T + 1.02318 \times G_T^2 + 0.20178 T - 4.9886 \times 10^{-3} T^2$	T is the panel temperature (K), too many significant figures!!!	Jie et al. (2002)
$P = G_T (b_1 + b_2 G_T + b_3 T_a + b_4 V_f)$	EPTC model, b_j regression coefficients, V_w^f wind speed 10 m above ground	Farmer (1992)
$P = c_1 + (c_2 + c_3 T_a) G_T + (c_4 + c_5 V_w) G_T^2$	c_j regression coefficients based on STC module tests ^b	Taylor (1986)
$P_{mp} = D_1 G_T + D_2 T_c + D_3 [\ln(G_T)]^m + D_4 T_c [\ln(G_T)]^m$	D_j ($j = 1-4$), m parameters ^c	Rosell and Ibáñez (2006)
$P = V_c I_c \left[1 - \frac{G_T - 500}{2.0 \times 10^{-4}} + \frac{C_{T_c}}{4 \times 10^4} (50 - T_c)^2 \right]$	I_c = output current (A), V_c = output voltage (V), T_c in K, $C_{T_c} = 1$ if $T_c \leq 50$ °C or = 3 if $T_c \geq 50$ °C	Furushima et al. (2006)
$P = A(0.128 G_T - 0.239 \times 10^{-3} T_a)$	p-Si, hybrid PV-fuel cells system G_T in kW/m ² , P in kW, T_a in °C	Zervas et al. (2007)
$P = P_{ref} G_T K_{p1} K_w K_e K_c$ with $K_{p1} = 1 + \alpha(T_c - 25)$	K_w , K_e , K_c loss coefficients due to mounting, dirt etc., AC conversion. Semitransparent PV	Wong et al. (2005)

Notes:

- Ref. Bücher et al. (1998): reports power temperature coefficients for various module types in the range $[-0.0022/\text{K}$ to $0.0071/\text{K}]$, values around -0.002 referring to a-Si.
 - Refs. Radziemska (2003) and Radziemska and Klugmann (2006): report power temperature coefficients $-0.0065/\text{K}$ for c-Si.
 - Ref. Fathi and Salem (2007): reports a dimensional expression for “power” – actually specific energy!
 - Energy production correlation E_{out} {W hr} = $(e_0 + e_1 T_c) E$ {kW hr/m²}, with $36.41 \leq e_0 \leq 44.14$ and $-0.20 \leq e_1 \leq -0.16$ is given in del Cueto (2001).
 - Daily energy production (W h/day) is given by $E = A_1 H + A_2 H (T_{a,max})^{-2} + A_3 T_{a,max}$, with $T_{a,max}$ the maximum ambient temperature (°C), H the daily total insolation (W h/m²/day) and A_j regression coefficients, according to the EMAT model (Meyer and van Dyk, 2000).
 - Ref. Zhou et al. (2007) presents an expression for P_{max} based on BIPV data, which, for two states 0 and 1, is proportional to $(T_0/T_1)^\gamma$ with $\gamma = \frac{\ln(V_{oc0}/V_{oc1})}{\ln(T_0/T_1)}$.
 - There are few equations with no explicit temperature dependence. Among them, the single regression yearly average form $P_{yr} = 0.1103 G_{T,yr}$ (Liu et al, 2004) and the nonlinear expression $P = c_1 G_T + c_2 G_T^2 + c_3 G_T \ln G_T$, with c_j regression coefficients, known as the ENRA model (Gianolli Rossi and Krebs, 1988), which over-predicts the PV performance.
- ^a The V_{oc} and I_{sc} expressions have been combined as in Eq. (1).
^b The regression equation shown combines the original equation for P and the analogous expression for T_c .
^c For pc-Si, $D_1 = 0.000554$, $D_2 = -7.275 \times 10^{-5}$, $D_3 = 2.242 \times 10^{-5}$, $D_4 = -4.763 \times 10^{-8}$, $m = 7.0306$. Analogous sets are given for c-Si, a-Si, and thin film modules.

Figure 10. Published total array power equations as a function of temperature since 1979 [21]

Of the functions for PV array efficiency shown in Figure 9, nine call for cell or module temperature which, as stated above, can be accurately modeled without negatively affecting the overall model accuracy [21]. The same is true of 15 of the 28 PV array power functions shown in Figure 10 [21]. It is clear that the ambient temperature contributes significantly to the efficiency of a photovoltaic panel. At one point, research had concluded that operating temperature has a linear relationship with a PV system's electrical efficiency and is correlated specifically to the module, array, and mounting system [21]. However, SNL-published research has shown that the power efficiency factor does not hold a linear relationship to temperature. This is shown in Figure 11 for USSC UMP-880 tandem amorphous silicon and ASE Americas ASE-300-DG/50 [22].

SNL developed a twelve-step process to predict photovoltaic performance under any operating condition [22]. The efficiency factors for short circuit current and open circuit voltage can be calculated, as can the cell temperature, based on a known reference temperature at thermal equilibrium [22]. The only variable that still must be characterized is the module operating temperature which, as stated above, is dependent

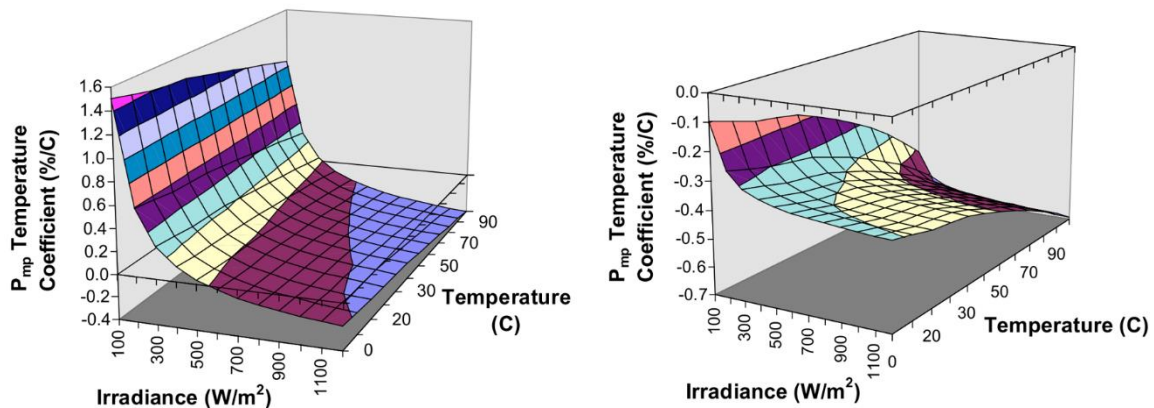


Figure 11. SNL published research showing the non-linearity of the Temperature-Irradiance relationship [22]

upon the mount system, wind, thermal radiation, and ambient temperature [22]. If this variable is accurately known or calculated, the overall accuracy of the SNL model is within approximately 3% [22]. The SNL database currently has information on over 200 modules [22]. Crystalline silicon (mono- and poly-) represents 70% to 90% of the market share [23]. It is also amongst the most efficient commercially-viable photovoltaic technology, with efficiencies ranging from 15% to 20% [23]. This research will focus specifically on methods for characterizing the power efficiency factors in regard to temperature for both monocrystalline and polycrystalline technologies [23].

Small-scale testing of photovoltaic technology temperature dependency found that cooler temperatures generally improved performance [23]. This effect is echoed by the SNL studies which found a non-linear relationship that is unique for each module, as shown in Figure 11. To further characterize the efficiency variables for the most commonly-used module types, extensive research must be conducted to establish the true, global factors that should be published for these technologies.

Characterizing Humidity Effects

Humidity may influence multiple variables affecting photovoltaic array performance, which are summarized below. Dust alone causes 1% to 65.8% loss of photovoltaic performance which is exacerbated by dew-induced coagulation or reduced by rain-induced cleaning of the panels [24] [25] [24, 25]. More directly, the microscopic water droplets can either refract, reflect, or diffract solar irradiance in a non-linear relationship [25]. Humidity levels under 23% generally allowed for a solar irradiance over 800 W/m², but a 2% increase in humidity led to a drop of 400 W/m², as shown in Figure 12 [25]. Additionally, as stated above, mono- and polycrystalline silicon panels represent up to 90% of the market share of photovoltaic panels. A change in water vapor from 1cm to 5cm alone has been found to have up to a 10% decrease of panel power output [26]. Most directly, increased humidity degraded the physical characteristics of panels through water ingress leading to encapsulating material embrittlement or crystalline silicon structure corrosion [25].

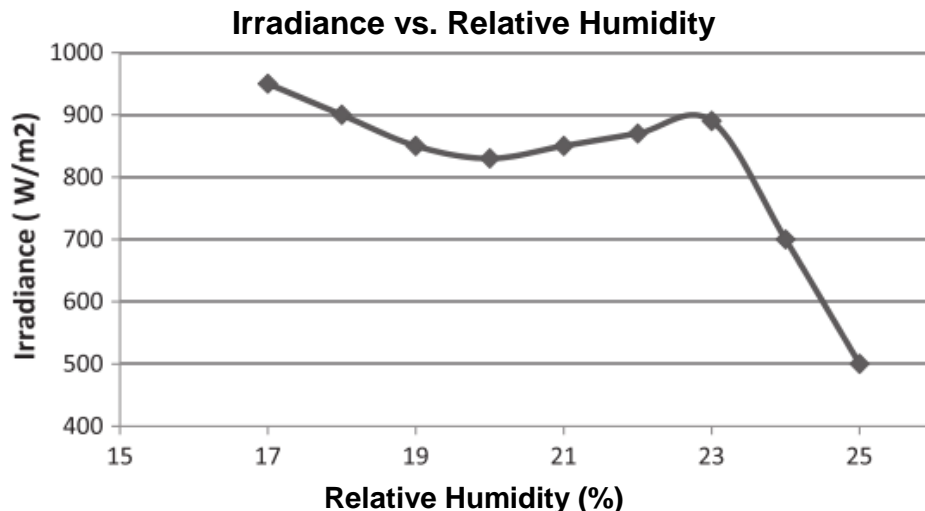


Figure 12. Relationship between ambient humidity and irradiance [25]

The SNL model assumed that the effects of variables like dust and humidity can be averaged over specific time frames (weekly, monthly, annually) as uniform linear variables [27]. These variables can be considered generic for photovoltaic systems with identical structures and materials, and they are claimed to have an average total effect of less than 3% on a specific PV panels based on empirical studies [27]. However, given that limited global experiments have revealed that dust alone can have an effect of up to 65.8%, and that humidity alone can reduce irradiance by nearly 38%, an average influence of 3% seems highly inaccurate [24] [25] [24, 25]. Currently, generic “derate factors,” or variables that reduce the performance of panels, are included in some models and increase model accuracy 2% to 10% when accurate weather data is incorporated [7]. However, as stated above, these derate factors are applied as universal, linear factors, which do not seem to provide an accurate impression of the effects of climactic conditions and the subsequent derate factors for which assumptions are being made.

Photovoltaic cell manufacturers generally use an Air Mass of 1.5 as the standard per ASTM. This Air Mass is a direct correlation between a 48.2° angle of the sun, from a zenith of 0° when directly overhead, as shown in Figure 13 [28]. However, the direct beam radiation angle is not the sole influence on irradiance as noted by the Atmospheric Model conditions noted on the right of Figure 13 [28]. Irradiance is also influenced by turbidity and humidity, as the wavelength distribution of photon flux varies directly with the water vapor content of the air through which this beam radiation travels [28]. While

the effects of turbidity are found to be greater than that of water vapor, they are also more difficult to quantify in this line of research [26].

The method by which clouds affect apparent Air Mass as well as measured global horizontal irradiance at ground level are shown in Figure 14 and have been found to be especially apparent as Air Mass equals a value of 1 [29]. Air Mass will appear to be higher with increased cloud cover due to a greater relative thickness when the zenith angle of the direct beam radiation is higher [29]. It can also be affected by sparse cloud cover due to reflections from the clouds bouncing photons back to a central point (P) increasing the mean value for global horizontal irradiance and reducing the apparent Air Mass.

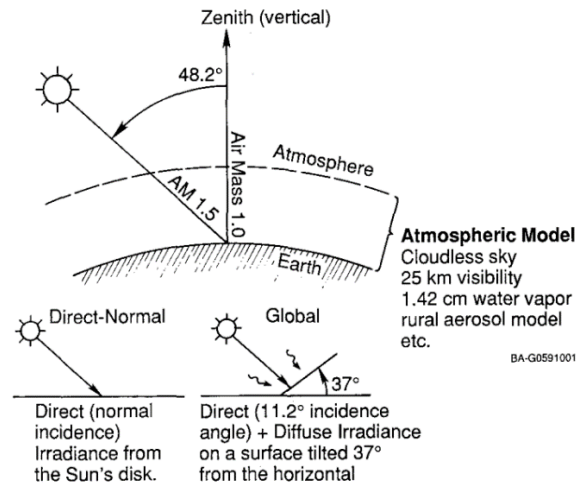


Figure 13. Diagram equating Air Mass to Zenith Angle. NOTE: climatic conditions are specified [28]

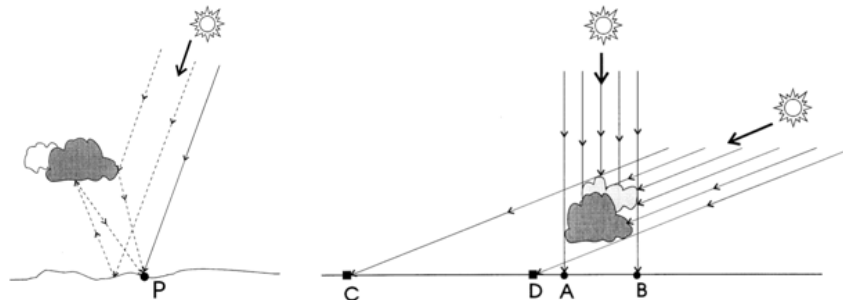


Figure 14. Diagrams clarifying how humidity can change apparent Air Mass [29]

Research into the Clearness Index, k_t , which is the ratio of global horizontal irradiance at ground level as compared to the horizontal extraterrestrial solar irradiation, has found that the function depends on Air Mass as well [29]. The probability density distributions have been found to have a bimodal nature, which became more apparent as the time frequency of measurements increased from hourly to by-the-minute, as shown in Figure 16 [29]. As the Air Mass increases, the lower of the two maxima increases and the higher decreases. Simultaneously, both moved towards a lower Clearness Index. This results in a more uniform, yet still bimodal, distribution that is shifted left as shown in Figure 15 [29]. Models developed to chart this bimodal probability distribution of clearness index, based on Air Mass, have been found to be accurate with an R^2 value between 97.5% and 99.9% [29]. Therefore, measurement of Air Mass is unnecessary as it can be modeled with a high level of accuracy.

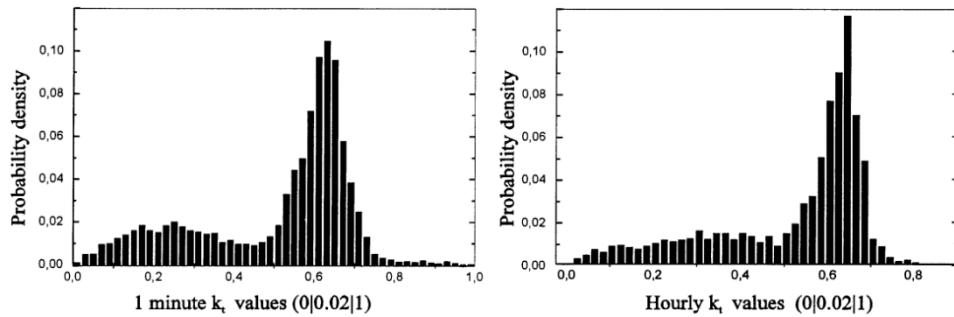


Figure 16. Comparison of the probability densities of Clearness Index by the minute versus by the hour [29]

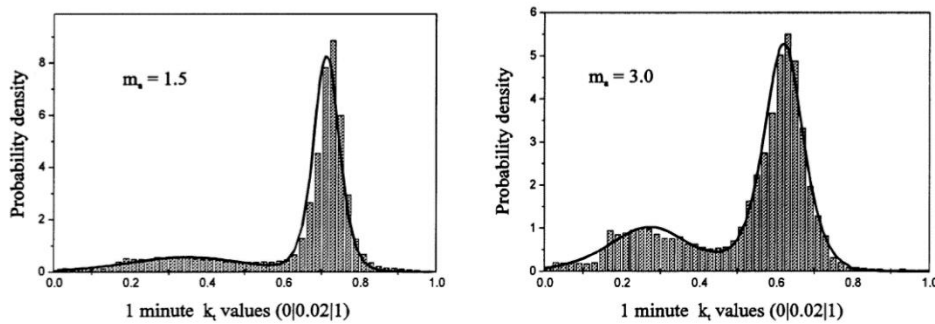


Figure 15. Comparison of the probability densities of Clearness Index measured at AM1.5 versus AM3 [29]

Foundations for Research

The effects of temperature are well known, though there are many proposed functions for both power and panel efficiency, as well as many published factors for temperature coefficients and module electrical efficiency. Models, such as the SNL model, require extensive information regarding the PV system's mounting, its make-up, and manufacturer-specific data. Simpler models apply a linear factor for temperature to analyze its effects on the efficiency of their products. To identify the range of factors, various climates impacts must be characterized, such that variables for the range of effects of each climate can be considered. The creation of categorical variables for each of these classifications requires on-site, long-term study.

Additionally, humidity has the potential to be used as a conglomerated variable--accounting for the effects of Clearness Index, Air Mass, dust, and the direct impacts of water infiltration into the system. While the impacts of humidity on irradiance appear to be well quantified, especially for silicone technologies for which the specific wavelength of light causing these types of solar cells to produce power is absorbed as shown in Figure 17, a correlation directly to photovoltaic performance was not able to be found in any existing published research [30]. Additionally, humidity could be characterized by categorical variables based on climate classifications through empirical analysis.

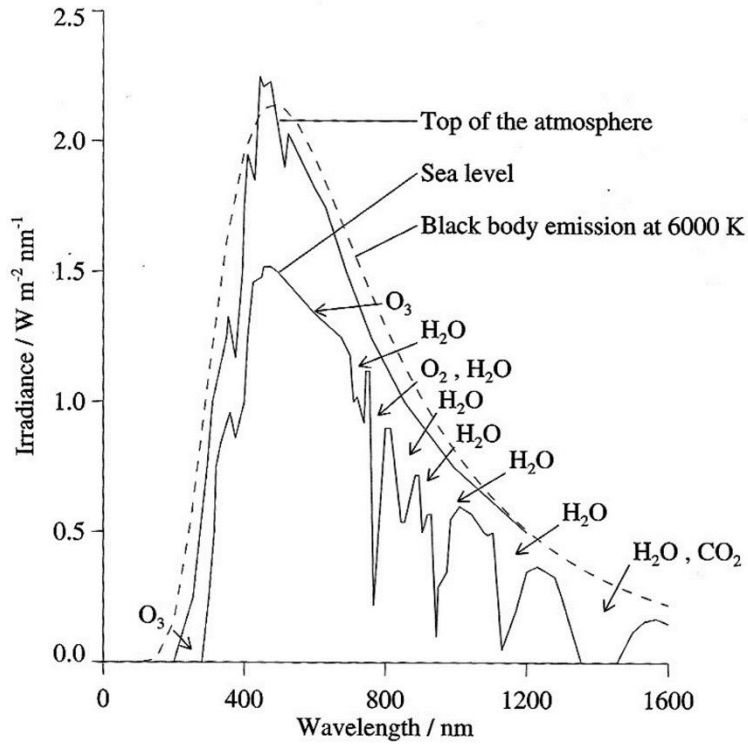


Figure 17. Atmospheric Absorption Spectrum of Irradiance [30]

Independently, temperature and humidity affect photovoltaic panels in known ways. Their combined effects, however, may exacerbate or negate their independent effects. Humidity could result in panel cooling, in the same way that sweat cools a human, and temperature could keep humidity from infiltrating a system. These combined effects are currently unknown and can best be characterized by long-term study on multiple sites around the world representing a broad spectrum of combinations of temperature and humidity climate classifications.

Research Question 2: Risk Modeling of Photovoltaic Pavement Systems

A method of quantifying the risk of replacing traditional pavement systems with photovoltaic pavement systems is necessary because this study proposed implementation of this technology on USAF installations. Despite extensive testing on the products enabled by funding from the DoT, and the general public's rapidly-increasing interest, exemplified by the most successful fundraising campaign in Indiegogo's history, there is still an inherent risk in trying new technologies. Due to the unknown long-term performance characteristics of the technology, risk quantification must be established for decision makers to establish acceptable levels of risk.

All USAF real property is characterized by Category Code identifying the facility system and its specific use. These "CATCODES" reveal that there are 26 types of pavement systems within the inventory which could potentially be replaced by photovoltaic pavements. These pavement categories range from sidewalks to runways and the quantities of each are available.

Additionally, as well as having a CATCODE, which identifies the facility system type, there is a Mission Dependency Index (MDI), which correlates each CATCODE to a generically-established importance to the USAF mission [31]. MDI values do not identify the mission of an installation or necessarily even how directly that infrastructure system supports that mission. They simply identify the "interruptability," "relocatability," and "replicability" of an asset based on subjectively quantified scores of the CATCODE [31]. For example, a perimeter road around the national forest on Vandenberg Air Force Base, CA, may have the same MDI as the road accessing the Air

Traffic Control Tower on Andrews Air Force Base in Washington DC, as long as they are both assigned the same CATCODE.

With the combination of the various CATCODES, establishing pavement types and quantities, as well as the MDIs establishing their importance, a model that quantifies the risk of implementing technologies such as photovoltaic pavement systems relative to the total quantity of specific pavements can be established. Risk modeling is subjective as it is based upon the willingness of leadership to set acceptable risk thresholds. However, the ability to determine quantities of pavement for replacement within various categories based on the acceptance of risk creates an objective system of prioritized implementation while managing subsequent increased risk.

Foundations for Research

Controlling risk is a priority for no-fail organizations like the USAF. Therefore, the implementation of any new technology system or method of conducting business rightfully raises concern. The first step in being able to manage and control these risks is being able to quantify them objectively, thus removing emotion and opinion.

There are existing constructs within the service which parallel the ability to quantify the risk of implementing a photovoltaic pavement. By combining the concept that increasing quantities represent disproportionately increasing risks and various pavement uses represent a sliding scale of potential impacts, an methodology to analyze and quantify these risks comes into focus. This not only enables effective communication but enables a controlled introduction of risky ventures like the application of new technologies.

III. Methodology

The aforementioned qualitative analysis identifying proposed test standards to evaluate photovoltaic pavements through heuristics-based analysis enabled the use of photovoltaic pavements without the modification of pavement design methodologies. The greatest limitation of the analysis of these materialistically unique pavement systems is that current standards of analysis are not able to be directly applied to these glass/polymer/metallic structures. For example, the Superpave Shear Test traditionally used on pavements cannot be applied to the SR3 model paver unit as its shear strength is not gained from the interlocking of aggregates but the adherence of the layers within the laminated structure. This is why a specific qualitative analysis to identify the metrics necessary for design was required and heuristics were designed.

The remaining methodologies proposed in this new line of research are specific to the listed research questions. These include methodologies to calibrate the expected performance of photovoltaic pavement systems empirically, quantify the impacts of climate through linear and logistic regressions that may identify optimal conditions at locations different than the commonly accepted locations, and propose a system to control risk in implementing these new technologies. As research continues, the methodologies proposed herein may be adjusted or calibrated with greater fidelity than is currently available on the limited spectrum of research into photovoltaic pavement systems.

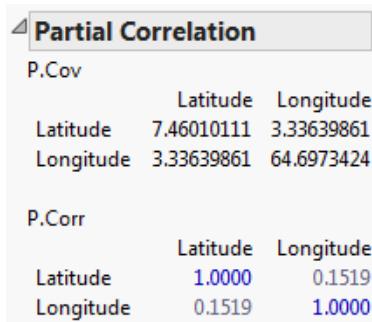
Research Question 1: Photovoltaic Performance Modeling

Site Selection

Statistical analysis of the latitude and longitude coordinates of 1,763 USAF installations, through an ANOVA of each variable, independently divided the world into five latitude bins and five longitude bins. For the purposes of this research, a “location” or “installation” is defined as any site with a unique Real Property Site Unique Identifier, or “RPSUID” code. The correlation between latitude and longitude for these installations was found to be statistically insignificant at 0.1519 as shown in Figure 18. There was a concern that, given the clustering of installations into geographically limited regions that there may be a more significant correlation.

When overlaid, these bins created 25 regions covering the entire earth. The break points between these bins may be adjusted left or right with minor affects to the R^2 value of the resulting bins. Therefore, a single point at the mean latitude and longitude of all sites within one of these 25 regions can be extrapolated to represent all other sites within that specific region in regards to the latitude and longitude variables.

This measure is relevant as the Air Mass is primarily based on the angle with which the sun strikes a panel, as outlined above. As the earth is constantly tilted at an



Partial Correlation		
P.Cov		
	Latitude	Longitude
Latitude	7.46010111	3.33639861
Longitude	3.33639861	64.6973424
P.Corr		
	Latitude	Longitude
Latitude	1.0000	0.1519
Longitude	0.1519	1.0000

Figure 18. Correlation Analysis of 1,763 Installation Latitudes and Longitudes as created by the JMP Software Package

angle of 23.5° , the optimal location for achieving the 48.2° angle of direct beam irradiation required for an Air Mass of 1.5 changes latitude throughout the seasons. Any photovoltaic pavement system at a latitude greater than 71.7° should never achieve an Air Mass of 1.5 due to the fact that photovoltaic pavements are generally horizontal.

However, as outlined above, Air Mass is also affected by humidity as well as latitude. A system at a low-humidity location above latitude 71.7° may outperform a system at a latitude under this threshold with high-humidity if the increased humidity results in significant reductions in irradiance due to diffraction, reflection, deflection, increased cloud cover, or reduced clearness index. Additionally, as temperatures generally decrease at higher latitudes, which corresponds to higher efficiency for photovoltaics, the same inverted performance expectations may occur for cooler systems above this latitude over hotter systems at lower latitudes.

To develop this global, long-term experiment, a statistical analysis of United States Air Force installations and sites is proposed. Rather than creating customized categories for temperature and humidity, this research capitalized on the Köppen-Geiger Climate Classification System. This is the most widely-used climate classification system and was updated by Kottek, et al. in 2005, which improved its accuracy to 0.5 degrees of latitude and longitude [32]. Using this climate classification system to ensure a diversity of climactic conditions allowed the linear regression analysis of independent effects of temperature and humidity as well as their combined effects. Additionally, categorical variables are developed for these classifications allowing for logistical regression analysis. The resultant models may identify characteristics of each type of

technology identifying optimum operational conditions and enhance product development for specific conditions.

To identify the effects of humidity and temperature on top of the latitudes established by these 25 regions, a Pareto analysis was conducted on all 1,763 sites based on the Köppen-Geiger Climate Classification System, as well as the 25 regions identified through the ANOVAs. This latter Pareto analysis identified which regions represented the majority of installations allowing a prioritized placement of additional test systems within regions. The climate-based Pareto analysis identified in which climates the majority of test sites should be selected to identify major effects and combined effects of temperature and humidity through linear regression analysis and climate classifications through logistic regression analysis.

It must be noted that the Köppen-Geiger Climate Classification system uses temperature metrics to establish both the “Temperature” classification and the “Main Climate” Classification. Therefore, the climate classification Pareto analysis was broken into two different methods: one method using “Main Climate” and “Precipitation” classifications and a second method using “Precipitation” and “Temperature” classifications.

Test System Design

To evaluate the effects of these classifications, temperatures, and humidities, a simple test system was designed for placement at each test site. The test system consists primarily of a 40W Monocrystalline Photovoltaic Panel, a 25W Polycrystalline Photovoltaic Panel, a Temperature/Humidity Probe, a Satellite Communication System,

and a computer. To save costs and enable shipping across international boundaries, batteries were not incorporated into the systems; so while it may be ironic, these photovoltaic test systems are not self-powering. However, at the request of some sites, a back-up battery system, with a photovoltaic panel to re-charge the battery, was specified. Sites were notified of the specifications of this battery back-up and trained regarding how to connect them. Additionally, the coding of the system allowed remote monitoring of the voltage of the battery so that the research team could notify site POCs when to replace the battery.

Once placed, the test systems will take measurements every 15 minutes to identify the instantaneous ambient temperature, humidity, and the Current-Voltage curves for both panels with 64 points used to establish them. This collection of data points will be stored in an on-board memory card. At the end of each day, the test system will send a message with generic performance information and system operations data to the research team. These messages will give a general idea of the system's performance and current condition. For schematics, programming code, and users guides of the test system see the corresponding appendices. At the end of a year's worth of data collection, or any time period within Phase I of this research, the memory card data will be downloaded, and a secondary card will be placed in the test system to start the next time period's data collection. This cycle may continue until the systems die in place allowing for Phase II of this research, which is intended to focus on the effects of various climates on the longevity of various photovoltaic technologies.

Data from Phase I will be analyzed to identify if there are statistically significant categorical variables for either the main effects of Main Climate, Precipitation, or

Temperature, or the combined effects of Main Climate/Precipitation or Precipitation/Temperature classification on the impact of photovoltaics. Separately, it will be analyzed to identify the correlations between ambient temperature and ambient humidity through the data collected by the probe to identify statistical significance. Additionally, it allows the analysis of temperature and humidity within specific climates to identify statistically significant correlations. The volume of data provided by identical test systems at all sites will create a dataset of greater breadth and depth than ever before. As well as analysis within the constructs of this research, this data may be able to be used to evaluate and validate the multitude of efficiency and power factors mentioned above.

Research Question 2: Risk Modeling of Photovoltaic Pavement Systems

Since this model did not take into account the specific location of the pavement to be replaced, it is predicated on the assumption that the least-risky pavements are to be replaced first within each CATCODE. For example, the roads on the airfield would be replaced last--whereas the roads to an on-base camping and recreation facility may be replaced first. Therefore, it can be assumed that as the quantity of pavement is replaced within a CATCODE, the corresponding risk increases at an accelerating rate in reference to the CATCODE's effects on the mission.

Additionally, there are specific CATCODEs which, if only a fraction fail, represent a total shut down to the mission--regardless of the MDI. For example, a single square yard of failed pavement in the runway landing zone represents a total shutdown of airfield operations until it is repaired. However, if all the sidewalks fail, the total risk to the mission is nearly negligible. The MDIs provide us a point-of-reference for a

CATCODE's importance but cannot be used to represent the actual risk of replacing portions of a pavement system.

A mathematical system must be developed with the MDI as a significant influence to identify the increase in risk when a portion of a CATCODE of pavement is replaced. However, there are specific CATCODES that result in a risk level of nearly 100% should they, individually, fail. Subjective opinions developed over years of experience must be gathered to quantify the impact to the mission of the failure of portions of pavement systems and form much of the methodology upon which this system is predicated. However, a system architecture for quantifying the risk may be proposed allowing research to be conducted to calibrate the system.

Conclusion

The proposed methodologies above are one way of answering the research questions. In answering Question 1, a statistical analysis was conducted of a broad spectrum of variables which can be analyzed in numerous ways. The goal of this method is to begin bringing light to a new area of research but the results of the work are not guaranteed to provide the answers necessary. However, the volume of data represented in 15-minute measurements of photovoltaic performance in congruence with ambient temperature and humidity at 37 test sites around the world during the same 365-day technical period of performance is immense. It will aid in clarifying current research that disagrees regarding specific metrics, be a solid foundation for the identification of potentially unidentified correlations, and represent an entirely new method of identifying optimum locations for photovoltaic power plants. In answering Question 2, a

methodology is proposed that is admittedly untested and subjectively designed based on the expertise of members of the research team. It resolves currently known issues regarding the accuracy of specific metrics but is still based heavily upon subjective evaluations of risk. Each of these questions represent the beginnings of new lines of research that have the potential to add significant data to the academic community.

IV. Analysis and Results

Some of the data analyzed for this research is proprietary and cannot be presented, although the results of the analysis can be presented. Additionally, some of the data represents federally sensitive information and will not be published either. However, the minimum data required to present the analysis for consideration has been provided.

As with all statistical analysis, the same data can be viewed and presented multiple ways. Additionally, due to funding shortfalls, some of the analysis proposed stopped short of actual testing. Further research will complete this testing and identify if the results of this analysis prove to be effective and correct or if alternative methods may prove more fruitful.

Research Question 1: Photovoltaic Performance Modeling

As identified above, the primary variables for this study are Temperature and Humidity. The Köppen-Geiger Climate Classification System provides an architecture for the design of this experiment which ensure a broad spectrum of climate conditions as well as providing categorical variables for subsequent regressions in future research. Additionally, since this experiment is intended to identify the potential for photovoltaic systems across the USAF enterprise, analysis to ensure a broad spectrum of latitudes and longitudes are considered must be conducted.

Histograms for both the latitudes and longitudes of 1,763 locations are shown in Figure 19 and Figure 20, respectively, along with their corresponding Analysis of Variance (ANOVA) bins. From the histogram clusters, multiple possible groupings

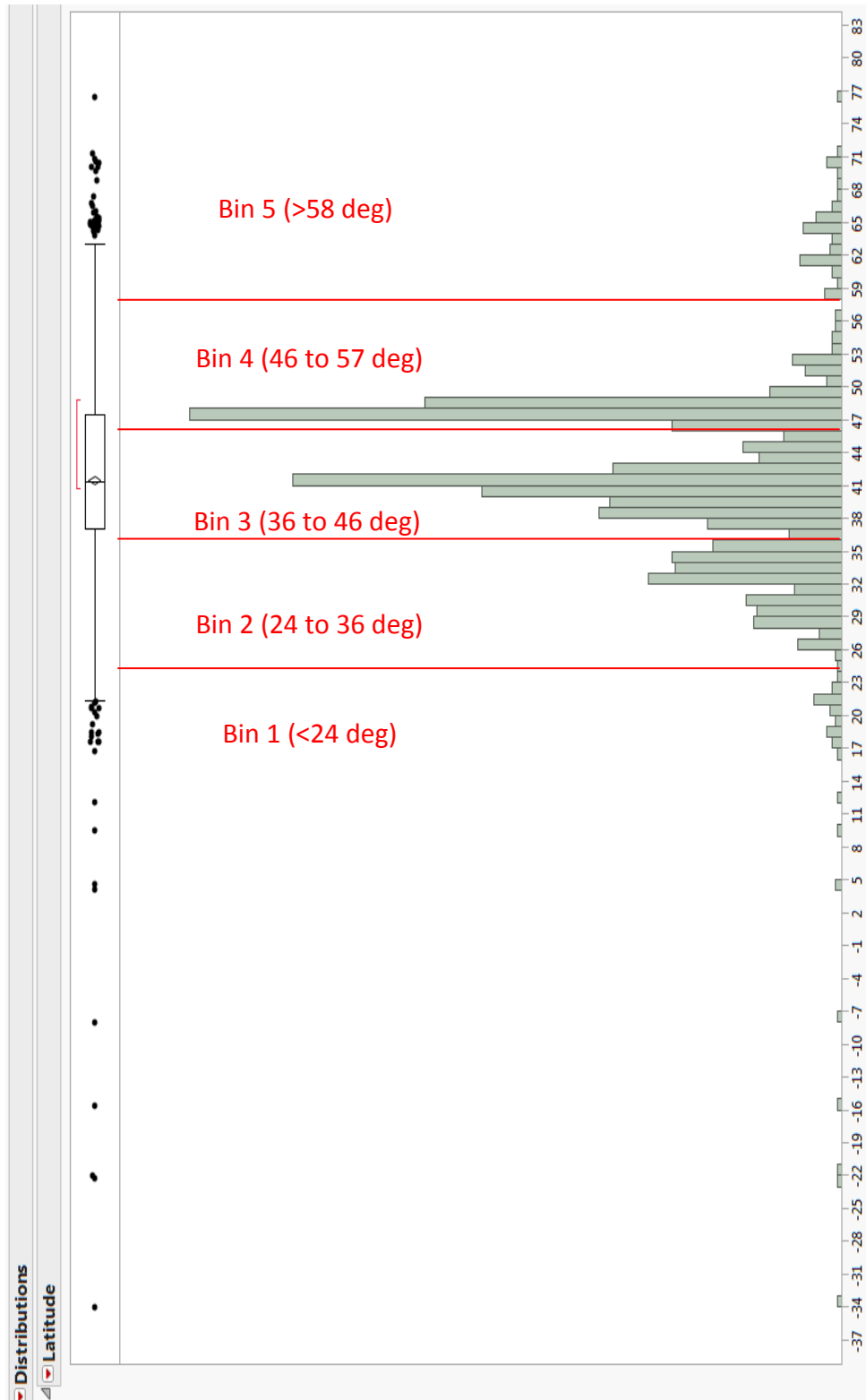


Figure 19. Histogram of all latitudes with a bin size of 1 degree as created by the JMP Software Package and ANOVA bins shown

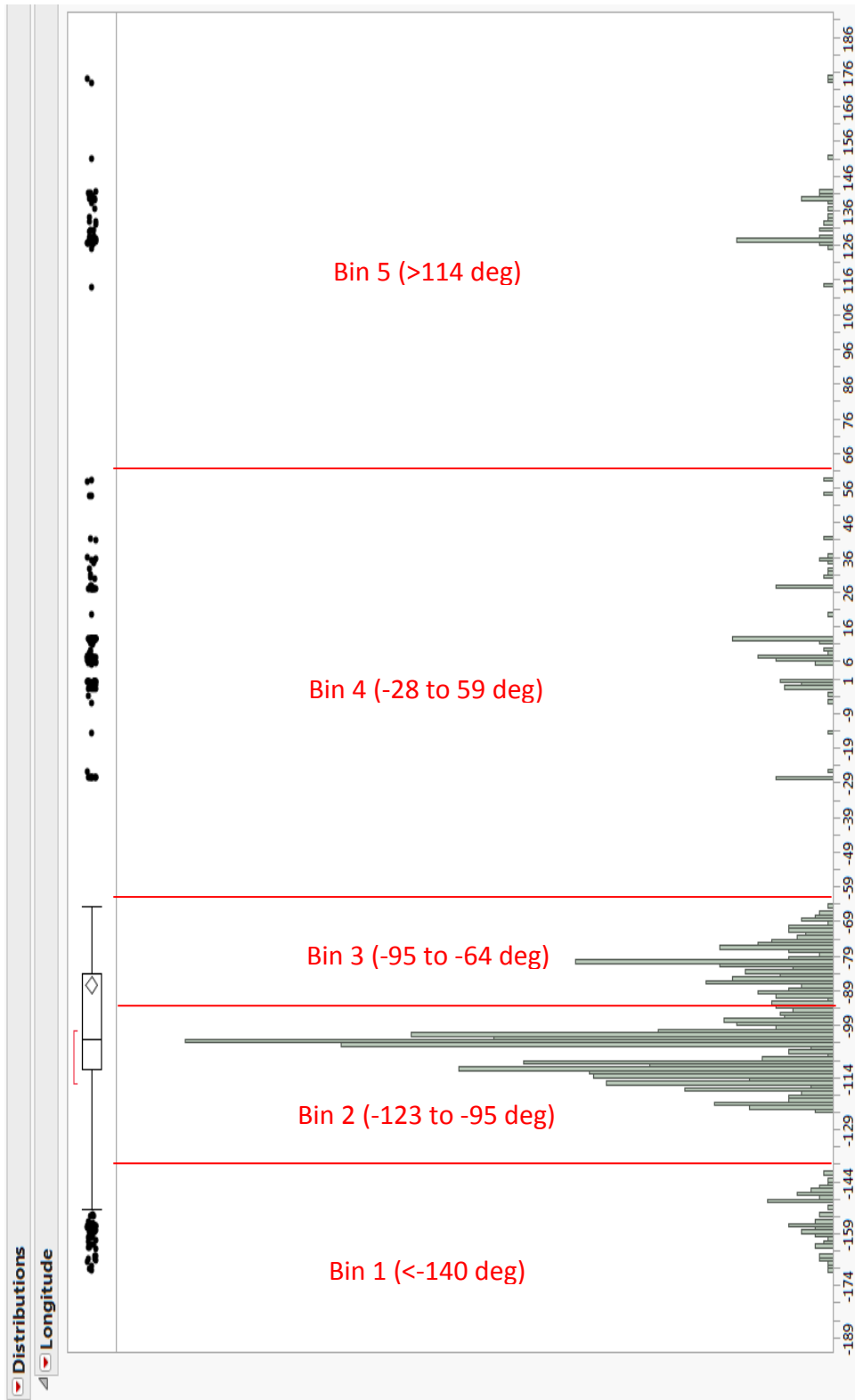


Figure 20. Histogram of all longitudes with a bin size of 1 degree as created by the JMP Software Package and ANOVA bins shown

for an ANOVA for each metric can be identified. The median and mean for latitudes are nearly in the same location. However, the median and the mean for the longitudes are dislocated from each other. The histograms also show many outliers as identified by the JMP software package. Eliminating these outliers may increase the accuracy of the analysis, thus improving the R^2 value, and align the mean and median of the longitudes. However, it would eliminate a large number of potential test sites and corresponding climates which could affect the climate portions of the analysis. Therefore, all installations were retained and the bins for the ANOVA analysis spanned the full breadth of published latitudes and longitudes.

This research team chose the clustering shown in Figure 19 and Figure 20 based on a bin size of one degree for both latitude and longitude histograms. The subsequent bins were subjected to an ANOVA as shown in Figure 21 for latitude and Figure 22 for longitude, which result in R^2 values of 0.89 and 0.98, respectively. The relatively low R^2 value for the latitude ANOVA is largely due to the outliers in the southern hemisphere, but these outliers must be accounted for to include all possible climate types in the final analysis. Further analysis, through a Connecting Letters report and Ordered Differences report produced by the JMP software package, show that the probability of bin overlap is negligible.

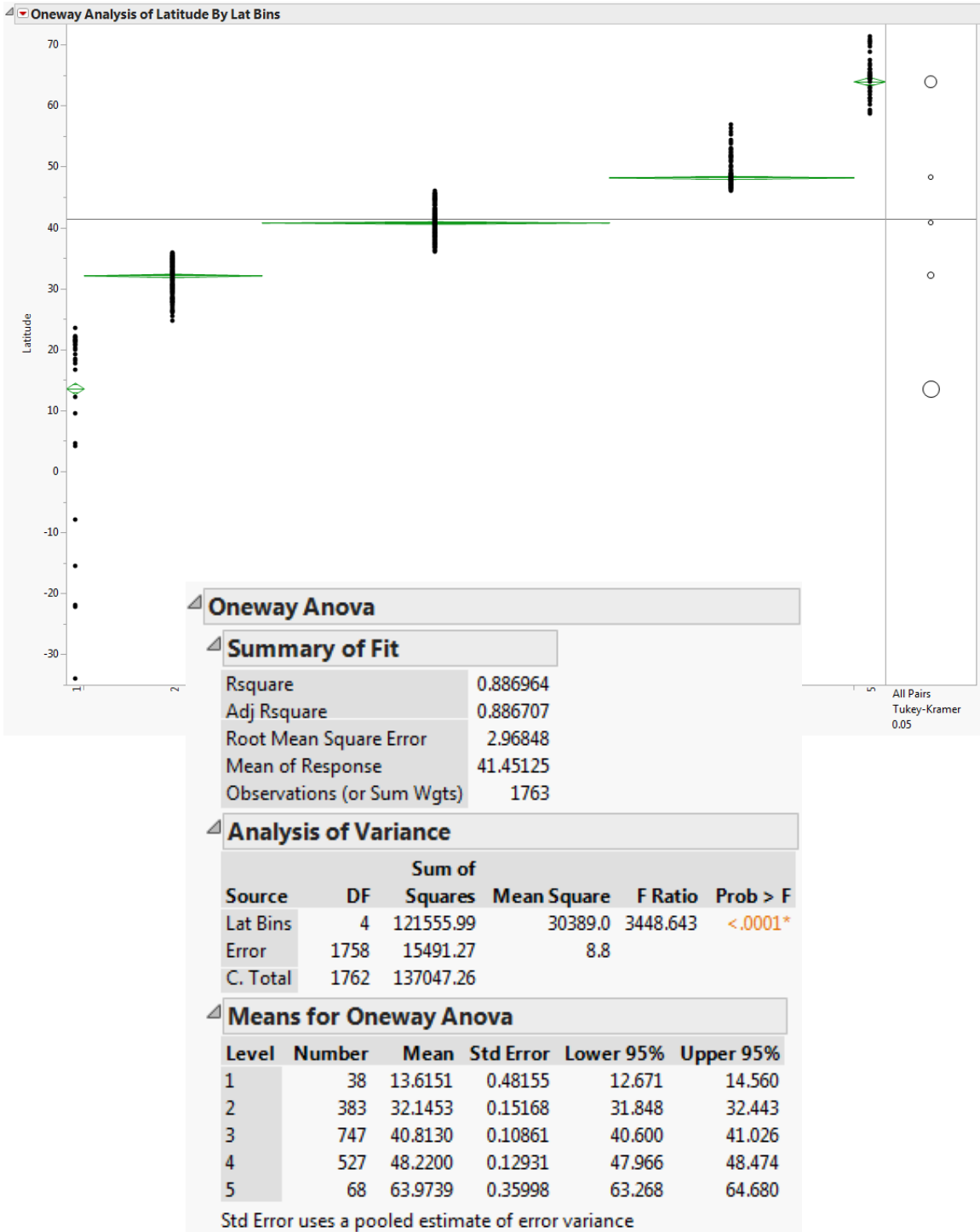


Figure 21. ANOVA for Latitude Bins of all USAF Installations evaluated by the JMP Software Package

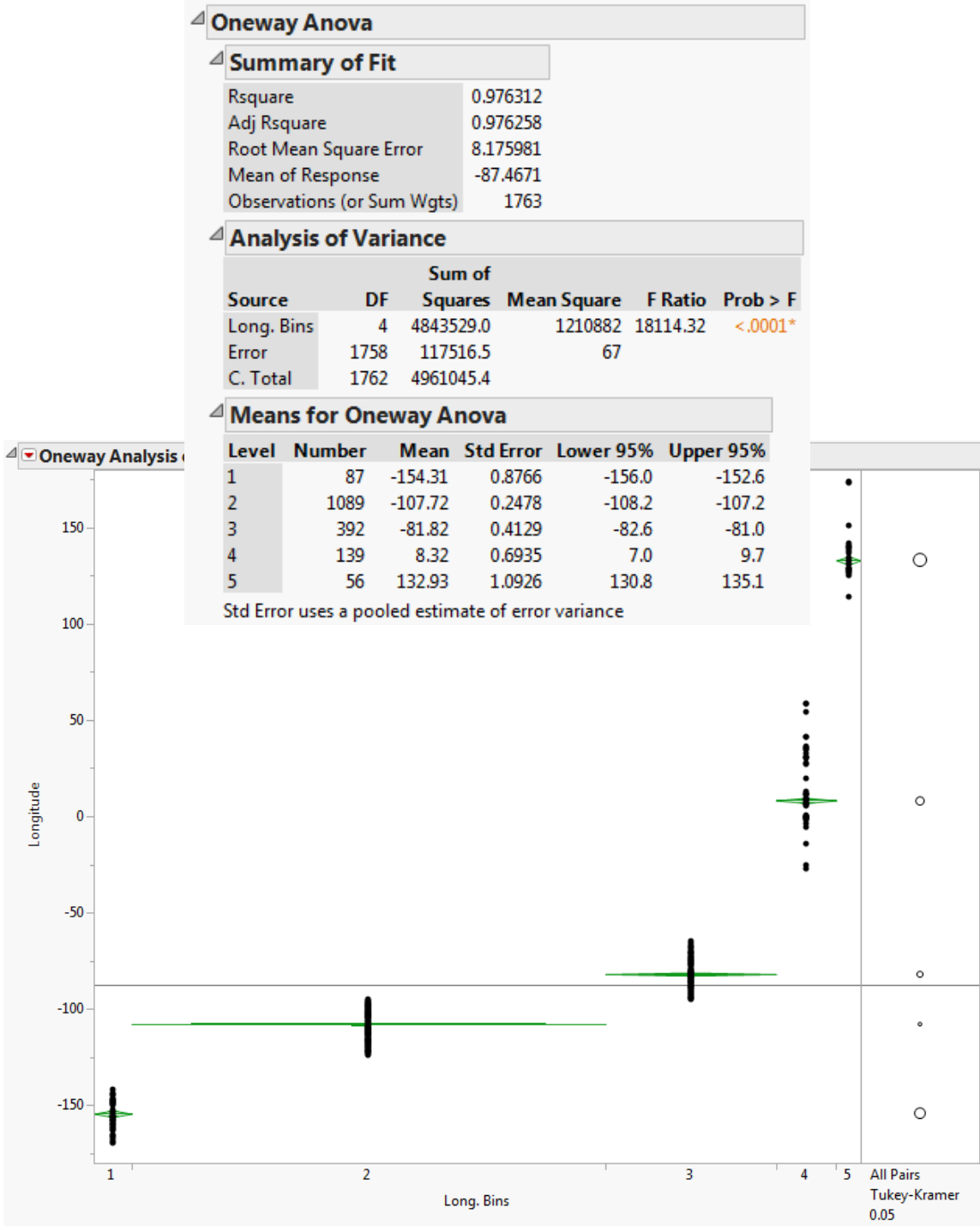


Figure 22. ANOVA for Longitude Bins of all USAF Installations evaluated by the JMP Software Package

When overlaid, these latitude and longitude bins resulted in 25 regions of unequal size as shown in Figure 23. As seen from this figure, not all regions have installations inside of them, due to the fact that the ANOVAs were conducted independently of each other. The mean of a region may be greatly different than the mean of a bin, due to the outliers, which is made apparent when looking at Latitude Bin 1.

Within Bin 1, comparing the latitude of Region A to Region E shows a great variance in the mean latitude across regions within the same bin. Subsequently, 190 pairwise comparisons between each of the final 25 defined regions were analyzed, and only 22 comparisons were found to have statistically similar longitudes; each of these pairs was found to be within the same bin, which is to be expected. The same pairwise analysis was conducted on latitudes, and 20 were found to be statistically similar. Again, each was found to be within the same bin--except for five which were found to be either up or down by a single bin. As stated above, this is explained by considering that the mean for the bin includes all installations in that bin but the mean for a region will have a much smaller population size. Reviewing the locations of Region P and Region X shows how two regions in two different bins could have statistically similar mean latitudes despite being in different bins. Reviewing the statistically similar regions while considering the information presented in Figure 23, which gives a visual of the ANOVA based bins and 25 Regions, aids in explaining the results of the pairwise comparisons discussed above.

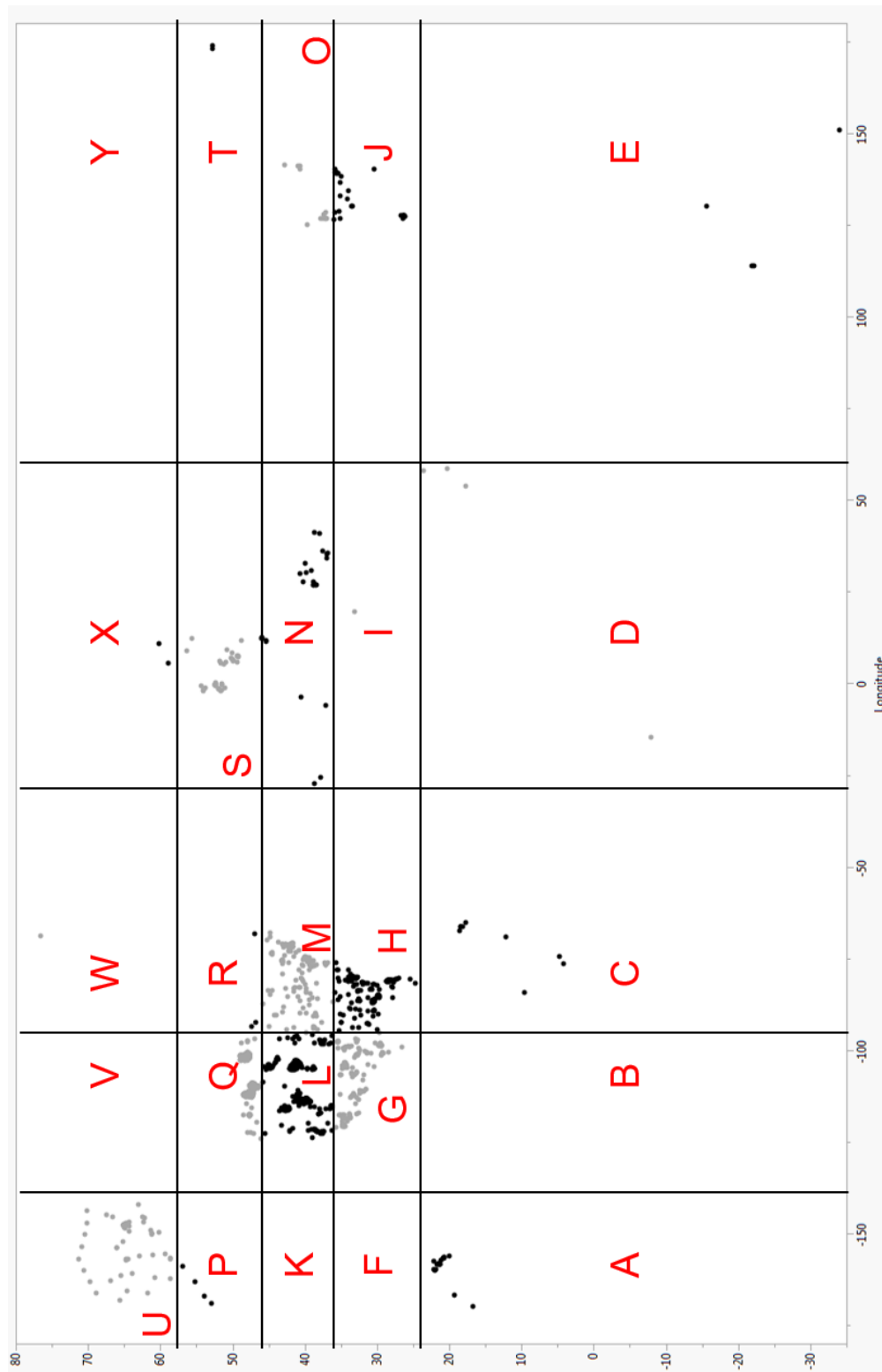


Figure 23. Chart of Latitude and Longitude ANOVA Bins and subsequent 25 Regions Labeled produced by JMP Software Package

Through this analysis, installations closest to the mean of each defined region can be assumed to represent all installations within that region. Deference was given to matching latitudes as closely as possible as longitude generally does not affect irradiance. Therefore, to satisfy the desire to accurately represent the potential for photovoltaic power across the enterprise, these installations formed the foundation of the test sites for this experiment. To identify these installations, Table 1 shows the mean location of the installations in each region, that of the nearest installation, and the deltas.

Table 1. Comparison of Regional Mean Lat/Long to Nearest Installation Lat/Long

Region	Mean Lat	Mean Long	Desired Site Lat	Desired Site Long	Lat Delta	Long Delta
A	21.01796316	-158.8819526	20.8817	-156.4675	0.136263	2.414453
B	0	0	N/A	N/A	0	0
C	14.03258	-70.07715	12.1833	-69	1.84928	1.07715
D	13.80936667	42.30361667	17.6669	54.0328	3.857533	11.72918
E	-23.401475	127.46385	-22.19	114.103	1.211475	13.36085
F	0	0	N/A	N/A	0	0
G	33.10169884	-106.1646988	33.1061	-101.665	0.004401	4.499699
H	31.293064	-83.62521143	31.3217	-85.4512	0.028636	1.825989
I	33.1833	19.7167	29.346964	47.521819	3.836336	27.805119
J	31.63523824	132.2586029	30.48	140.3061	1.155238	8.047497
K	0	0	N/A	N/A	0	0
L	40.96126303	-108.2169311	40.961	-103.974	0.000263	4.242931
M	41.01970582	-79.92033386	40.9846	-85.1768	0.035106	5.256466
N	39.26723409	9.109268182	39.16	31.12	0.107234	22.01073
O	38.396	130.6304375	37.7519	127.0278	0.6441	3.602638
P	54.787125	-164.28625	55.2629	-162.807	0.475775	1.47925
Q	47.79719507	-107.3443075	47.7959	-111.776	0.001295	4.431693
R	46.9237875	-89.2779125	46.9344	-67.913	0.010612	21.36491
S	50.04802442	5.847924419	50.0263	6.799	0.021724	0.951076
T	52.77605	173.6425	52.8326	173.179	0.05655	0.4635
U	64.02361129	-152.6679081	63.8841	-160.559	0.139511	7.891092
V	0	0	N/A	N/A	0	0
W	76.5311	-68.7031	76.5311	-68.7031	0	0
X	59.37473333	7.517366667	58.9633	5.7331	0.411433	1.784267
Y	0	0	N/A	N/A	0	0

Consideration was given to each installation at these locations. However, some of the sites represent unoccupied environmental restoration sites, closed sites, or other locations which are unable to be accessed. Therefore, Nearest Neighbor Analysis was completed until the nearest occupied, and willing, installation for each of the regional means was identified. This results in Table 2. This means every selected installation intended to represent the span of all USAF installations is within 3.84 degrees with an average delta of 0.699 degrees of latitude, with 14 of 20 sites being within 0.5 degrees of the regional mean that the site is meant to represent, which matches the range of accuracy of the climate data from the updated Köppen-Geiger Climate System.

Table 2. Comparison of Regional Mean Lat/Long to Selected Installation Lat/Long

Region	Desired Lat	Desired Long	Selected Site Lat	Selected Site Long	Lat Delta	Long Delta
A	21.01796316	-158.8819526	20.8817	-156.4675	0.136263	2.414453
B	0	0	N/A	N/A	0	0
C	14.03258	-70.07715	12.1833	-69	1.84928	1.07715
D	13.80936667	42.30361667	11.5172	43.0644	2.292167	0.760783
E	-23.401475	127.46385	-22.19	114.103	1.211475	13.36085
F	0	0	N/A	N/A	0	0
G	33.10169884	-106.1646988	32.9186	-106.134	0.183099	0.030699
H	31.293064	-83.62521143	31.1671	-92.62	0.125964	8.994789
I	33.1833	19.7167	29.346964	47.521819	3.836336	27.805119
J	31.63523824	132.2586029	33.5667	130.4333	1.931462	1.825303
K	0	0	N/A	N/A	0	0
L	40.96126303	-108.2169311	40.9428	-113.412	0.018463	5.195069
M	41.01970582	-79.92033386	40.6703	-86.1469	0.349406	6.226566
N	39.26723409	9.109268182	38.7808	-27.1453	0.486434	36.25457
O	38.396	130.6304375	39.65	125.3333	1.254	5.297138
P	54.787125	-164.28625	55.2629	-162.807	0.475775	1.47925
Q	47.79719507	-107.3443075	47.7949	-101.298	0.002295	6.046308
R	46.9237875	-89.2779125	46.9344	-67.913	0.010612	21.36491
S	50.04802442	5.847924419	50.0263	6.799	0.021724	0.951076
T	52.77605	173.6425	52.7195	174.106	0.05655	0.4635
U	64.02361129	-152.6679081	64.2905	-149.187	0.266889	3.480908
V	0	0	N/A	N/A	0	0
W	76.5311	-68.7031	76.5311	-68.7031	0	0
X	59.37473333	7.517366667	58.9633	5.7331	0.411433	1.784267
Y	0	0	N/A	N/A		

These installations represent the spread of potential across USAF installations based on latitude and longitude as well as forming the starting point of the climatological analysis. They represent 20 of the total 37 test sites able to be evaluated. Therefore, Pareto analysis of the number of installations within each region was conducted to determine in which regions the research team would attempt to select the remaining 17 test locations. This Pareto analysis resulted in the data shown in Table 3. The majority of installations are in Regions L and Q while less than 1% are in each of O, C, R, D, E, P, X, T, W, and I. These percentages are not intended to equate the total square footage of installations within these regions but solely the number of installations. Therefore, efforts will be made to ensure the majority of test sites are in the more populous regions.

Table 3. Pareto Analysis of Installations per Region

Region	Installation Count	Percent
L	498	28.24730573
Q	427	24.22007941
M	189	10.72036302
H	175	9.926262053
G	173	9.812819058
S	86	4.87804878
U	64	3.630175837
N	44	2.495745888
J	34	1.928530913
A	19	1.077708452
O	16	0.907543959
C	10	0.567214974
R	8	0.45377198
D	5	0.283607487
E	4	0.22688599
P	4	0.22688599
X	3	0.170164492
T	2	0.113442995
W	1	0.056721497
I	1	0.056721497
B, F, K, V, Y	0	0

However, before the remaining sites can be selected, the climates of the existing sites must be known, and a Pareto analysis of all known climates must be completed so as to know which regions to prioritize for additional test sites and which can be disregarded for this study. Ideally, multiple test systems would be placed in each possible climate type. There are 30 possible climate types using the Köppen-Geiger Climate Classification system [32]. An ideal study would place 30 test systems in each of these climate classifications, which provides a statistically large sample size in each. This would require 900 test systems which exceeds the research team’s budget. Of the 30 existing classifications, the USAF has installations in 23. The classifications that will remain uninvestigated are shown in Table 4. There is no method by which this study could identify the possible impacts of these climate classifications. Furthermore, even though statistical identification of climate impacts with less than 30 test systems on site, a single test system in a climate does not allow true analysis of a impact. Therefore, if a minimum of two test systems is required per climate classification, a minimum of 46 test systems would be required. This also is beyond the scope of this research team’s budget. Additionally, as shown in Table 5, there are 15 climate classifications that each retain less than 1% of all USAF installations, representing less value than other climates.

Table 4. Uninvestigated Köppen-Geiger Climate Classification Types

Main Climate	Precipitation	Temperature
Polar		Polar Frost
Snow	Fully Humid	Extremely Continental
Snow	Winter Dry	Cool Summer
Snow	Winter Dry	Extremely Continental
Warm Temperate	Summer Dry	Cool Summer
Warm Temperate	Winter Dry	Cool Summer
Warm Temperate	Winter Dry	Warm Summer

Table 5. Pareto Analysis of All Possible USAF Installation Climate Classifications

Climate Classifications	Count	Percent
Arid/Steppe/Cold Arid	613	34.77028
Warm Temperate/Fully Humid/Hot Summer	340	19.28531
Snow/Fully Humid/Warm Summer	307	17.4135
Warm Temperate/Fully Humid/Warm Summer	97	5.501985
Warm Temperate/Summer Dry/Warm Summer	82	4.651163
Snow/Fully Humid/Hot Summer	55	3.119682
Snow/Fully Humid/Cool Summer	54	3.062961
Warm Temperate/Summer Dry/Hot Summer	49	2.779353
Arid/Desert/Cold Arid	17	0.964265
Arid/Steppe/Hot Arid	16	0.907544
Polar//Polar Tundra	12	0.680658
Arid/Desert/Hot Arid	11	0.623936
Snow/Winter Dry/Hot Summer	11	0.623936
/Fully Humid/	10	0.567215
/Summer Dry/	10	0.567215
Snow/Summer Dry/Warm Summer	7	0.39705
/Monsoonal/	5	0.283607
Snow/Summer Dry/Cool Summer	3	0.170164
/Winter Dry/	3	0.170164
Warm Temperate/Winter Dry/Hot Summer	2	0.113443
Snow/Summer Dry/Hot Summer	1	0.056721
Snow/Winter Dry/Warm Summer	1	0.056721
Warm Temperate/Fully Humid/Cool Summer	1	0.056721

These budgetary restrictions limited analysis to a reduced spectrum of climate classifications. Therefore, the research team broke down the Köppen-Geiger Climate Classification System to create a smaller number of possible climate classifications. This enables the research team to analyze this modified system in greater depth and with more accuracy. Solely considering the combination of Main Climate and Precipitation classifications results in the Pareto analysis shown in Table 6, and the combination of Precipitation and Temperature classifications results in the Pareto analysis shown in Table 7. Both modified climate classification systems include “Fully Humid,” “Summer Dry,” “Monsoonal,” and “Winter Dry” Precipitation Classifications. In comparing the

results of the analysis in Table 5, it can be seen that the only installations with a Main Climate Classification of “Polar” are also those with a Temperature Classification of “Polar Tundra” and vice versa. Additionally, there are five classifications that appear on both modified classifications systems, allowing for a reduced total number of sites. Furthermore, sites that are “Arid/Steppe” from Table 6 could be “Steppe/Cold Arid” or “Steppe/Hot Arid” from Table 7. Therefore, it is apparent that the research team must select test sites that allow analysis within one modified classification system but also allow multiple analyses within the other modified classification system.

Table 6. Pareto Analysis of All USAF Installation Main Climate/Precipitation Classifications

Main/Precip Classification	Count	Percent
Arid/Steppe	629	35.67782189
Warm Temperate/Fully Humid	438	24.84401588
Snow/Fully Humid	416	23.59614294
Warm Temperate/Summer Dry	131	7.430516166
Arid/Desert	28	1.588201929
Snow/Winter Dry	12	0.680657969
Polar	12	0.680657969
Snow/Summer Dry	11	0.623936472
Fully Humid	10	0.567214974
Summer Dry	10	0.567214974
Monsoonal	5	0.283607487
Winter Dry	3	0.170164492
Warm Temperate/Winter Dry	2	0.113442995

Table 7. Pareto Analysis of All USAF Installation Precipitation/Temperature Classifications

Precip/Temp Classification	Count	Percent
Steppe/Cold Arid	613	34.77027794
Fully Humid/Warm Summer	404	22.91548497
Fully Humid/Hot Summer	395	22.40499149
Summer Dry/Warm Summer	89	5.048213273
Fully Humid/Cool Summer	55	3.11968236
Summer Dry/Hot Summer	50	2.836074872
Desert/Cold Arid	17	0.964265457
Steppe/Hot Arid	16	0.907543959
Winter Dry/Hot Summer	13	0.737379467
Polar Tundra	12	0.680657969
Desert/Hot Arid	11	0.623936472
Fully Humid	10	0.567214974
Summer Dry	10	0.567214974
Monsoonal	5	0.283607487
Winter Dry	3	0.170164492
Summer Dry/Cool Summer	3	0.170164492
Winter Dry/Warm Summer	1	0.056721497

Starting with the Starting with the Regional Mean test sites, a baseline set of test sites with modified climate classifications as shown in Table 8 were identified. Viewed in reverse, these modified climate classifications result in the Test Site Climate Pareto Analyses shown in Table 9 and Table 10. It makes sense that, without focusing on climate types of these initial test sites, the climates are relatively closely aligned to the Pareto analysis results. The probability of selecting a test site in a populous climate classification is greater than selecting one in a less populous climate classification. The remaining 17 sites were selected to prioritize placement in the most populous regions as well as the most populous modified climate classifications based on the Pareto Analysis in Table 3, Table 6, and Table 7. In order to select these sites, the climate types of each Region must be identified. Table 11 below shows the possible Main

Climate/Precipitation classifications and Table 12 shows the possible Precipitation/Temperature classifications within each occupied Region, as well as the percentage of total installations within each climate classification and Region from Table 3, Table 6, and Table 7.

Table 8. Climate Classifications of Lat/Long Based Test Sites

Region	Main Climate/Precipitation	Precipitation/Temperature
A	/Fully Humid	Fully Humid/
C	Arid/Steppe	Steppe/Hot Arid
D	Warm Temperate/Summer Dry	Summer Dry/Warm Summer
E	Arid/Desert	Desert/Hot Arid
G	Arid/Steppe	Steppe/Cold Arid
H	Warm Temperate/Fully Humid	Fully Humid/Hot Summer
I	Arid/Desert	Desert/Hot Arid
J	Warm Temperate/Fully Humid	Fully Humid/Hot Summer
L	Arid/Steppe	Steppe/Cold Arid
M	Snow/Fully Humid	Fully Humid/Hot Summer
N	Warm Temperate/Summer Dry	Summer Dry/Warm Summer
O	Snow/Winter Dry	Winter Dry/Hot Summer
P	Warm Temperate/Fully Humid	Fully Humid/Cool Summer
Q	Snow/Fully Humid	Fully Humid/Warm Summer
R	Snow/Fully Humid	Fully Humid/Warm Summer
S	Warm Temperate/Fully Humid	Fully Humid/Warm Summer
T	Snow/Fully Humid	Fully Humid/Cool Summer
U	Snow/Fully Humid	Fully Humid/Cool Summer
W	Polar/	/Polar Tundra
X	Warm Temperate/Fully Humid	Fully Humid/Warm Summer

Table 9. Alignment of Lat/Long Test Sites to Pareto Analysis of Main Climate/Precipitation Climate Classifications

Main Climate/Precipitation	Pareto Analysis	Test Site Count
Arid/Steppe	35.67782189	3
Warm Temperate/Fully Humid	24.84401588	5
Snow/Fully Humid	23.59614294	5
Warm Temperate/Summer Dry	7.430516166	2
Arid/Desert	1.588201929	2
Snow/Winter Dry	0.680657969	1
Polar/	0.680657969	1
Snow/Summer Dry	0.623936472	0
/Fully Humid	0.567214974	1
/Summer Dry	0.567214974	0
/Monsoonal	0.283607487	0
/Winter Dry	0.170164492	0
Warm Temperate/Winter Dry	0.113442995	0

Table 10. Alignment of Lat/Long Test Sites to Pareto Analysis of Precipitation/Temperature Climate Classifications

Precipitation/Temp	Pareto Analysis	Test Site Count
Steppe/Cold Arid	34.77027794	2
Fully Humid/Warm Summer	22.91548497	4
Fully Humid/Hot Summer	22.40499149	3
Summer Dry/Warm Summer	5.048213273	2
Fully Humid/Cool Summer	3.11968236	3
Summer Dry/Hot Summer	2.836074872	0
Desert/Cold Arid	0.964265457	0
Steppe/Hot Arid	0.907543959	1
Winter Dry/Hot Summer	0.737379467	1
/Polar Tundra	0.680657969	1
Desert/Hot Arid	0.623936472	2
Fully Humid/	0.567214974	1
Summer Dry/	0.567214974	0
Monsoonal/	0.283607487	0
Winter Dry/	0.170164492	0
Summer Dry/Cool Summer	0.170164492	0
Winter Dry/Warm Summer	0.056721497	0

Table 11. Options for Additional Climate Based Test Sites for Main Climate/Precipitation Effects Analysis for Top 90% of Pareto Analysis from Table 9

Main Climate/Precipitation	Climate Pareto Analysis	Region	Region Pareto Analysis
Arid/Steppe	35.67782189	L	28.24730573
Arid/Steppe	35.67782189	Q	24.22007941
Arid/Steppe	35.67782189	G	9.812819058
Arid/Steppe	35.67782189	C	0.567214974
Arid/Steppe	35.67782189	I	0.056721497
Warm Temperate/Fully Humid	24.78729438	L	28.24730573
Warm Temperate/Fully Humid	24.78729438	M	10.72036302
Warm Temperate/Fully Humid	24.78729438	H	9.926262053
Warm Temperate/Fully Humid	24.78729438	G	9.812819058
Warm Temperate/Fully Humid	24.78729438	S	4.87804878
Warm Temperate/Fully Humid	24.78729438	N	2.495745888
Warm Temperate/Fully Humid	24.78729438	J	1.928530913
Warm Temperate/Fully Humid	24.78729438	A	1.077708452
Warm Temperate/Fully Humid	24.78729438	O	0.907543959
Warm Temperate/Fully Humid	24.78729438	C	0.567214974
Warm Temperate/Fully Humid	24.78729438	E	0.22688599
Warm Temperate/Fully Humid	24.78729438	P	0.22688599
Warm Temperate/Fully Humid	24.78729438	X	0.056721497
Snow/Fully Humid	23.53942144	L	28.24730573
Snow/Fully Humid	23.53942144	Q	24.22007941
Snow/Fully Humid	23.53942144	M	10.72036302
Snow/Fully Humid	23.53942144	U	3.630175837
Snow/Fully Humid	23.53942144	O	0.907543959
Snow/Fully Humid	23.53942144	R	0.45377198
Snow/Fully Humid	23.53942144	P	0.22688599
Snow/Fully Humid	23.53942144	T	0.113442995
Warm Temperate/Summer Dry	7.487237663	L	28.24730573
Warm Temperate/Summer Dry	7.487237663	Q	24.22007941
Warm Temperate/Summer Dry	7.487237663	G	9.812819058
Warm Temperate/Summer Dry	7.487237663	N	2.495745888
Warm Temperate/Summer Dry	7.487237663	D	0.397050482

Table 12. Options for Additional Climate Based Test Sites for Precipitation/Temperature Effects Analysis for Top 90% of Pareto Analysis from Table 10

Precipitation/Temperature	P/T Pareto Percent	Region	Region Pareto Percent
Steppe/Cold Arid	34.77027794	L	28.24730573
Steppe/Cold Arid	34.77027794	Q	24.22007941
Steppe/Cold Arid	34.77027794	G	9.812819058
Fully Humid/Warm Summer	22.80204197	L	28.24730573
Fully Humid/Warm Summer	22.80204197	Q	24.22007941
Fully Humid/Warm Summer	22.80204197	M	10.72036302
Fully Humid/Warm Summer	22.80204197	G	9.812819058
Fully Humid/Warm Summer	22.80204197	S	4.87804878
Fully Humid/Warm Summer	22.80204197	N	2.495745888
Fully Humid/Warm Summer	22.80204197	A	1.077708452
Fully Humid/Warm Summer	22.80204197	O	0.907543959
Fully Humid/Warm Summer	22.80204197	C	0.567214974
Fully Humid/Warm Summer	22.80204197	R	0.45377198
Fully Humid/Warm Summer	22.80204197	X	0.056721497
Fully Humid/Hot Summer	22.40499149	L	28.24730573
Fully Humid/Hot Summer	22.40499149	M	10.72036302
Fully Humid/Hot Summer	22.40499149	H	9.926262053
Fully Humid/Hot Summer	22.40499149	G	9.812819058
Fully Humid/Hot Summer	22.40499149	N	2.495745888
Fully Humid/Hot Summer	22.40499149	J	1.928530913
Fully Humid/Hot Summer	22.40499149	O	0.907543959
Fully Humid/Hot Summer	22.40499149	E	0.22688599
Summer Dry/Warm Summer	5.10493477	L	28.24730573
Summer Dry/Warm Summer	5.10493477	Q	24.22007941
Summer Dry/Warm Summer	5.10493477	G	9.812819058
Summer Dry/Warm Summer	5.10493477	N	2.495745888
Summer Dry/Warm Summer	5.10493477	D	0.397050482
Fully Humid/Cool Summer	3.11968236	L	28.24730573
Fully Humid/Cool Summer	3.11968236	U	3.630175837
Fully Humid/Cool Summer	3.11968236	P	0.22688599
Fully Humid/Cool Summer	3.11968236	T	0.113442995
Summer Dry/Hot Summer	2.836074872	L	28.24730573
Summer Dry/Hot Summer	2.836074872	G	9.812819058
Summer Dry/Hot Summer	2.836074872	N	2.495745888

As can be seen, regardless of whether analyzing the Main Climate/Precipitation Classifications or Precipitation/Temperature Classifications, Region L appears to have the greatest span of climate types and could serve to provide test sites for nearly all of the top five classifications. However, Region L only represents 28% of all installations. Therefore, placing all 17 additional test sites within that region would leave 72% of all installations without proportionate representation.

Priority was given to identifying large installations occupied by active duty personnel within the most populous regions and in climate types that were of significance for either or both classification methods. The resulting spread of final test sites shown in Table 13 was selected based on installations that were in desired regions, climate types, and willing to participate in the study. Note that the latitudes and longitudes listed are the nearest point--rounding up or down to XX.25 or XX.75 degrees, whichever is closer. This was because the updated Köppen-Geiger Climate Classification database used these points. Additionally, the actual test site latitude and longitude may be sensitive.

Table 13. Climate Classifications of the Final Selection of Test Sites

Region	Site	Lat	Long	MAIN/PRECIP	PRECIP/TEMP
A	Site 1:	20.75	-156.25	/Fully Humid	Fully Humid/
C	Site 1:	12.25	-69.25	Arid/Steppe	Steppe/Hot Arid
D	Site 1:	11.75	43.25	Warm Temperate/Summer Dry	Summer Dry/Warm Summer
E	Site 1:	-22.25	114.25	Arid/Desert	Desert/Hot Arid
G	Site 1:	32.75	-106.25	Arid/Steppe	Steppe/Cold Arid
G	Site 2:	29.25	-100.25	Arid/Steppe	Steppe/Hot Arid
G	Site 3:	34.25	-103.25	Arid/Steppe	Steppe/Cold Arid
G	Site 4:	33.75	-117.25	Warm Temperate/Summer Dry	Summer Dry/Hot Summer
H	Site 1:	31.25	-92.75	Warm Temperate/Fully Humid	Fully Humid/Hot Summer
H	Site 2:	25.75	-80.25	/Fully Humid	Fully Humid/
I	Site 1:	33.25	19.75	Arid/Desert	Desert/Hot Arid
J	Site 1:	33.75	130.25	Warm Temperate/Fully Humid	Fully Humid/Hot Summer
L	Site 1:	40.75	-113.25	Arid/Steppe	Steppe/Cold Arid
L	Site 2:	41.25	-95.75	Snow/Fully Humid	Fully Humid/Hot Summer
L	Site 3:	38.25	-121.75	Warm Temperate/Summer Dry	Summer Dry/Hot Summer
L	Site 4:	38.75	-104.75	Arid/Steppe	Steppe/Cold Arid
L	Site 5:	38.75	-104.75	Arid/Steppe	Steppe/Cold Arid
L	Site 6:	41.25	-111.75	Snow/Fully Humid	Fully Humid/Warm Summer
M	Site 1:	40.75	-86.25	Snow/Fully Humid	Fully Humid/Hot Summer
M	Site 2:	37.25	-76.25	Warm Temperate/Fully Humid	Fully Humid/Hot Summer
M	Site 3:	40.25	-74.25	Warm Temperate/Fully Humid	Fully Humid/Hot Summer
M	Site 4:	44.75	-93.25	Snow/Fully Humid	Fully Humid/Hot Summer
N	Site 1:	38.75	-27.25	Warm Temperate/Summer Dry	Summer Dry/Warm Summer
O	Site 1:	39.75	125.25	Snow/Winter Dry	Winter Dry/Hot Summer
O	Site 3:	37.25	128.75	Snow/Winter Dry	Winter Dry/Hot Summer
P	Site 1:	55.25	-162.75	Warm Temperate/Fully Humid	Fully Humid/Cool Summer
Q	Site 1:	47.75	-101.25	Snow/Fully Humid	Fully Humid/Warm Summer
Q	Site 2:	47.25	-122.75	Warm Temperate/Summer Dry	Summer Dry/Warm Summer
Q	Site 4:	48.25	-101.25	Snow/Fully Humid	Fully Humid/Warm Summer
Q	Site 5:	47.75	-111.25	Arid/Steppe	Steppe/Cold Arid
R	Site 1:	46.75	-67.75	Snow/Fully Humid	Fully Humid/Warm Summer
S	Site 1:	50.25	6.75	Warm Temperate/Fully Humid	Fully Humid/Warm Summer
T	Site 1:	52.75	174.25	Snow/Fully Humid	Fully Humid/Cool Summer
U	Site 1:	64.25	-149.25	Snow/Fully Humid	Fully Humid/Cool Summer
U	Site 2:	65.75	-167.75	Polar/	/Polar Tundra
W	Site 1:	76.75	-68.75	Polar/	/Polar Tundra
X	Site 1:	58.75	5.75	Warm Temperate/Fully Humid	Fully Humid/Warm Summer

Pulling the information from Table 3, Table 6, and Table 7, and comparing the Pareto analyses in those tables to a Pareto analysis of the final selection of sites, the research team created the results shown in Table 14, Table 15, and Table 16. As can be seen from these tables, the final test site selection aligns well with the Pareto analysis of all installations with a high level of accuracy. Generally, the most populated regions and climate classifications are those with the most test sites. There is one case for each climate classification method, where a more-populated category is bypassed for a less-populated category. In both cases, this is to place test systems in the “Fully Humid” classification, which is only 0.0567% less populated than the next-higher classification.

Table 14. Installation-to-Region versus Test Site-to-Region Pareto Analyses

Region	Total Installation Count	Installation Pareto Analysis	Total Test Site Count	Test Site Pareto Analysis
L	498	28.24730573	6	16.21622
Q	427	24.22007941	4	10.81081
M	189	10.72036302	4	10.81081
H	175	9.926262053	2	5.405405
G	173	9.812819058	4	10.81081
S	86	4.87804878	1	2.702703
U	64	3.630175837	2	5.405405
N	44	2.495745888	1	2.702703
J	34	1.928530913	1	2.702703
A	19	1.077708452	1	2.702703
O	16	0.907543959	2	5.405405
C	10	0.567214974	1	2.702703
R	8	0.45377198	1	2.702703
D	5	0.283607487	1	2.702703
E	4	0.22688599	1	2.702703
P	4	0.22688599	1	2.702703
X	3	0.170164492	1	2.702703
T	2	0.113442995	1	2.702703
W	1	0.056721497	1	2.702703
I	1	0.056721497	1	2.702703
B, F, K, V, Y	0	0	0	0

Table 15. Comparison of Main Climate/Precipitation Classification Pareto Analyses of All Installations versus Final Test Site Selection

Main Climate/Precipitation Classification	Total Installation Count	Installation Pareto Analysis	Total Test Site Count	Test Site Pareto Analysis
Arid/Steppe	629	35.67782189	8	21.62162
Warm Temperate/Fully Humid	438	24.84401588	7	18.91892
Snow/Fully Humid	416	23.59614294	9	24.32432
Warm Temperate/Summer Dry	131	7.430516166	5	13.51351
Arid/Desert	28	1.588201929	2	5.405405
Snow/Winter Dry	12	0.680657969	2	5.405405
Polar	12	0.680657969	2	5.405405
Snow/Summer Dry	11	0.623936472	0	0
Fully Humid	10	0.567214974	2	5.405405
Summer Dry	10	0.567214974	0	0
Monsoonal	5	0.283607487	0	0
Winter Dry	3	0.170164492	0	0
Warm Temperate/Winter Dry	2	0.113442995	0	0

Table 16. Comparison of Precipitation/Temperature Classification Pareto Analysis of All Installations versus Final Test Site Selection

Precipitation/Temperature Classification	Total Installation Count	Installation Pareto Analysis	Total Test Site Count	Test Site Pareto Analysis
Steppe/Cold Arid	613	34.77027794	6	16.21622
Fully Humid/Warm Summer	404	22.91548497	6	16.21622
Fully Humid/Hot Summer	395	22.40499149	7	18.91892
Summer Dry/Warm Summer	89	5.048213273	3	8.108108
Fully Humid/Cool Summer	55	3.11968236	3	8.108108
Summer Dry/Hot Summer	50	2.836074872	2	5.405405
Desert/Cold Arid	17	0.964265457	2	5.405405
Steppe/Hot Arid	16	0.907543959	2	5.405405
Winter Dry/Hot Summer	13	0.737379467	2	5.405405
Polar Tundra	12	0.680657969	2	5.405405
Desert/Hot Arid	11	0.623936472	0	0
Fully Humid	10	0.567214974	2	5.405405
Summer Dry	10	0.567214974	0	0
Monsoonal	5	0.283607487	0	0
Winter Dry	3	0.170164492	0	0
Summer Dry/Cool Summer	3	0.170164492	0	0
Winter Dry/Warm Summer	1	0.056721497	0	0

In both climate classification methods, the top three classifications do not have quantities of test sites in prioritized order when compared to the installation Pareto analysis. However, all have a significant number of test sites within them which allows effective analysis of the effects of that climate classification on photovoltaic performance.

Despite selecting sites based on this split classification method, the test sites align relatively closely to the three-part classification system as shown in Table 17. However, given that the analysis is designed to evaluate a logistic regression based on the Köppen-Geiger Climate Classification System in future research, using the three-classification system may result in interference between the “Main Climate” and “Temperature” variables as both use temperature to establish their definitions. The divided system is still considered optimal for this study.

Table 17. Comparison of Köppen-Geiger Climate Classification Pareto Analysis of All Installations versus Final Test Site Selection

Köppen-Geiger Climate Classifications	Total Installation Count	Installation Pareto Analysis	Total Test Site Count	Test Site Pareto Analysis
Arid/Steppe/Cold Arid	613	34.77028	6	16.66667
Warm Temperate/Fully Humid/Hot Summer	340	19.28531	4	11.11111
Snow/Fully Humid/Warm Summer	307	17.4135	4	11.11111
Warm Temperate/Fully Humid/Warm Summer	97	5.501985	2	5.555556
Warm Temperate/Summer Dry/Warm Summer	82	4.651163	3	8.333333
Snow/Fully Humid/Hot Summer	55	3.119682	3	8.333333
Snow/Fully Humid/Cool Summer	54	3.062961	2	5.555556
Warm Temperate/Summer Dry/Hot Summer	49	2.779353	2	5.555556
Arid/Desert/Cold Arid	17	0.964265	0	0
Arid/Steppe/Hot Arid	16	0.907544	2	5.555556
Polar//Polar Tundra	12	0.680658	2	5.555556
Arid/Desert/Hot Arid	11	0.623936	2	5.555556
Snow/Winter Dry/Hot Summer	11	0.623936	2	5.555556
/Fully Humid/	10	0.567215	2	5.555556
/Summer Dry/	10	0.567215	0	0
Snow/Summer Dry/Warm Summer	7	0.39705	0	0
/Monsoonal/	5	0.283607	0	0
Snow/Summer Dry/Cool Summer	3	0.170164	0	0
/Winter Dry/	3	0.170164	0	0
Warm Temperate/Winter Dry/Hot Summer	2	0.113443	0	0
Snow/Summer Dry/Hot Summer	1	0.056721	0	0
Snow/Winter Dry/Warm Summer	1	0.056721	0	0
Warm Temperate/Fully Humid/Cool Summer	1	0.056721	1	2.777778

In establishing the methodologies, the impacts of temperature were clearly outlined, as well as the foundation for the hypothesis that humidity may have a correlation to photovoltaic power performance--if it is able to be used to quantify the impacts of cloud cover, ambient humidity, and precipitation--all of which have an effect on irradiation and air mass. By using the Köppen-Geiger Climate Classification system as an architecture to ensure a broad spectrum of possible Temperature and Humidity, the relationship of these variables to photovoltaic performance may be better quantified. As

well as enabling logistic and linear regression analysis in future research, the statistical analysis of location allows a conceptual analysis of the potential for photovoltaic power systems on all 1,763 USAF installations analyzed.

Research Question 2: Risk Modeling of Photovoltaic Pavement Systems

To establish a risk quantification method for implementation of photovoltaic pavement system technology, an understanding or characterization of the possible failure methods must be achieved. For the purposes of this research, failure is considered to occur in one of two methods: failure to produce sufficient power or failure to perform as a pavement. There is potential for additional modes of failure for the SR3 product, due to the integrated LEDs and self-heating system. However, as solutions to those problems currently exist (e.g., painted lines and Snow and Ice Removal Operations), those methods of failure have mitigation methods in place that would return the operation of the pavements.

Failure to produce sufficient, or any, power is unlikely to affect the mission as current proposals only seek to replace the standby power systems on installations. Since this power is produced, but not stored, in the photovoltaic pavement systems, the risk is deemed by this research team to be relatively low. The power storage systems, such as batteries, pumped hydro, or compressed air energy storage, should supply sufficient standby power until an alternate, non-renewable energy mechanism can be activated to continue to support the mission. As the current method consists primarily of back-up generators, the risk of the photovoltaic pavement system failing to produce power is deemed to be acceptable. Therefore, the only failure mode deemed necessary for

quantification is a structural system failure. Of the 1,544 installations, for which Real Property Records from the second quarter of Fiscal Year 2016 were made available, 1261 owned paved surfaces. These are as identified by the 26 types of pavement shown in Table 18.

Table 18. Pareto Analysis of All CATCODES of Pavements Considered Eligible for Replacement with Photovoltaic Pavement Systems

CATCODE	TITLE	QUANTITY (SY)
851147	ROAD	125,163,378
852262	VEH PKING N/ORGN	65,998,507
113321	APRON	65,582,527
111111	RUNWAY	37,195,711
112211	TAXIWAY	36,474,639
116642	SHLDR, PAVED	22,520,439
852261	VEH PKING OPS	19,655,968
852289	SIDEWALK	16,790,171
851145	DRIVEWAY	13,306,592
111115	OVERRUN, PAVED	5,400,960
111411	RUNWAY, UNPAVED	3,746,935
852201	VEH PKING SRF	2,589,761
852267	VEH/EQUIP PRK R/D	2,267,169
116663	PAD, HELICOPTER	1,998,215
116666	PAD, WRMUP HLDG	1,901,054
132133	PAD, EQUIP	1,881,040
852271	PVT VEH PKING COMPD	1,790,155
852269	VEH PKING REFL	1,470,068
852273	ACFT SPT/E STOR YD	1,469,448
116662	PAD, DANG CARGO	1,323,854
116661	PAD, ARM/DISARM	1,294,675
116664	PAD, POWER CHK	876,074
116116	SH FLD T.O. & LND	766,060
852301	VEH STG AREA, SURF/UNSURF	603,039
116667	PAD, CALIBRATION	188,288
116665	PAD, POWER CHK W/SPR	183,906

These Category Codes (CATCODEs) were identified by this research team as having the potential for implementation of photovoltaic pavement technologies and range from runways and aircraft parking aprons to roads, sidewalks, and parking lots. Each of these CATCODEs has a different level of risk to the mission, should it fail, and has different quantities of pavement.

“Failure” is defined as the point at which the surface cannot be used for its intended purpose, as defined by the rules and regulations for that surface type. With this definition, it was identified that a single failed unit on a runway renders the runway unusable, as there are rules regarding the smoothness of runways and the presence of foreign objects. Compared to that standard of “failure,” failure of a single unit on a road would be roughly the equivalent of a pothole, as far as pavement system failure, and is simply a maintenance concern rather than a system failure.

The Mission Dependency Index (MDI) is the established method of quantifying the correlation of a CATCODE to the mission. While research is proving that this system is in need of refinement, it is still an established and accepted method for identifying an asset’s importance. For example, a runway is essential to the mission of most USAF bases, and its failure would result in a mission shut-down. Therefore, the MDI of a runway is 99, whereas a sidewalk has relatively little impact to the mission of an installation, and its MDI is 25. Overall, the MDIs of all 26 CATCODEs are shown in Table 19.

Table 19. Table of CATCODEs and Corresponding MDIs

CATECODE	TITLE	MDI
111111	RUNWAY	99
111411	RUNWAY, UNPAVED	99
116116	SH FLD T.O. & LND	99
112211	TAXIWAY	95
113321	APRON	95
116642	SHLDR, PAVED	95
116661	PAD, ARM/DISARM	95
116662	PAD, DANG CARGO	95
116664	PAD, POWER CHK	95
116665	PAD, POWER CHK W/SPR	95
116666	PAD, WRMUP HLDG	95
111115	OVERRUN, PAVED	90
116663	PAD, HELICOPTER	86
116667	PAD, CALIBRATION	76
852269	VEH PKING REFL	75
851147	ROAD	69
852201	VEH PKING SRF	51
852261	VEH PKING OPS	51
852262	VEH PKING N/ORGN	51
852267	VEH/EQUIP PRK R/D	51
852271	PVT VEH PKING COMPD	50
852273	ACFT SPT/E STOR YD	50
851145	DRIVEWAY	40
852301	VEH STG AREA, SURF/UNSURF	40
132133	PAD, EQUIP	35
852289	SIDEWALK	25

One important nuance not captured in MDIs is that installations without an aircraft-based mission rely on their pavements in a different manner than those oriented towards airfield operations. For example, Peterson Air Force Base (AFB), CO hosts a Space Wing whose primary mission is the control and operations of missile warning and space-control organizations. With no aircraft-based mission, the most important pavement on the installation is the road network, which facilitates transportation of assets and personnel around the installation. Therefore, failure of these pavements results in a different risk quantification than Altus AFB, OK, where the installation mission revolves

nearly exclusively around aircraft operations and training. These differing subjective considerations of risk do not mean that failure of the roads on Peterson AFB would result in total mission failure as the personnel on site would create and implement work-arounds. However, there are significantly more restrictions and standards for failed airfield pavement work-arounds--resulting in a different quantification of risk for road failure for these two installations.

Therefore, two systems of risk analysis must be developed: one for aircraft operation missions and one for non-aircraft operation missions. For aircraft operation missions, temporary mission failure exists with any damage to the runway pavements. For non-aircraft operation missions, total mission failure cannot take place simply due to pavement system failure, although it can be significantly impacted.

Due to these sliding scales which measure each CATCODEs failure impact, a risk quantification system for each mission will require significant research into subjective and historical effects to the mission, based on specific quantities of various pavement types that fail. For example, leadership must be surveyed to identify the answer to questions such as, "If 10% of the road pavements were un-traversable, what would be the impact to your mission on a scale of 1 (none) to 100 (total mission failure)?" These subjective impacts must be statistically analyzed and will calibrate the sliding scales of risk for each mission type for each CATCODE of pavement.

A mission risk quantification system architecture may be proposed based on these principles. Additionally, it must be noted that there may be scenarios where the location of the failure impacts the mission disproportionately to the quantity of failed pavement. For example, a failure of 1% of the runway on one of its four corners may not result in

subjective mission failure, whereas a 1% failure in the center of the landing zone may render the runway totally failed until repaired. Therefore, these scales only provide a potential for risk to the mission but do not provide the actual risk or impacts of that risk.

The top ten CATCODES, based on the Pareto analysis shown in Table 18, account for 408,088,892 square yards of pavement, or just over 94% of all pavements in the inventory. For reference, if we assume a 0° inclination, 500W/m², and 10% efficiency, this much pavement roughly represents a 20.4GW power plant which is over 1,400 times as large as the 140 acre, 14MW array at Nellis Air Force Base without taking up a single square inch of additional real estate to produce power. If we assume 10% soiling and 50% shading, the PVWatts calculator reveals this size array could produce 10.29TWh of usable energy if we use the TMY3 dataset at the average Air Force location, which would be the south side of Chicago.

By using a simple set of heuristics based on a selection of these priority pavements, a series of scenarios can be created to establish of the sliding scales that equate pavement structural failure to mission risk. The first heuristic is that any quantity of failed runway pavement should result in a mission risk score of nearly 100. In other words, the sliding scales must maximize the mission risk of high MDI pavement systems as quickly as possible. The second heuristic is that, even at 100% failure, the risk to the mission for the failure of sidewalks has a minimal value. This is simply the inverse of the first heuristic and it anchors the other end of the sliding scale.

Quantification of these sliding scales will rely on future research, but using these heuristics to develop a set of proposed rules can exemplify the system architecture on which that quantification may be placed. Table 20 provides a set of conceptual rules used

to develop these sliding scales for aircraft operation missions. The resulting scale developed from following this set of proposed, theoretical rules is shown in Figure 24. As can be seen, the greater the MDI, the more quickly the quantity of failed pavement impacts the mission and vice versa. To use these scales, begin by assessing how much pavement failed, connect that value to the MDI, and continue that line until it intersects the Risk scale. This identifies the risk score incurred by a structural failure of a specific quantity of a specific CATCODE of pavement.

Table 20. Aircraft Operation Missions Pavement Failure Impact Conceptual Rules

Rule	Pavement Type	Percent Failed	MDI	Risk to Mission
1	111111 – RUNWAY	ANY	99	~100
5	112211 – TAXIWAY	1%	95	0
6	112211 – TAXIWAY	50%	95	50
7	112211 – TAXIWAY	100%	95	100
2	851147 – ROAD	1%	69	0
3	851147 – ROAD	50%	69	33
4	851147 – ROAD	100%	69	66
8	852262 – VEH PKING N/ORGN	1%	51	0
9	852262 – VEH PKING N/ORGN	50%	51	16
10	852262 – VEH PKING N/ORGN	100%	51	33
11	852289 – SIDEWALK	1%	25	0
12	852289 – SIDEWALK	50%	25	2
13	852289 – SIDEWALK	100%	25	5

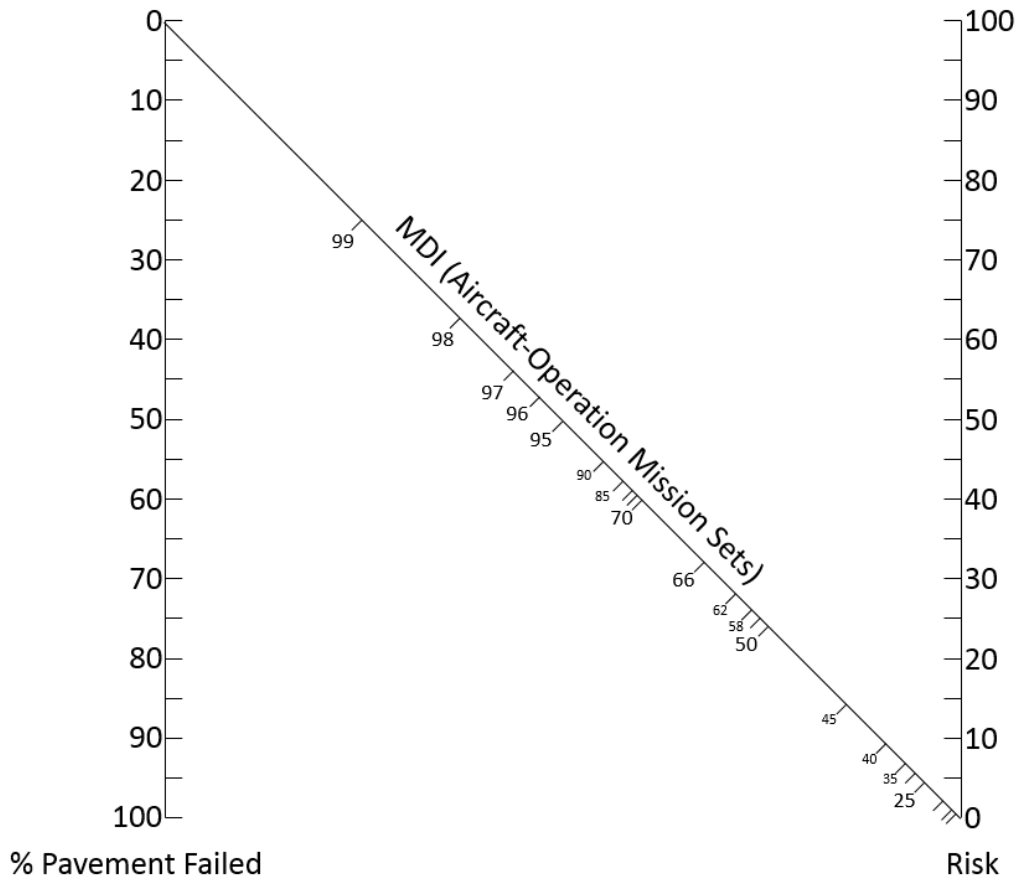


Figure 24. Aircraft Operations Mission Pavement Failure Impact Scale

The same scale can be developed for non-aircraft operation missions. However, the scale of MDI changes significantly due to the difference in risk for pavement types other than airfields. To develop this scale, the rules shown in Table 21 were used as a reference. The risk to the mission is significantly higher for roads as well as other pavement types. However, whereas a runway can be considered a total failure if even 1% of it is failed, as shown in Table 20, there is no pavement system that could result in a total mission shut down for non-aircraft operation missions.

The rules listed in Table 21 result in the scale for non-aircraft operating mission shown in Figure 25. From this scale, it can be clearly seen that the risk to the mission for lower-MDI pavement types has grown. This is due to the fact that more of the mission relies on these transportation networks than installations whose primary mission revolves around airfield operations.

Table 21. Non-Aircraft Operation Missions Pavement Failure Impact Conceptual Rules

Rule	Pavement Type	Percent Failed	MDI	Risk to Mission
2	851147 – ROAD	1%	69	0
3	851147 – ROAD	50%	69	45
4	851147 – ROAD	100%	69	90
8	852262 – VEH PKING N/ORGN	1%	51	0
9	852262 – VEH PKING N/ORGN	50%	51	25
10	852262 – VEH PKING N/ORGN	100%	51	50
11	851145 – DRIVEWAY	1%	40	0
12	851145 – DRIVEWAY	50%	40	5
13	851145 – DRIVEWAY	100%	40	10
14	852289 – SIDEWALK	1%	25	0
15	852289 – SIDEWALK	50%	25	2
16	852289 – SIDEWALK	100%	25	5

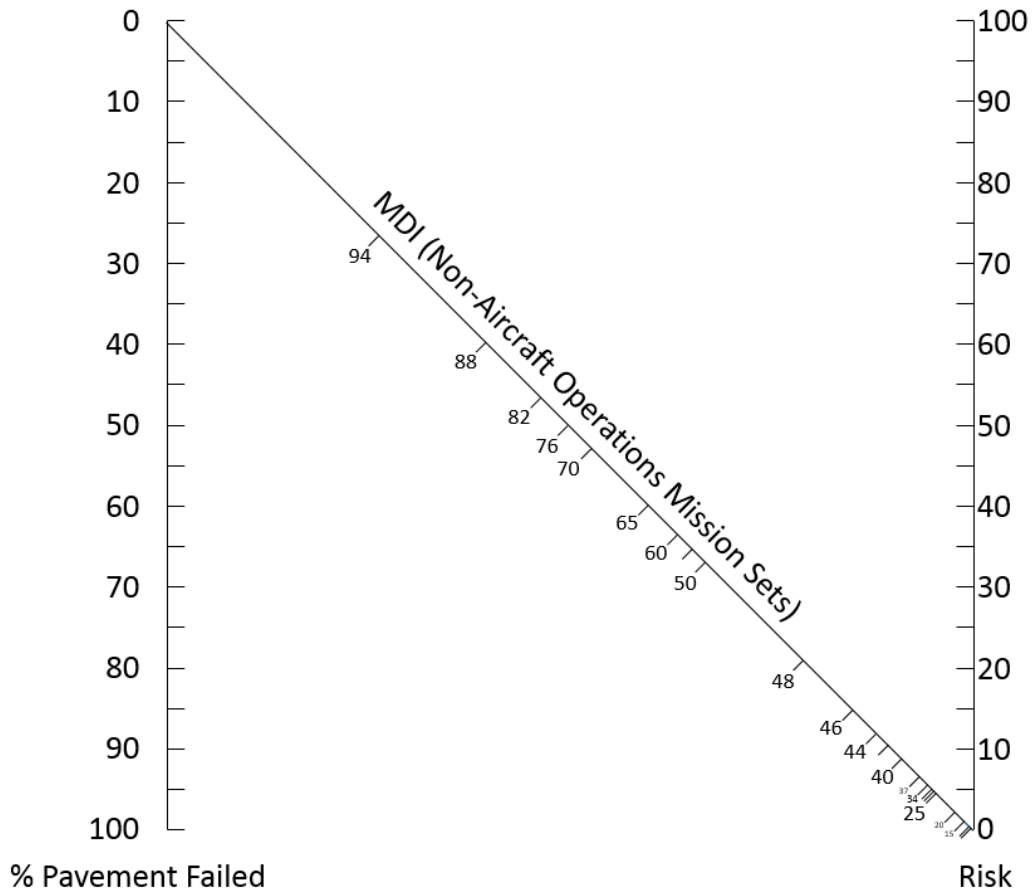


Figure 25. Non-Aircraft Operations Mission Pavement Failure Impact Scale

As an example, a 45% failure of the road network (CATCODE 851147) on an installation with an aircraft operation mission results in a total mission risk score of approximately 30, whereas it results in a total mission risk score of approximately 40 on a installation with a non-aircraft operation mission. By canting the MDI line on an angle, the influence of higher MDI items is increased based on the true mission risk for the specific mission set a scale is calibrated to represent.

Using these scales, leadership can state that no pavement system is allowed to exceed a risk score of 50. Therefore, only 60% of road networks on installation with a non-aircraft operation mission may be replaced with photovoltaic pavement systems until

they are proven to perform as effectively as traditional pavements. However, 100% of all lower-MDI pavement systems may be replaced. For installations with an aircraft operation mission, this results in the option to replace approximately 80% of the roads or 50% of the taxiways, aprons, etc. If diversified locations are desired, the sum of their respective risk scores may be required to remain below the threshold or thresholds can be set for various functional areas of the installation such as a risk of 30 to the airfield and 50 to the rest of the installation.

As a reminder, each pavement CATCODE has an individual risk to the mission with this system architecture. Synergistic effects of replacing multiple pavement types are not analyzed using this system. It is possible for the combined failure of multiple pavement CATCODEs to have a compound effect on the mission risk. Therefore, decision-making regarding which pavements to replace with photovoltaic pavement systems is still subjective, even with quantification systems such as this, to aid with decision-making.

Conclusion

The above analysis of the data available to answer these questions is intended to propose a starting point for advanced research into this unique application of photovoltaic technology. There are numerous questions which must be researched and answered which are not covered herein. However, given the potential apparent in this application there is a clear and present need to identify if this represents a disruptive, revolutionary concept. Decentralized power production without additional disruption to the environment and in a method already proven, though it is being slightly altered in this

application, is one way to revolutionize the power industry without fundamentally changing it. In order to continue the analysis of the possible secondary and tertiary benefits of systems such as the SR3 paver, optimization modeling must be done for specific case studies to determine, based on acceptable risk levels and the energy needs of the installation, how much and what locations should photovoltaic pavements be implemented to provide energy security and autonomy.

V. Conclusions and Recommendations

The potential behind implementing a concept like a photovoltaic pavement system is demonstrably immense. Not only does it prevent the need for large expanses of land for photovoltaic installations, damaging their reputation as a “green” source of energy, but the large quantity of pavements even on small installations render the systems a more flexible application of the technology. With test installations going in for all three current market products, the results will be critical in determining the value of the application to the market and to unique requirements such as those of the USAF.

Research Question 1: Photovoltaic Performance Modeling

Photovoltaic panel performance models are highly accurate, when extensive studies of the specific panel, configuration, and mounting system are completed. Some models allow for performance prediction if a significant number of variables regarding the system and its integral components are known. All of these models, however, rely on temperature in some manner. There are models that can accurately determine internal component temperature based on ambient temperature for those advanced models requiring these variables.

With 24 functions for efficiency as a function of temperature and 27 functions for power as a function of temperature, models for photovoltaic power as a function of ambient temperature have much greater variance. Therefore, a large-scale study of the correlation of ambient temperature to panel performance for the most common types of

panels may help hone in these functions, identify performance coefficients, and improve existing models' ability to accurately predict performance using ambient temperature.

Additionally, parallel to a study regarding the effects of ambient temperature, a study on humidity may prove eye-opening. Current models apply uniform derate factors for ambient humidity, but focused studies have found great variance in the effects of humidity on panel performance--due to the broad range of ways in which humidity can affect panel performance. Documented affects in synergy with dust, changes in air mass due to humidity, and ingress of water all are measured ways in which humidity affects panel performance.

Therefore, a global study using the Köppen-Geiger Climate Classification as an architecture to develop categorical variables and create great variance in linear variables may help illuminate the empirical effects of ambient temperature and ambient humidity on panel performance for both mono- and poly-crystalline panels. This proposed study includes 37 test sites based on a statistical analysis of all USAF installations. This study identified 25 global regions in which test systems would need to be placed. Test systems are first proposed to be at installations close to the statistical mean location of each region. Additional test systems should be placed in specific climate zones within each region--prioritizing the most populous Regions and most populous climate zones.

With this global spread of test systems, the effects of ambient temperature and humidity will be more effectively measured and quantified. This may improve the accuracy of current models and functions. It may also identify if the power efficiency coefficients currently published are accurate or identify if their accuracy can be improved by establishing categorical coefficients depending on climate types. The data can be

broken down to analyze the impacts of either mono- or poly-crystalline technologies through two different systems of analysis based on two categorical variables established in each of the two systems, which allows for the development of multiple models. However, it can also be used to improve existing models, quantify assumptions within them, and provide information to improve assumed uniform factors and develop models to more accurately analyze the impacts of temperature and humidity.

Research Question 2: Risk Modeling of Photovoltaic Pavement Systems

Risk modeling is a subjective exercise based on local leadership. However, objective tools to quantify risk, based on current systems, aid in communicating acceptable risk. By considering the specific missions of installations, quantities of pavements, and the correlation of pavement types to the mission, the research team was able to establish a set of scales that quantify the risk caused by the failure of a specific category of pavement. Conversely, leadership can set a maximum total amount of risk to be accepted for engineers to implement technologies such as photovoltaic pavement systems.

The proposed system scales the impact of the failure of a percentage of pavement by its current established Mission Dependency Index. Although it is known that the pavement failure location has a significant mission impact, as well as quantity, an objective risk factor helps provide a foundation for effectively communicating risk acceptance. By canting the MDI scale, greater influence was given to those pavements more closely tied to the mission than not in determining their actual risk to said mission.

Significance of Research

This research forms a foundation for continued studies into the potential applications for photovoltaic pavements on USAF installations. Preliminary case studies have shown that there is significant potential for photovoltaic pavements to replace current standby power systems, which have known weaknesses posing a risk to installation missions [33]. With the great volume of paved surfaces on USAF installations, the potential exists to expand these current case studies and power large portions of the installation from photovoltaic pavement systems.

Not only could photovoltaic pavements provide energy security and autonomy for USAF installations, but photovoltaic pavement systems can also be implemented more simply and more broadly than other renewable energy systems. As road surfaces must be repaved at specific intervals, photovoltaic pavement installations can be done without impacting the use of infrastructure systems more than currently expected. Rooftop systems typically require extensive renovations to a facility's structure and many installations do not have large plots of unused land on which traditional arrays can be erected.

Additionally, the results of the GP3L experiment may improve the accuracy of all current photovoltaic models. By making data publicly available, improvement is enabled in renewable energy systems across the market. This upholds the federal government's goal of enabling growth in energy markets and manufacturing.

Recommendations for Future Research

Future research must include testing non-traditional materials to serve as pavements. The previously published research conducted its qualitative analysis on over 70,000 standards of which nearly 17,000 are test methods. Using key word filters and the methodologies, analysis, and results of those potential test standards identified through those filters and comparing them with the heuristics in Appendix D, the research team was able identify optimum test standards to evaluate the products. This analysis identified that products such as these glass/composite laminate sandwich constructions can be implemented using existing pavement design methodologies.

However, the most pressing need for continued research is the sustainment of the GP3L experiment, due the broad impacts of the study's results. The initial year's results could help validate and improve existing models and coefficients. Continued years of study into multiple climate types' life-cycle impacts on photovoltaic technologies also help to quantify long-term photovoltaic performance modeling. Data from multiple years of study may be used to help improve photovoltaic system material selection and design to expand the spectrum of locations where the technology is used and improve its longevity in harsh climates.

Summary

Extensive potential has been identified for photovoltaic pavement systems in the current research. While multiple tests and evaluations, as well as the results of the GP3L experiment, are necessary to firmly identify the viability of photovoltaic pavements for use on USAF installations, the pathway to quantifying performance has been outlined.

This emerging technology has the potential to be disruptive to current economies and incite growth in several markets while also stabilizing critical infrastructure systems and providing energy security rapidly in a dynamic global environment.

Appendix A – GP3L Test System Physical Design

Test System Hardware Design

The Node Chip diagrams how the node chip evaluates the performance of each panel attached to the test system. The chip identifies 64 measurements of current coming from the panel through both a Hall Sensor and a proprietary method. The panel is connected to the board through the (+) and (-) connections on the bottom left and sends the data to the Base Chip through either of the RJ45 connections on the top of the chip.

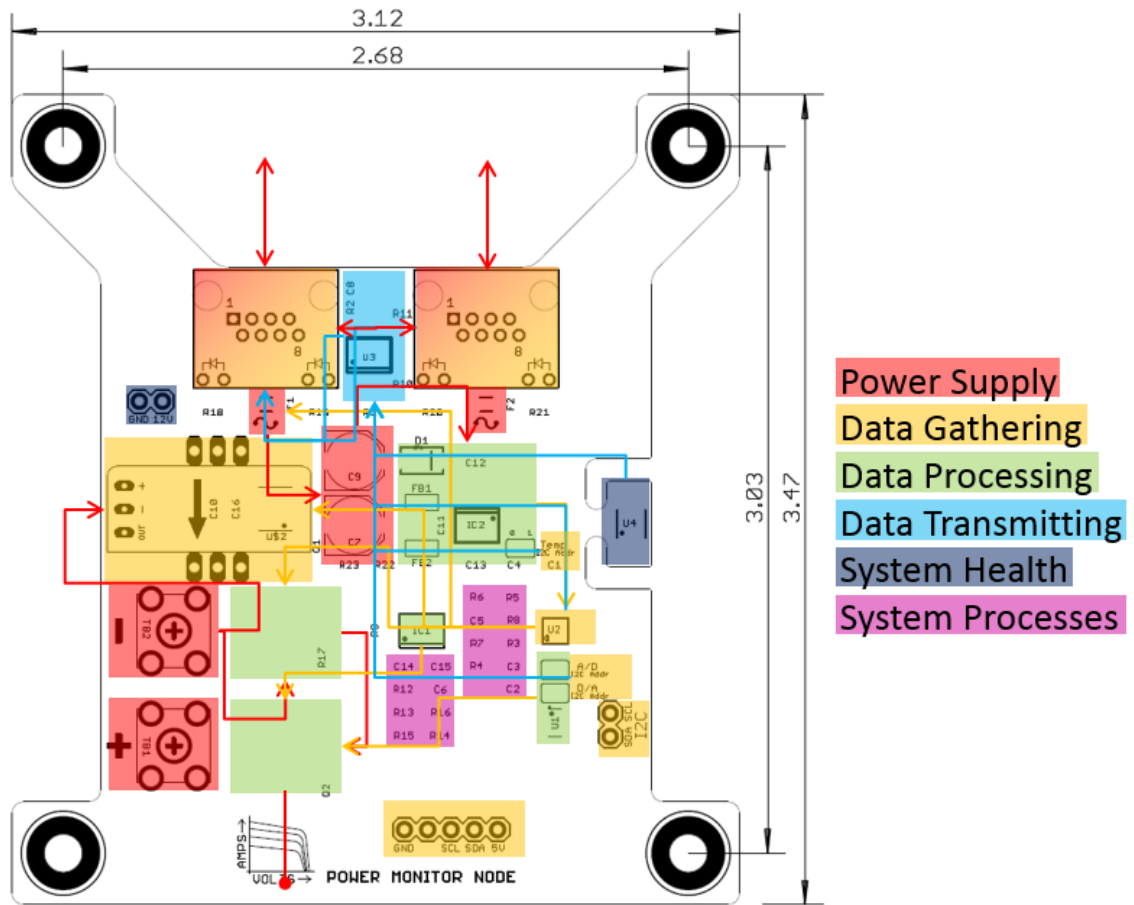


Figure 26. Node Chip diagram with component functions identified

The Base Chip acts as a power control device, pulling power either from a prime connection or a dedicated battery at the connections on the bottom of the right hand side. It also pulls information from the Node Chips through the RJ45 connection on the top of the right hand side and the Temperature/Humidity Probe at the connection on the right of the bottom side. The Raspberry Pi computer system connects to with a ribbon cable to the left side and the RockBlock MK2 connects to the back through the string of through-hole connections on the right hand side, just inside the RJ45 connection. LEDs connected at “NET/AV,” “STAT1,” and “STAT2” and mounted on the outside of the box provide system condition information to on-site POCs.

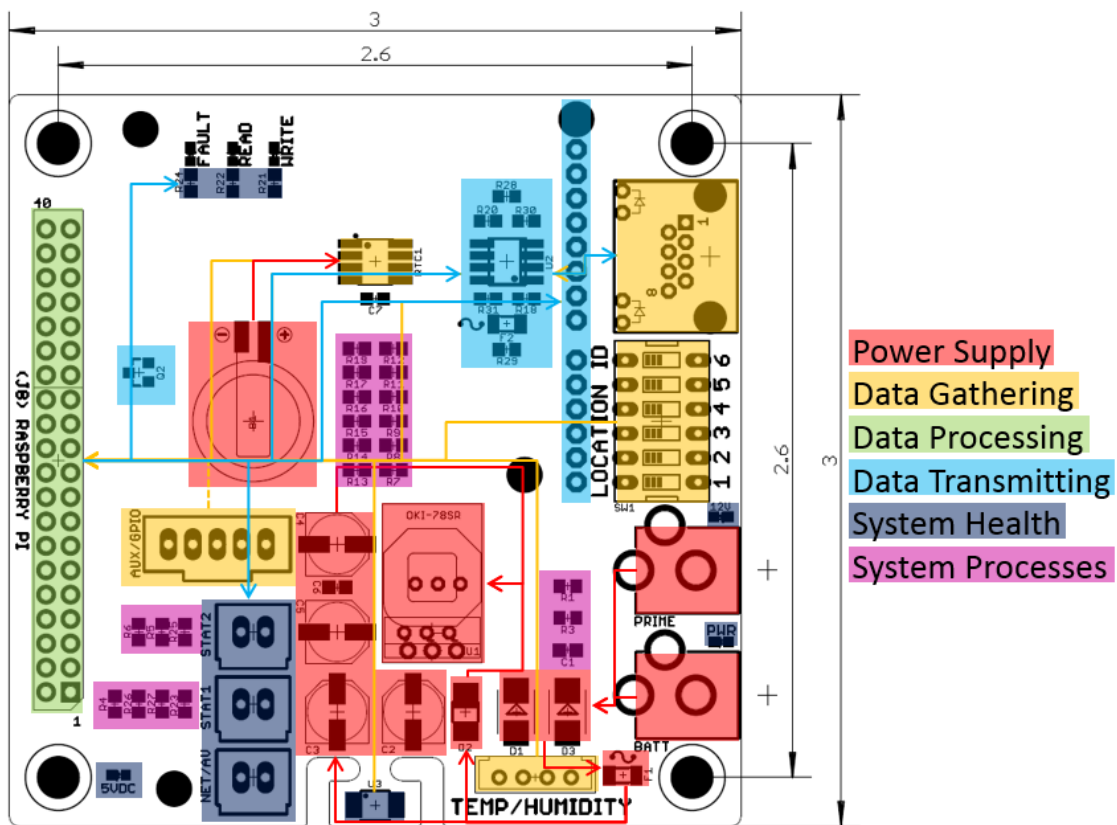


Figure 27. Base Chip diagram with component functions identified

Test System Structure Design

This figure shows the test system dubbed “Omega” operating on the roof of Building 640 at AFIT. The connection to prime power can be seen on the right and the connection to the test panel can be seen coming out the front. The large connection on the left of the front is for a back-up battery for test sites unable to connect to prime power. Nestled between these can be seen the temperature and humidity probe. Just above them are the LEDs indicating the system is operating. The yellow LED flashes continually indicating the system has power. The green LED flashes at the start and stop of a reading from the panels which is done every 15 minutes. The red LED illuminates if the system identifies an error with the satellite connection. Internal to the box is another LED that identifies an internal fault within the system hardware or software. Because Omega operated without a satellite connection and with only one panel, both red LEDs were lit.



Figure 28. “Omega” Test System

The internal connections of the GP3L Test system show the Raspberry Pi computer on the left which is connected to the Base Chip with a ribbon cable. Between the Base Chip and the lid of the case can be seen the RockBlock MK2. The prime power connection is seen as a large, black cylinder on the left of the body of the case. The LEDs can be seen with their red and black wires connecting them to the Base Chip. Beneath them, from left to right, are the connections to the panels, the Temperature/Humidity Probe, and the connection for a back-up battery.



Figure 29. “Omega” Internal Components

“Omega” is connected to prime power through the yellow extension cord coming from its right side. It is connected to a single, 50W panel with the black Cat5 cable protruding from the front of the case and connecting to a standard, plastic electronics case attached to the back of the panel. The panel is lifted off the ground using jugs to keep it from sitting in water, but bricks or sandbags work as well. The case is connected to the steel lighting protection system cable with a nylon strap. The panel is connected with a 1/8 inch steel rope looped under the same cable. This simply keeps the system from blowing off the roof of the building. In a standard configuration, a second panel would extend off of the one seen here. This test system was used to confirm the code in Appendix B operated correctly and a satellite connection was achieved, therefore a second panel was not necessary.



Figure 30. Basic setup for a GP3L Test System (second panel not shown)

Appendix B – GP3L Test System Coding

Test System Software Design

The test system was encoded to meet the following requirements:

- 1) The test system must automatically initiate its code once receiving power.
- 2) Data must taken every 15 minutes to increase fidelity from the industry standard of 1-hour readings for photovoltaic systems.
- 3) The system must measure 64 points along the power curve for current and voltage, allowing a highly accurate power curve to be established to find the peak power produced at every measurement.
- 4) The system must simultaneously log the ambient temperature and humidity measured from the incorporated probe with the power curve measurements.
- 5) The system must date/time stamp each reading.
- 6) The system must log the voltage provided by the primary power source which may be a battery system or prime power supplied by a local source.
- 7) Data must be logged into a .csv file on a partitioned MicroSD card which site POCs can use to download the information and transmit it.
- 8) The test system must automatically send a system health update every morning between 0600 and 1200 EST via an iridium satellite link.

- 9) The messages transmitted must consist of a string of 18 digits encoded as shown in Figure 31.

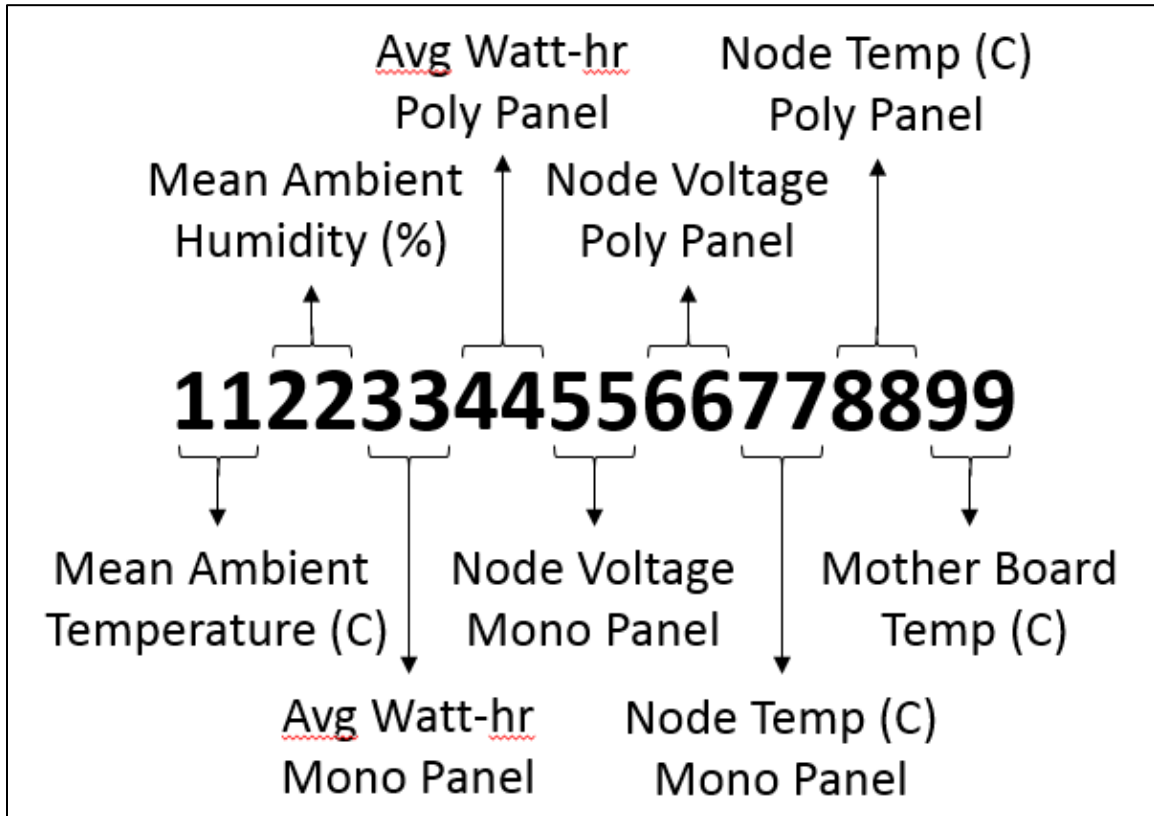


Figure 31. GP3L Test System Daily Status Message Code

Photovoltaic Panel Monitoring Code

```
#!/usr/bin/python
import sys
import os.path
import RPi.GPIO as PiGPIO
import Adafruit_GPIO.GPIO as GPIO
import Adafruit_GPIO.I2C as I2C
import time
import mysql.connector
import operator
import Adafruit_MCP9808.MCP9808 as MCP9808
import Adafruit_ADS1x15.ADS1x15 as ADC
import Adafruit_MCP4725
import rblface as rblk
from subprocess import call
```



```

#####
#####
# setting date note
# sudo date -s "Tue Sep 20 08:25:00 EST 2016" auto converts to UTC
# best to set using UTC instead of EST just to be safe
#Some functions

#celsius to farenheight conversion
def c_to_f(c):
    return c * 9.0 / 5.0 + 32.0

# channel 0 = solar Voltage
# channel 1 = solar current
# channel 2 = Vdd
# channel 3 = Hall Current
#####
#####
#Convert the ADC reading to voltages and currents
def adc_to_V(v,k):
    #cval = 6.144/32767 = 0.0001875
#6.144*(ADCVal/32767)*conv factor from data sheet for GAIN = 2/3
    if (k==0):
        return v*0.001125    #Conv Factor = 30/5
    if (k==1):
        return v*0.0001875    #Conv Factor = 1
    if (k==2):
        return v*0.000775    #Conv Factor = 20.667/5
    if (k==3):
        return ((v*0.0001875)-2.5)*1.333    #Conv
Factor = 1

def blink(statuspin,pol): # pol is the value that turns the LED on
    if (pol == PiGPIO.LOW):
        PiGPIO.output(statuspin, PiGPIO.LOW)
        time.sleep(blinkdel)
        PiGPIO.output(statuspin, PiGPIO.HIGH)
        time.sleep(blinkdel)
    else:
        PiGPIO.output(statuspin, PiGPIO.HIGH)
        time.sleep(blinkdel)
        PiGPIO.output(statuspin, PiGPIO.LOW)
        time.sleep(blinkdel)
    return

def syncTime(radio):
    try:
        RBData = radio.getDateTime()
        print(RBData)#for debugging
        if (len(RBData) == 28):
            call(["sudo", "date", "-s", str(RBData)])

```

```

        call(["sudo", "hwclock", "-w"])
        return True
    print("Trying to synchronize time with the rockblock
network.")
    return False
except:
    print("Problem synchronizing with rock block, using system
time.")
    return False

```

```

def msgFormat(val):
    rtnVal = ''
    try:#error code value (string, not number)
        chrs = len(val)
        val = int(val)
    except:
        return val
    if (val>=0):
        sign = '+'
    else:
        sign = '-'
    val = abs(val)
    if (chrs < 2):
        rtnVal = sign + '0' + str(val)
    else:
        rtnVal = sign + str(val)
    return rtnVal

```

```

#####
#####
#Init Monitoring Program

```

```

#In future version, should find better way to secure password and
connection information
delta = 900          #number of seconds between readings 1min =
60sec, 1hr = 3600sec etc

```

```

# LED GPIO Pins

```

```

RedLED = 40# on Main board

```

```

YellowLED = 38 # on field unit
Stat2LED = 18 #on Beta

```

```

GreenLED = 36 #on field unit
Stat1LED = 16 #on Beta

```

```

N1LED = 21
N2LED = 23

```

```

#Location GPIO Pins
ADD1 = 19 #Switch 1

```

```

ADD2 = 15 #Switch 2
ADD3 = 13 #Switch 3
ADD4 = 11 #Switch 4
ADD5 = 7 #Switch 5
ADD6 = 26 #Switch 6

#RockBlock GPIO Pins
RBSlp = 31
NETAV = 29
NETREC = 12

# Module addresses
MainTemp = 0x19 #Main Board Temp Probe
N1Temp = 0x1b
N2Temp = 0x1a
D1 = 0x64
D2 = 0x63
A1 = 0x48
A2 = 0x49
ExTemp = 0x28
bus = 1

#Database Variables
tbl = "PVDataTable"
base = "PVDataBase"
UIDw = 'loggy'
PWDw = 'Lets_L0g'
UIDr = 'viewy'
PWDr = 'Letm3C'
HST = 'localhost'
csvpath = "/media/pi/DATA/IVCurveData.csv"
Col = 'Date'
Col2 = 'Time'
#Main Board Error Codes:
# Error codes are two character string starting with Z

# A - E = Main Board Errors
MBErr1 = 'ZA' #Failed to Initialize
MBErr2 = 'ZB' #Communication failure
LErr = 'ZC'
ExtErrT = 'ZD'
ExtErrH = 'ZE'

# F - J = Node 1 Error Codes:
N1Err1 = 'ZF' #Failed to Initialize
N1Err2 = 'ZG' #Communication Failure
V1Err = 'ZH'
C1Err = 'ZI'
V1RErr = 'ZJ'

# K - O = Node 2 Error Codes:
N2Err1 = 'ZK' #Failed to initialize

```

```

N2Err2 = 'ZL' #Communication Failure
V2Err = 'ZM'
C2Err = 'ZN'
V2RErr = 'ZO'

# P - T = Transmission section Error Codes:
DTEErr = 'ZP'
DWErr = 'ZQ'
DTErr = 'ZR'
DHErr = 'ZS'
DVErr = 'ZT'

#Other Variables
abet = ['
','A','B','C','D','E','F','G','H','I','J','K','L','M','N','O','P','Q
','R','S','T','U','V','W','X','Y','Z']
mdel = 0.001 #Measure delay between DAC voltage sets
blinkdel = 0.2 #LED Blink Delay
lpblink = 4 #modifier of blinkdel for loop status
GAIN = 2/3 # Range for ADC Readings 2/3 = +/-6V range; See data
sheet for other settings
collection = list(range(4096,0,-64))
fmt5 = '.5f'
fmt0 = '.0f'
secs = 0
sent = False
ExRead = 0x00#Read for external probe
ExWrite = ExTemp
nightstart = 11
nightend = 17
prevdate = ""
starttime = str(nightstart*100)
if (nightstart <10):
    starttime = '0'+starttime
failcount = 0
slpctr = 0
SLPDEL = 300

#####
#####
#setup LED status Pin
PiGPIO.setwarnings(False)

#initialize output GPIOs
PiGPIO.setmode(PiGPIO.BOARD)

PiGPIO.setup(RedLED, PiGPIO.OUT)
PiGPIO.output(RedLED,PiGPIO.LOW)

PiGPIO.setup(YellowLED, PiGPIO.OUT)
PiGPIO.output(YellowLED,PiGPIO.LOW)

```

```

PiGPIO.setup(GreenLED, PiGPIO.OUT)
PiGPIO.output(GreenLED, PiGPIO.LOW)

PiGPIO.setup(N1LED, PiGPIO.OUT)
PiGPIO.output(N1LED, PiGPIO.LOW)

PiGPIO.setup(N2LED, PiGPIO.OUT)
PiGPIO.output(N2LED, PiGPIO.LOW)

PiGPIO.setup(Stat1LED, PiGPIO.OUT)
PiGPIO.output(Stat1LED, PiGPIO.LOW)

PiGPIO.setup(Stat2LED, PiGPIO.OUT)
PiGPIO.output(Stat2LED, PiGPIO.LOW)

PiGPIO.setup(RBSlp, PiGPIO.OUT)
PiGPIO.output(RBSlp, PiGPIO.HIGH)

#Initialize Input GPIOs
PiGPIO.setup(ADD1, PiGPIO.IN)
PiGPIO.setup(ADD2, PiGPIO.IN)
PiGPIO.setup(ADD3, PiGPIO.IN)
PiGPIO.setup(ADD4, PiGPIO.IN)
PiGPIO.setup(ADD5, PiGPIO.IN)
PiGPIO.setup(ADD6, PiGPIO.IN)
PiGPIO.setup(NETAV, PiGPIO.IN)
PiGPIO.setup(NETREC, PiGPIO.IN)#

## Init RockBlock Interface
iblk = rblk.rockDat()

#####
#####
#Boot Sequence to let the user know its entering loop
for i in range(0,2):
    blink(Stat1LED, PiGPIO.HIGH)
    blink(Stat2LED, PiGPIO.HIGH)
    blink(N1LED, PiGPIO.HIGH)
    blink(N2LED, PiGPIO.HIGH)
    time.sleep(blinkdel/2)
    PiGPIO.output(RedLED, PiGPIO.HIGH)
    time.sleep(blinkdel/2)
    PiGPIO.output(YellowLED, PiGPIO.HIGH)
    time.sleep(blinkdel/2)
    PiGPIO.output(GreenLED, PiGPIO.HIGH)
    time.sleep(blinkdel/2)
    PiGPIO.output(GreenLED, PiGPIO.LOW)
    time.sleep(blinkdel/2)
    PiGPIO.output(YellowLED, PiGPIO.LOW)
    time.sleep(blinkdel/2)
    PiGPIO.output(RedLED, PiGPIO.LOW)
    time.sleep(blinkdel/2)

```

```

#####
#####
#Make sure clock is sync'd to appropriate date time
synct = syncTime(iblk)
if(not(synct)):
    syncDel = SLPDEL

#####
#####
# Start Logging Loop
try:
    while True:
#####  Read Location Data
        try:
            loc = PiGPIO.input(ADD6)
            loc = loc + (PiGPIO.input(ADD5)*2)
            loc = loc + (PiGPIO.input(ADD4)*4)
            loc = loc + (PiGPIO.input(ADD3)*8)
            loc = loc + (PiGPIO.input(ADD2)*16)
            loc = loc + (PiGPIO.input(ADD1)*32)
        except:
            loc = LErr
##### Add GPS sync section here

#####  get date and time from Pi
cur = time.localtime()

if (len(str(cur.tm_min)) == 2):
    tmm = str(cur.tm_min)
else:
    tmm = "0" + str(cur.tm_min)

if (len(str(cur.tm_hour)) == 2):
    tmh = str(cur.tm_hour)
else:
    tmh = "0" + str(cur.tm_hour)
tim = tmh +tmm
if (len(str(cur.tm_mon)) == 2):
    cm = str(cur.tm_mon)
else:
    cm = "0" + str(cur.tm_mon)
if (len(str(cur.tm_mday)) == 2):
    cd = str(cur.tm_mday)
else:
    cd = "0" + str(cur.tm_mday)
cy = str(cur.tm_year)
date = cy + cm + cd
if (prevdate == ""):
    if (len(str(cur.tm_mday-1)) == 2):
        cd = str(cur.tm_mday-1)
    else:

```

```

        cd = "0" + str(cur.tm_mday-1)
    prevdate = cy + cm + cd
    startdate = prevdate
    enddate = date
else:
    if (prevdate != date):
        startdate = prevdate
        enddate = date

#####    take reading approximately every delta seconds
secs = cur.tm_sec + (cur.tm_min*60) + (cur.tm_hour*3600)
if ((cur.tm_sec%(lpblink)) == 0):    #blink approx every 3
sec when not taking readings
    blink(YellowLED,PiGPIO.HIGH) #let user know the program
is running
    blink(Stat2LED,PiGPIO.HIGH)    #

if(not(syncct)):
    if(syncDel > 0):
        syncDel = syncDel - 1
        time.sleep(blinkdel)
    else:
        syncct = syncTime(iblk)
        if(not(syncct)):
            syncDel = SLPDEL

#####    Time to take a reading!
if ( (secs%delta == 0) ):
#####
#####
#####    connect to database
        PiGPIO.output(Stat1LED,PiGPIO.HIGH)    #Reset Faut1
LED, incase fixed errors since last read
        try:
            connw =
mysql.connector.connect(user=UIDw,password=PWDw,host=HST)
            mycursorw = connw.cursor()
        except:
            PiGPIO.output(RedLED, PiGPIO.HIGH) #error occurred
            PiGPIO.output(Stat1LED,PiGPIO.LOW)
        try:
            mycursorw.execute("USE "+base)
            connw.commit()
        except:
            PiGPIO.output(RedLED, PiGPIO.HIGH) #error occurred
            PiGPIO.output(Stat1LED,PiGPIO.LOW)

#####
#####
#####    Turn on status LED to show a data collection in progress
        blink(GreenLED,PiGPIO.HIGH)
        blink(N1LED,PiGPIO.HIGH)

```



```

#####
#####
#####      Init Main Board Temp Probe for Readings
            try:
                MBTemp = MCP9808.MCP9808(address = MainTemp, busnum
= bus)
            except:
                PiGPIO.output(RedLED, PiGPIO.HIGH) #error occurred
                PiGPIO.output(Stat1LED,PiGPIO.LOW)
            try:
                mbt = 0
                MBTemp.begin()
            except:
                mbt = MBErr1 #Error with Main board temp sensor
init
                PiGPIO.output(RedLED, PiGPIO.HIGH) #error occurred
                PiGPIO.output(Stat1LED,PiGPIO.LOW)
            try:
#####      Read Temperature
                if (mbt == 0):
                    mbt = MBTemp.readTempC()
            except:
                mbt = MBErr2 #Error with Main board temp sensor
temp read
                PiGPIO.output(RedLED, PiGPIO.HIGH) #error occurred
                PiGPIO.output(Stat1LED,PiGPIO.LOW)
                #print("Read : "+str(mbt)+" deg C")
#####
#####
#####      Init NODE Temp Probe for Readings
#####
            try:
                N1Temp = MCP9808.MCP9808(address = N1Temp, busnum =
bus)
            except:
                PiGPIO.output(RedLED, PiGPIO.HIGH) #error occurred
                PiGPIO.output(Stat1LED,PiGPIO.LOW)
#####      Initialize communication with the sensor.
            try:
                n1t = 0
                N1Temp.begin()
            except:
                n1t = N1Err1 #Error with Node1 temp sensor init
                PiGPIO.output(RedLED, PiGPIO.HIGH) #error occurred
                PiGPIO.output(Stat1LED,PiGPIO.LOW)
            try:
#####      Read Temperature
                if (n1t == 0):
                    n1t = N1Temp.readTempC()
            except:

```

```

n1t = N1Err2 #Error with Node1 temp sensor temp
read
    PiGPIO.output(RedLED, PiGPIO.HIGH)#error occurred
#####
    try:
        N2Temp = MCP9808.MCP9808(address = N2Temp, busnum =
bus)
    except:
#
Temp Probe')
        PiGPIO.output(RedLED, PiGPIO.HIGH) #error occurred
        PiGPIO.output(Stat1LED,PiGPIO.LOW)
##### Initialize communication with the sensor.
    try:
        n2t = 0
        N2Temp.begin()
    except:
        n2t = N2Err1 #Error with Main board temp sensor
init
        PiGPIO.output(RedLED, PiGPIO.HIGH) #error occurred
        PiGPIO.output(Stat1LED,PiGPIO.LOW)
    try:
##### Read Temperature
        if (n2t == 0):
            n2t = N2Temp.readTempC()
        except:
            n2t = N2Err2 #Error with Main board temp sensor
temp read
        PiGPIO.output(RedLED, PiGPIO.HIGH) #error occurred
        PiGPIO.output(Stat1LED,PiGPIO.LOW)
#####
#####
##### Init Dacs and take Panel readings 0-Vdd = 0-4096
##### Connect to DAC1
    try:
        n1v = 0
        n1c = 0
        dac1 = Adafruit_MCP4725.MCP4725(address=D1,
busnum=bus)
    except:
        n1v = V1Err #Error initializing DAC1
        n1c = C1Err
        PiGPIO.output(RedLED, PiGPIO.HIGH) #error occurred
        PiGPIO.output(Stat1LED,PiGPIO.LOW)

##### Connect to DAC2
    try:
        n2v = 0
        n2c = 0
        dac2 = Adafruit_MCP4725.MCP4725(address = D2, busnum
= bus)
    except:

```

```

        n2v = V2Err #Error initializing DAC2
        n2c = C2Err
        PiGPIO.output(RedLED, PiGPIO.HIGH) #error occurred
        PiGPIO.output(Stat1LED, PiGPIO.LOW)
#####
Init ADCs
#####
Connect to ADC1
    try:
        adc1 = ADC.ADS1115(address = A1, busnum = bus)
    except:
        n1c = C1Err #Error initializing ADC1
        PiGPIO.output(RedLED, PiGPIO.HIGH) #error occurred
        PiGPIO.output(Stat1LED, PiGPIO.LOW)
#####
Connect to ADC2
    try:
        adc2 = ADC.ADS1115(address=A2, busnum=bus)
    except:
        n2c = C2Err #Error initializing ADC2#####
        PiGPIO.output(RedLED, PiGPIO.HIGH) #error occurred
        PiGPIO.output(Stat1LED, PiGPIO.LOW)

#####
#####
##### Take Readings ADC/DAC 1

        max1v = 0
        max1c = 0
        max2v = 0
        max2c = 0
        maxv = 0
        maxc = 0
        LRV = [0]*len(collection)
        LRC = [0]*len(collection)
        LRV2 = [0]*len(collection)
        LRC2 = [0]*len(collection)
        hall1c = [0]*len(collection)
        hall2c = [0]*len(collection)
        values = [0]*4
        ctr = 0
        ctr2 = 0
        for k in collection:
            try:
                dacl.set_voltage(k, True)
                time.sleep(mdel)
                values = [0]*4
                for i in range(4):
                    vv = adc1.read_adc(i, gain=GAIN)
                    values[i] = adc_to_V(vv, i)
                if (values[0] > max1v):
                    max1v = values[0]
                if (values[1] > max1c):
                    max1c = values[1]
                if (values[2] > maxv):

```

```

        maxv = values[2]
        if (values[3] > maxc):
            maxc = values[3]
        LRV[ctr] = format(values[0],fmt5)
        LRC[ctr] = format(values[1],fmt5)
        hall1c[ctr] = format(values[3],fmt5)
        ctr = ctr +1
    except:
#                                     print('Error Reading Node1
Data')
        PiGPIO.output(RedLED, PiGPIO.HIGH) #error
occurred
        PiGPIO.output(Stat1LED,PiGPIO.LOW)
        nlv = V1RErr #Error setting dacl voltage for
read
        n1c = C1Err
        if (str(nlv) != V1RErr and str(nlv) != V1Err):
            nlv = format(max1v,fmt5)
        if (str(n1c) != C1Err):
            n1c = format(max1c,fmt5)
        if ((maxv!=0) and (maxv != MBErr1)):
            mbv = format(maxv,fmt5)
        else:
            mbv = MBErr1mbv = format(maxv,fmt5)

##### Take Readings ADC/DAC 2
        values = [0]*4
        try:
            dac2.set_voltage(k, True)
            time.sleep(mdel)
            values = [0]*4
            for i in range(4):
                vv = adc2.read_adc(i, gain=GAIN)
                values[i] = adc_to_V(vv,i)
            if (values[0] > max2v):
                max2v = values[0]
            if (values[1] > max2c):
                max2c = values[1]
            if (values[2] > maxv):
                maxv = values[2]
            if (values[3] > maxc):
                maxc = values[3]#
            LRV2[ctr2] = format(values[0],fmt5)
            LRC2[ctr2] = format(values[1],fmt5)
            hall2c[ctr2] = format(values[3],fmt5)
            ctr2 = ctr2 +1
        except:
#                                     print('Error Reading Node2
Data')
        PiGPIO.output(RedLED, PiGPIO.HIGH) #error
occurred
        PiGPIO.output(Stat1LED,PiGPIO.LOW)

```

```

n2v = V2RErr #Error setting dacl voltage for
read
n2c = C2Err
if (str(n2v) != V2RErr and str(n2v) != V2Err):
    n2v = format(max2v,fmt5)
if (str(n2c) != C2Err):
    n2c = format(max2c,fmt5)
if ((maxv!=0) and (maxv != MBErr1)):
    mbv = format(maxv,fmt5)
else:
    mbv = MBErr1

#####
#####
# channel 0 = solar Voltage
# channel 1 = solar current
# channel 2 = Vdd
# channel 3 = Hall Current
#####
#####
#####      Log last read to CSV File

    try:
        STRG =
"Location,"+str(loc)+",Date,"+str(date)+",Time,"+str(tim)+",Humidity
,"+str(mbh)+",ExtTemp,"+str(extTemp)+",IntTemp,"+str(mbt)+",VoltsN1,
"+str(LRV)+",CurrentN1,"+str(LRC)+",Hall1,"+str(hall1c)+",Temp1,"+st
r(n1t)+",VoltsN2,"+str(LRV2)+",CurrentN2,"+str(LRC2)+",Hall2c,"+str(
hall2c)+",Temp2,"+str(n2t)+'\n'
        #print(STRG)
        if (os.path.isfile(csvpath)):
            with open(csvpath,"a") as fh:
                fh.write(STRG)
        else:
            with open(csvpath,"a") as fh:
                HDR = str(list(range(20+(len(LRV)*4))))+'\n'
                fh.write(HDR)
                fh.write(STRG)
            #print('Write Success!')
    except:
        PiGPIO.output(RedLED, PiGPIO.HIGH)#error occurred
        print('Failed to Write to File')
#write to database
    try:

#print(str(date)+' ','+str(tim)+' ','+str(loc)+' ','+str(mbt)+' ','+str(n1t)
+', '+str(n2t)+' ','+str(extTemp)+' ','+str(mbh)+' ','+str(mbv)+' ','+str(n1v)
')+', '+str(n2v)+' ','+str(n1c)+' ','+str(n2c)')
        mycursorw.execute("INSERT into
"+tbl+"(Date,Time,Loc,MTemp,N1Temp,N2Temp,ETemp,MHum,MVolt,N1Volt,N2
Volt,N1Curr,N2Curr) values

```

```

(%s,%s,%s,%s,%s,%s,%s,%s,%s,%s,%s,%s,%s,%s)", (date,tim,loc,mbt,n1t,n2t,
extTemp,mbh,mbv,n1v,n2v,n1c,n2c))
    connw.commit()
except:
    PiGPIO.output(RedLED, PiGPIO.HIGH)#error occurred
    print('Failed to Write to Database')

blink(GreenLED,PiGPIO.HIGH)
blink(N2LED,PiGPIO.HIGH)
try:
    mycursorw.close()
    connw.close()
except:
    print('Error Closing Database Connection')
    PiGPIO.output(RedLED, PiGPIO.HIGH) #error occurred
    PiGPIO.output(Stat1LED,PiGPIO.LOW)
#####
#####
#####
else:
##Non-read section
    t1 = (cur.tm_hour >= nightstart)
    t2 = (cur.tm_hour <= nightend)
    if ( (t1 and t2) and (sent == False)):# time to send
daily TX
        PiGPIO.output(RBSlp,PiGPIO.HIGH)#wakeup rockblock
        time.sleep(1)
        try:
            day = cur.tm_yday
            c1 = int(round((day/26),1))
            if (c1 == 0):
                c1=c1+1
            c2 = int(round((day%26),1))
            if (c2 == 0):
                c2=c2+1
            dte = abet[c1]+abet[c2]
        except:
            dte = DTEErr#error
            PiGPIO.output(RedLED, PiGPIO.HIGH) #error
occurred
            PiGPIO.output(Stat1LED,PiGPIO.LOW)
        try:
            connr =
mysql.connector.connect(user=UIDr,password=PWDr,host=HST)
            mycursorr = connr.cursor()
        except:
            PiGPIO.output(RedLED, PiGPIO.HIGH) #error
occurred
            PiGPIO.output(Stat1LED,PiGPIO.LOW)
        try:
            mycursorr.execute("USE "+base)
            connr.commit()

```

```

except:
    print('Error Initializing Read Connection')
    PiGPIO.output(RedLED, PiGPIO.HIGH) #error
occurred

    PiGPIO.output(Stat1LED,PiGPIO.LOW)

    cdd = "SELECT * from "+tbl+" WHERE ("+Col+" =
"+'''+startdate+'''+ and "+Col2+" >= "+'''+starttime+'''+)"+" or
"+("'+Col+" = "+'''+enddate+'''+ and "+Col2+" <=
"+'''+starttime+'''+)"
    #cdd = "SELECT * from "+tbl          #selects
whole table
    #print (cdd) #for debugging

    # Database Structure
    # 1, 2, 3, 4, 5, 6, 7, 8, 9
, 10, 11, 12, 13
    #Date,Time,Loc,MTemp,N1Temp,N2Temp,ETemp
,MHum,MVolt,N1Volt,N2Volt,N1Curr,N2Curr
    #date,tim ,loc,mbt ,n1t ,n2t ,extTemp,mbh ,mbv
,n1v ,n2v ,n1c , n2c

#####
#####
    # Initialize average variables
    avgMT = 0
    ctrmt = 0
    avgET = 0
    ctret = 0
    avgMH = 0
    ctrmh = 0
    totW1 = 0
    ctrw1 = 0
    totW2 = 0
    ctrw2 = 0
    avgTN1 = 0
    ctrt1 = 0
    avgTN2 = 0
    ctrt2 = 0
    mvolt = 0
    ctrv = 0
    # initialize message strings
    InMsg = ''
    ETstr = ''
    MTstr = ''
    TN1str = ''
    TN2str = ''
    MHstr = ''
    MVstr = ''
    W1str = ''
    W2str = ''
    try:

```

```

        #read database
        mycursorr.execute(cdd)
    except:
        print("Database Read error")
        PiGPIO.output(RedLED, PiGPIO.HIGH) #error
occurred

        PiGPIO.output(Stat1LED, PiGPIO.LOW)
    try:

        for row in mycursorr:
            if ((str(row[4]) != MBErr1) and (str(row[4])
!= MBErr2)):
                avgMT = avgMT + float(row[4])
                ctrmt = ctrmt + 1
            if ((str(row[5]) != N1Err1) and (str(row[5])
!= N1Err2)):
                avgTN1 = avgTN1 + float(row[5])
                ctrt1 = ctrt1 + 1
            if ((str(row[6]) != N2Err1) and (str(row[6])
!= N2Err2)):
                avgTN2 = avgTN2 + float(row[6])
                ctrt2 = ctrt2 + 1
            if (str(row[7]) != ExtErrT):
                avgET = avgET + float(row[7])
                ctret = ctret + 1
            if (str(row[8]) != ExtErrH):
                avgMH = avgMH + float(row[8])
                ctrmh = ctrmh + 1
            if (str(row[9]) != MBErr1):
                mvolt = mvolt + float(row[9])
                ctrv = ctrv + 1
            if ((str(row[10]) != V1RErr) and
(str(row[10]) != V1Err) and (str(row[12]) != C1Err)):
                totW1 = totW1 +
float(row[10])*float(row[12])
                ctrw1 = ctrw1 + 1
            if ((str(row[11]) != V2RErr) and
(str(row[11]) != V2Err) and (str(row[13]) != C2Err)):
                totW2 = totW2 +
float(row[11])*float(row[13])
                ctrw2 = ctrw2 + 1
            #convert to string, rounding to whole integer
values

    except:
        print('Data Extraction Error')
        print(row)
        PiGPIO.output(RedLED, PiGPIO.HIGH) #error
occurred

        PiGPIO.output(Stat1LED, PiGPIO.LOW)
    try:
        if (ctret != 0):

```



```

        ETstr = str(format(avgET/ctret,fmt0))
    else:
        ETstr = DTErr
    if (ctrmt != 0):
        MTstr = str(format(avgMT/ctrmt,fmt0))
    else:
        MTstr = DTErr
    if (ctrmh != 0):
        MHstr = str(format(avgMH/ctrmh,fmt0))
    else:
        MHstr = DHErr
    if (ctr1 != 0):
        TN1str = str(format(avgTN1/ctr1,fmt0))
    else:
        TN1str = DTErr
    if (ctr2 != 0):
        TN2str = str(format(avgTN2/ctr2,fmt0))
    else:
        TN2str = DTErr
    if (ctrv != 0):
        MVstr = str(format(mvolt/ctrv,fmt0))
    else:
        MVstr = DVErr
    if (ctrw1 != 0):
        W1str = str(format(totW1,fmt0))
    else:
        W1str = DWErr
    if (ctrw2 != 0):
        W2str = str(format(totW2,fmt0))
    else:
        W2str = DWErr

#####
#####
#Ensure each digit is appropriate length
ETstr = msgFormat(ETstr)
MTstr = msgFormat(MTstr)
TN1str = msgFormat(TN1str)
TN2str = msgFormat(TN2str)
if (len(MHstr) == 1):
    MHstr = '0'+ MHstr
if (len(W1str) == 1):
    W1str = '0' + W1str
if (len(W2str) == 1):
    W2str = '0' + W2str

#####
#####
#InMsg =
str(dte)+str(loc)+ETstr+MTstr+MHstr+TN1str+TN2str+MVstr+W1str+W2str

```

```

        InMsg =
ETstr+MHstr+W1str+W2str+MVstr+MVstr+TN1str+TN2str+MTstr

        except:
            print('Data Convert Error')
            PiGPIO.output(RedLED, PiGPIO.HIGH) #error
occurred

            PiGPIO.output(Stat1LED, PiGPIO.LOW)
        try:
            mycursorr.close()
            connr.close()
        except:
            print('Error closing read connection')
            PiGPIO.output(RedLED, PiGPIO.HIGH) #error
occurred

            PiGPIO.output(Stat1LED, PiGPIO.LOW)
        try:
            #talk to rockblock and send data
            if (slpctr > 0):
                slpctr = slpctr - 1
                time.sleep(blinkdel)

            else:
                print(InMsg)
                tmpblk = iblk.rb.s
                signal = iblk.rb.requestSignalStrength()
                print(signal)
                if (signal > 0):
                    sent = iblk.sendDat(InMsg)
                    iblk.rb.s = tmpblk
                    print("Message sent: "+str(sent))

                    if(sent):
                        print("Fails before success:
"+str(failcount))

                            failcount = 0
                            slpctr = 0
                        else:
                            failcount = failcount + 1
                            print("Giving the rockBlock a
moment....")

                                slpctr = SLPDEL
                    except KeyboardInterrupt:
                        raise KeyboardInterrupt
                except:
                    print("rockblock error")
                    PiGPIO.output(RedLED, PiGPIO.HIGH) #error
occurred

                    PiGPIO.output(Stat1LED, PiGPIO.LOW)

            else:
                if (synct):

```

```

        PiGPIO.output(RBSlp, PiGPIO.LOW)
    if (t1 and t2):
        time.sleep(blinkdel)
    else:
        if (synct):
            PiGPIO.output(RBSlp, PiGPIO.LOW)
            time.sleep(blinkdel)
            sent = False
            failcount = 0
            slpctr = 0
        prevdate = date

except KeyboardInterrupt:
    mycursorw.close()
    connw.close()
    PiGPIO.output(RedLED, PiGPIO.HIGH) #error occurred
    PiGPIO.output(Stat1LED, PiGPIO.LOW)

finally:
    PiGPIO.cleanup()

```

Code to Communicate with RockBlock Iridium Satellite Link

```

# Copyright 2015 Makersnake
#
# Licensed under the Apache License, Version 2.0 (the "License");
# you may not use this file except in compliance with the
License.
# You may obtain a copy of the License at
#
# http://www.apache.org/licenses/LICENSE-2.0
#
# Unless required by applicable law or agreed to in writing,
software
# distributed under the License is distributed on an "AS IS"
BASIS,
# WITHOUT WARRANTIES OR CONDITIONS OF ANY KIND, either express or
implied.
# See the License for the specific language governing permissions
and
# limitations under the License.

import glob
import signal
import sys
import time

import serial

class rockBlockProtocol(object):

```

```

def rockBlockConnected(self):pass
def rockBlockDisconnected(self):pass

#SIGNAL
def rockBlockSignalUpdate(self,signal):pass
def rockBlockSignalPass(self):pass
def rockBlockSignalFail(self):pass

#MT
def rockBlockRxStarted(self):pass
def rockBlockRxFailed(self):pass
def rockBlockRxReceived(self,mtmsn,data):pass
def rockBlockRxMessageQueue(self,count):pass

#MO
def rockBlockTxStarted(self):pass
def rockBlockTxFailed(self):pass
def rockBlockTxSuccess(self,momsn):pass

class rockBlockException(Exception):
    pass

class rockBlock(object):

    IRIDIUM_EPOCH = 1399818235000    #May 11, 2014, at 14:23:55 (This
will be 're-epoched' every couple of years!)
    #IRIDIUM_EPOCH = 1399818235000
    TIME_LIMIT = 15
    def __init__(self, portId, callback):
#        print("init"+str(0))
        self.s = None
        self.portId = portId
        self.callback = callback
        self.autoSession = True    #When True, we'll automatically
initiate additional sessions if more messages to download

        try:

            self.s = serial.Serial(self.portId, 19200, timeout=5)
            if( self._configurePort() ):

                self.ping() #KEEP SACRIFICIAL!

                self.s.timeout = self.TIME_LIMIT

                if( self.ping() ):

                    if(self.callback != None and
callable(self.callback.rockBlockConnected) ):
                        self.callback.rockBlockConnected()
                        return

```

```

        if(self.callback != None and
callable(self.callback.rockBlockConnected) ):
            self.callback.rockBlockConnected()
            return
        print("Init Failed")

    except (Exception):

        raise rockBlockException()

#Ensure that the connection is still alive
def ping(self):
    self._ensureConnectionStatus()
    command = b'AT'
    cr = b'\r'
    self._writeCmd(b''.join([command,cr]))

    if(self._ReadStatus(command)):
        if(self._ReadStatus(b'OK')):
            return True

    return False

#Handy function to check the connection is still alive, else
throw an Exception
def pingception(self):
    self._ensureConnectionStatus()

    self.s.timeout = 5
    if(self.ping() == False):

        raise rockBlockException

    self.s.timeout = self.TIME_LIMIT

def requestSignalStrength(self):
    self._ensureConnectionStatus()

    command = b'AT+CSQ'

    cr = b'\r'
    self._writeCmd(b''.join([command,cr]))

    if(self._ReadStatus(command)):

        response = self.s.readline().strip()
        print(response)
        if( response.find(b'+CSQ') >= 0 ):

            self.s.readline().strip()    #OK

```

```

        self.s.readline().strip()      #BLANK
        if( len(response) == 6):
            return int(response.decode('ascii')[5])

    return -1

def messageCheck(self):
    self._ensureConnectionStatus()

    if(self.callback != None and
callable(self.callback.rockBlockRxStarted) ):
        self.callback.rockBlockRxStarted()

    if( self._attemptConnection() and self._attemptSession() ):

        return True

    else:

        if(self.callback != None and
callable(self.callback.rockBlockRxFailed) ):
            self.callback.rockBlockRxFailed()

def networkTime(self):
    self._ensureConnectionStatus()

    command = b'AT-MSSTM'
    cr = b'\r'
    self._writeCmd(b''.join([command,cr]))

    if(self._ReadStatus(command)):

        response = self.s.readline().strip()

        self.s.readline().strip()      #BLANK
        self.s.readline().strip()      #OK

        if( not(b'no network service' in response) ):
#            print(str(1))
#            print(response)
            utc = int(response[8:], 16)
#            print(str(2))
#            print(utc)
            utc = int((self.IRIDIUM_EPOCH + (utc * 90))/1000)
#            print(str(3))
#            print(utc)
            return utc

    else:

```

```

        return 0;

def sendMessage(self, msg):

    self._ensureConnectionStatus()

    if(self.callback != None and
callable(self.callback.rockBlockTxStarted) ):
        self.callback.rockBlockTxStarted()
    else:
        print("SendMessage, no call back or not callable")
    if( self._queueMessage(msg)):
        if( self._attemptConnection() ):

            SESSION_DELAY = 1
            SESSION_ATTEMPTS = 3

            while(True):

                SESSION_ATTEMPTS = SESSION_ATTEMPTS - 1

                if(SESSION_ATTEMPTS == 0):

                    break

                if( self._attemptSession() ):

                    return True

                else:

                    time.sleep(SESSION_DELAY)
            else:
                print("SendMeessage, queue message or attempt connection
failed")
                if(self.callback != None and
callable(self.callback.rockBlockTxFailed) ):

                    self.callback.rockBlockTxFailed()
                print("SendMessage, Session Attempt Timeout")
                return False

def getSerialIdentifier(self):
    self._ensureConnectionStatus()

    command = b'AT+GSN'
    cr = b'\r'
    self._writeCmd(b''.join([command,cr]))

    if(self._ReadStatus(command)):

```

```

        response = self.s.readline().strip()

        self.s.readline().strip()    #BLANK
        self.s.readline().strip()    #OK

        return response

    #One-time initial setup function (Disables Flow Control)
    #This only needs to be called once, as is stored in non-volatile
memory

    #Make sure you DISCONNECT RockBLOCK from power for a few minutes
after this command has been issued...
    def setup(self):
        self._ensureConnectionStatus()

        #Disable Flow Control
        command = b'AT&K0'
        cr = b'\r'
        self._writeCmd(b''.join([command,cr]))

        if(self._ReadStatus(command) and self._ReadStatus(b'OK')):

            #Store Configuration into Profile0
            command = b'AT&W0'
            self._writeCmd(b''.join([command,cr]))

            if(self._ReadStatus(command) and
self._ReadStatus(b'OK')):

                #Use Profile0 as default
                command = b'AT&Y0'
                self._writeCmd(b''.join([command,cr]))

                if(self._ReadStatus(command) and
self._ReadStatus(b'OK')):

                    #Flush Memory
                    command = b'AT*F'
                    self._writeCmd(b''.join([command,cr]))

                    if(self._ReadStatus(command) and
self._ReadStatus(b'OK')):

                        self.close()

                        return True

        return False

```



```

def close(self):

    if(self.s != None):

        self.s.close()
        self.s = None

    @staticmethod
    def listPorts():

        if sys.platform.startswith('win'):

            ports = ['COM' + str(i + 1) for i in range(256)]

            elif sys.platform.startswith('linux') or
sys.platform.startswith('cygwin'):

                ports = glob.glob('/dev/tty[A-Za-z]*')

            elif sys.platform.startswith('darwin'):

                ports = glob.glob('/dev/tty.*')

        result = []

        for port in ports:
            try:
                s = serial.Serial(port)
                s.close()
                result.append(port)
            except (OSError, serial.SerialException):
                pass

        return result

    #Private Methods - Don't call these directly!
    def _queueMessage(self, msg):
        self._ensureConnectionStatus()

        if( len(msg) > 340):

            print("sendMessageWithBytes bytes should be <= 340
bytes")

            return False

        try:
            #self._disableFlowControl()

```

```

        command = b''.join([b'AT+SBDWT=',msg.encode('ascii')])
        cr = b'\r'
        self._writeCmd(b''.join([command,cr]))

        if(self._ReadStatus(command)):
            if(self._ReadStatus(b'OK')):
                print('Msg Load Success')
                return True

        print("Queue Message Load Failed")
        return False
    except:
        print("Queue Message Exception")
        return False

def _configurePort(self):
    if( self._enableEcho()):
        time.sleep(0.25)
    if (self._disableFlowControl):
        time.sleep(0.25)
    if(self._disableRingAlerts()):
        time.sleep(0.25)
    if(self.ping()):
        time.sleep(0.25)
    return True
print("Config port failed")
return False

def _enableEcho(self):
    self._ensureConnectionStatus()
    command = b'ATE1'
    cr = b'\r'
    self._writeCmd(b''.join([command,cr]))
    time.sleep(1)
    if(self._ReadStatus(command)):
        time.sleep(1)
        if( self._ReadStatus(b'OK')):
            return True
    else:
        if (self._ReadStatus(b'')):
            time.sleep(1)
            if( self._ReadStatus(b'OK')):
                return True
    print("Enable Echo Failed")
    return False

def _disableFlowControl(self):
    self._ensureConnectionStatus()
    command = b'AT&K0'
    cr = b'\r'

```

```

self._writeCmd(b''.join([command,cr]))
if(self._ReadStatus(command)):
    if( self._ReadStatus(b'OK')):
        return True
print("Disable Flow Control Failed")
return False

def _disableRingAlerts(self):
self._ensureConnectionStatus()
command = b'AT+SBDMTA=0'
cr = b'\r'
self._writeCmd(b''.join([command,cr]))
if( self._ReadStatus(command) ):
    if( self._ReadStatus(b'OK')):
        return True
print("Disable Ring Alerts Failed")
return False

def _attemptSession(self):
self._ensureConnectionStatus()
SESSION_ATTEMPTS = 3
while(True):
    if(SESSION_ATTEMPTS == 0):
        print("Attempt Session Failed, Timeout")
        return False

    SESSION_ATTEMPTS = SESSION_ATTEMPTS - 1

    command = b'AT+SBDIX'
    cr = b'\r'
    self._writeCmd(b''.join([command,cr]))
    time.sleep(10)
    if( self._ReadStatus(command) ):

        response = self.s.readline().strip()
        response = str(response.decode('ascii'))
        if( response.find("+SBDIX:") >= 0 ):

            self.s.readline()    #BLANK
            self.s.readline()    #OK

            response = response.replace("+SBDIX: ", "")
#+SBDIX:<MO status>,<MOMSN>,<MT status>,<MTMSN>,<MT
length>,<MTqueued>

            parts = response.split(",")

            moStatus = int(parts[0])
            moMsn = int(parts[1])
            mtStatus = int(parts[2])
            mtMsn = int(parts[3])

```

```

        mtLength = int(parts[4])
        mtQueued = int(parts[5])

        #Mobile Originated
        if(moStatus <= 4):
            self._clearMoBuffer()
            if(self.callback != None and
callable(self.callback.rockBlockTxSuccess) ):
                self.callback.rockBlockTxSuccess( moMsn
)
                pass
            else:
                if(self.callback != None and
callable(self.callback.rockBlockTxFailed) ):
                    self.callback.rockBlockTxFailed()
                    if(mtStatus == 1 and mtLength > 0): #SBD message
successfully received from the GSS.
                        self._processMtMessage(mtMsn)
                        #AUTOGET NEXT MESSAGE
                        if(self.callback != None and
callable(self.callback.rockBlockRxMessageQueue) ):
                            self.callback.rockBlockRxMessageQueue(mtQueued)
                            #There are additional MT messages to queued to
download
                                if(mtQueued > 0 and self.autoSession == True):
                                    self._attemptSession()
                                    if(moStatus <= 4):
                                        return True
                                print("Attempt Session Failed")
                                return False

def _attemptConnection(self):
    self._ensureConnectionStatus()

    TIME_ATTEMPTS = 10
    TIME_DELAY = 1

    SIGNAL_ATTEMPTS = 10
    RESCAN_DELAY = 10
    SIGNAL_THRESHOLD = 2

    #Wait for valid Network Time
    while True:
        if(TIME_ATTEMPTS == 0):
            if(self.callback != None and
callable(self.callback.rockBlockSignalFail) ):
                self.callback.rockBlockSignalFail()
                print("Attempt connection Failed, Timeout 1")
                return False
            if( self._isNetworkTimeValid() ):
                break

```

```

TIME_ATTEMPTS = TIME_ATTEMPTS - 1;

print("Checking For Signal: " + str(TIME_ATTEMPTS))
time.sleep(TIME_DELAY)

#Wait for acceptable signal strength
while True:

    signal = self.requestSignalStrength()
    if(SIGNAL_ATTEMPTS == 0 or signal < 0):
        print("NO SIGNAL")
        if(self.callback != None and
callable(self.callback.rockBlockSignalFail) ):
            self.callback.rockBlockSignalFail()
            print("Attempt connection Failed, Timeout 2")
            return False

        self.callback.rockBlockSignalUpdate( signal )

    if( signal >= SIGNAL_THRESHOLD ):

        if(self.callback != None and
callable(self.callback.rockBlockSignalPass) ):
            self.callback.rockBlockSignalPass()

            return True;

    SIGNAL_ATTEMPTS = SIGNAL_ATTEMPTS - 1

    time.sleep(RESCAN_DELAY)

def _processMtMessage(self, mtMsn):
    self._ensureConnectionStatus()
    command = b'AT+SBDRB'
    cr = b'\r'
    self._writeCmd(b''.join([command,cr]))

    response =
self.s.readline().strip().replace(command,"").strip()
    if( response == b'OK' ):
        print("No message content.. strange!")
        if(self.callback != None and
callable(self.callback.rockBlockRxReceived) ):
            self.callback.rockBlockRxReceived(mtMsn, "")
    else:
        content = response[2:-2]
        if(self.callback != None and
callable(self.callback.rockBlockRxReceived) ):

```

```

        self.callback.rockBlockRxReceived(mtMsn, content)
        self.s.readline()    #BLANK?

def _isNetworkTimeValid(self):
    self._ensureConnectionStatus()
    command = b'AT-MSSTM'
    cr = b'\r'
    self._writeCmd(b''.join([command,cr]))
    if( self._ReadStatus(command) ): #Echo
        response = self.s.readline().strip()
        if( response.startswith(b'-MSSTM') ):    #-MSSTM:
a5cb42ad / no network service
            self.s.readline()    #OK
            self.s.readline()    #BLANK
            if( len(response) == 16):
                return True
    time.sleep(1)
    return False

def _clearMoBuffer(self):
    self._ensureConnectionStatus()

    command = b'AT+SBDD0'
    cr = b'\r'
    self._writeCmd(b''.join([command,cr]))

    if(self._ReadStatus(command)):

        if(self._ReadStatus(b'0')):

            self.s.readline()    #BLANK

            if(self._ReadStatus(b'OK')):

                return True

    return False

def _ensureConnectionStatus(self):

    if(self.s == None or self.s.isOpen() == False):
        print("Ensure Connection Status Failed")
        raise rockBlockException()

def _ReadStatus(self,condition):
    self._ensureConnectionStatus()
    try:
        if (self.s != None or self.s.isOpen() != False):

            rstat = self.s.readline().strip()
            rstat = rstat.strip(b'\x00')
            #print(rstat)

```

```

        if (rstat == condition):
            return True
        else:
            print("ReadStatus Failed for condition;
expected: " + str(condition) + ", got: " + str(rstat) )
            return False
    else:
        print("Read Status Failed")
except:
    print("Read Status Exception thrown")

def _writeCmd(self,cmd):
    self._ensureConnectionStatus()
    try:
        if (self.s != None or self.s.isOpen() != False):

            self.s.write(cmd)
            return True
        else:
            print("Device Busy cannot write command: " +
str(cmd))
            return False
    except:
        print("Write command Exception thrown")

def _softReset(self):
    if (self.s != None):
        command = b'ATZ0'
        cr = b'\r'
        self.s.write(b''.join([command,cr]))
        if (self._ReadStatus(command)):
            if (self._ReadStatus(b'OK')):
                return True
    else:
        return False

```

Interface between PV Monitoring Code and RockBlock Communications Code

```

#####
#####

import modrockBlock
from modrockBlock import rockBlockProtocol

#####
#####

class rockDat (rockBlockProtocol):
    rb = None
    stat = None
    def __init__(self):
        if (self.rb == None):

```

```

        self.rb =
modrockBlock.rockBlock('/dev/ttyAMA0',self)
        if ((self.rb.s != None) and (self.rb.s.isOpen() ==
False)):
            self.rb.s.open()
    def sendDat(self,msg):
        if (self.rb == None):
            self.rb =
modrockBlock.rockBlock('/dev/ttyAMA0',self)
            if ((self.rb.s != None) and (self.rb.s.isOpen() == False)):
                self.rb.s.open()
            signal = self.rb.requestSignalStrength()
            if (signal > 0):
                self.rb.sendMessage(msg)
            self.rb.close()
            return self.stat

    def rockBlockTxStarted(self):
        print("rockBlockTxStarted")

    def rockBlockTxFailed(self):
        print("rockBlockTxFailed")
        self.stat = False

    def rockBlockTxSuccess(self,mtmsn):
        print("rockBlockTxSuccess: " + str(mtmsn))
        self.stat = True

    def rockBlockRxMessageQueue(self,count):
        print("Message Queued: " + str(count))

    def getDateTime(self):
        mytime = ""
        #"Tue Sep 20 08:25:00 EST 2016"
        dtfmt = "%a %b %d %H:%M:%S UTC %Y"
        if (self.rb == None):
            self.rb = modrockBlock.rockBlock('/dev/ttyAMA0',self)
            if ((self.rb.s != None) and (self.rb.s.isOpen() == False)):
                self.rb.s.open()
            signal = self.rb.requestSignalStrength()
            if (signal > 0):
                dt = self.rb.networkTime()
                print(dt)
                mytime =
modrockBlock.time.strftime(dtfmt,modrockBlock.time.gmtime(dt))
                print(mytime)
            return mytime
    def resetRb(self):
        if(self.rb != None):
            if (self.rb._softReset()):
                return True
            else:

```



```
        return False
    else:
        self.rb = modrockBlock.rockBlock('/dev/ttyAMA0',self)
        self.rb.setup()
        self.rb.close()

if(__name__ == '__main__'):
    print("Don't Run directly. Call methods with other Programs.")
```

Operations Manual

GLOBAL PHOTOVOLTAIC POWER POTENTIAL LABORATORY (GP3L)



Thank you for volunteering to be part of the first truly global, experimental evaluation of photovoltaic technology and the potential for its applications to the USAF. Without you, our on-site teams, we would not be able to conduct this research.

This research has several goals. First, we aim to establish the theoretical potential for monocrystalline and polycrystalline silicon photovoltaic technology, which together represent 70-90% of the market share, across the enterprise. Basically, we want to be able to tell any USAF location approximately how efficient a panel at their site will be based on empirical, not theoretical, data. Secondly, we aim to quantify the true impact of ambient temperature on this type of technology. There are currently 5 different published correlation coefficients for monocrystalline silicon technology showing disagreement amongst the industry and higher academics. Thirdly, we want to quantify if there is a statistical correlation between ambient humidity and photovoltaic performance. It's known that humidity affects irradiance, but no study has carried that through to actual photovoltaic performance, much less accounted for the additional impacts of humidity besides effects on irradiance.

For any questions, please contact the AFIT GP3L team at AFITGP3L@afit.edu. Thank you to the Civil Engineer School for the funding to purchase the test systems and the AFIT Renewable Energy Systems Research Group for monitoring the test system performance over the course of the next year.

TEST SYSTEM INVENTORY




Upon receipt of your test system, please inventory the shipment to ensure you received:

- 1) a yellow, labeled all-weather case
- 2) two photovoltaic panels, one approximately half the size of the other
- 3) 10 galvanized stakes, two steel cables, and a nylon strap with grommets in the ends.

Using the below graphic, ensure that you have all the remaining components of the shipment. If anything is missing or broken, contact AFITGP3L@afit.edu immediately.

TEST SYSTEM PLACEMENT

Each test system must be placed somewhere that it will not be shaded 24/7/365, but also where it's convenient for the on-site POCs to inspect regularly as noted in the POC Duties portion of this pamphlet. Generally, we've found that flat rooftops or open fields to the south of facilities (north if below the equator) are optimal. Some sites have found placement along sidewalks to/from office buildings to work well. Please notify your local Security Forces, or equivalent, of your identified site. Once on site, follow the below graphics for final placement details.



OBSTRUCTION

Place south (north if below the equator) of all obstructions with a clear line of site to the Southern, Eastern, and Western horizons. The incorporated extension cords provide a 25' standoff. Additional cords may be added as necessary.

Ensure panels are perfectly level

Place the panels on a rock, cinder block, sandbags, or bricks to level them and ensure they are not in standing water. Daisy chain the panels together so the larger one (gray aluminum edge) is the furthest away from the case and the smaller is nearest (black aluminum edge) as shown. The steel cables connect diagonally across the backs of the panels and can be staked down or weighted.



Raspberry Pi
MicroSD Card
RockBlock MK2
Base Chip
Auxiliary Battery Cable
Power Cable
Cat 5 Cable
Temp/Humidity Sensor
R/X/G LEDs
25' Extension Cord

Included should also be two packages of desiccant to keep the internal components dry. Once this inventory is completed, notify AFITGP3L@afit.edu.

ON-SITE POC RESPONSIBILITIES

Every site must have a Primary and Alternate POC. Both individuals must have access to the test system; neither should from a geographically separated unit.

Each of you is a steward of part of a \$50K line of research. Please ensure your test system is safe and secure. At the end of the year-long study, you will be provided the data from your site so you can make educated decisions about photovoltaics for your installation. Duties include:

- 1) No less than weekly, or within 24 hours of severe weather, visually inspect the system. Ensure the case is upright and the panels are not in standing water. Ensure no water is inside the case from recent heavy rain.
- 2) Ensure the panels are level and clean. A light dust is OK; snow, leaves, or excessive dust is not. Keep them as clean as your car windshield. In the event of snow/severe weather, check within 24 hours or the next duty day. Shading of/dirty panels significantly impacts the data.
- 3) Check the LEDs on the back of the case. Their functions are listed on the case labels. If the system is in an error state (Red LED), immediately unplug power from the system and check the connections of each solar panel. If those connections are secure, open the pelican case and check all connections to ensure they're secure. If all connections are secure, reconnect power. If the red LED illuminates any time within 20 minutes, immediately contact AFITGP3L@afit.edu for further instructions.

- 4) On the last duty day of each month, download and send the data from the MicroSD Card. To do this, disconnect power and open the pelican case. Remove the MicroSD card in the Raspberry Pi and replace it with the alternate, then reconnect power. The system will automatically begin operating again. Your local Communications Rep or Engineer Assistants can help you download the .csv and e-mail it to AFITGP3L@afit.edu. Once the .csv file has been e-mailed and receipt confirmed, delete the .csv file from the card and replace it in the system for the next months swap.

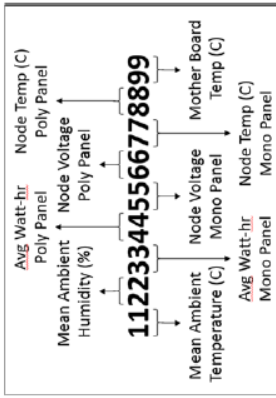
DO NOT REFORMAT THE MICROSD CARD!



DATA COLLECTION PROCESS

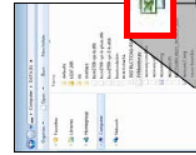


Every day, your test system will send a status message to AFITGP3L@afit.edu. This is formatted into a string of 18 digits as follows. Don't worry, there's no test. This is only provided if your local leadership is interested in the messages being sent via the satellite link.



MicroSD Card (a spare is in every case)

On the back of the Raspberry Pi computer the MicroSD card on which the data is stored. If you want the monthly data, we're able to provide it so that your leadership can have regular updates of its performance.



Once the MicroSD card has been opened on a computer, download the "IVCurveData.csv" and e-mail the file to AFITGP3L@afit.edu. Then, delete that file and replace the card in the case for the next month's data.

ON-SITE POC HANDOVER PROCEDURES

The AFIT GP3L Research Team is very aware of the time you take to sustain this line of research. We're very grateful for it.

We're also aware some test systems are located on remote, deployed, or contractor operated sites. We're especially thankful for the help of these POCs given their high operations tempo and turnover rates. If you are at one of these sites, please ensure that you connect your successor to the AFIT GP3L Research Team prior to your departure. This includes: providing the new POCs contact information, taking them to visit the test system, and providing them this pamphlet of and any instructions provided specifically for your site.

Additionally, we highly recommend that you connect them with any helpful individuals. This includes, but is not limited to, Communications Reps or Engineer Assistants who've helped download MicroSD Card data, Security Forces or equivalent personnel who area aware of the test system so it is not reported as an "unattended package," and leadership so that they're aware of their personnel's activities.

For any questions, contact:
AFITGP3L@afit.edu

Faculty Advisor:
Dr. Diedrich Prigge, AFIT/ENV
785-3636 x4648
2950 Hobson Way
WPAFB, OH 45433

Appendix D – Test System Beta Testing Results

Figure 32 shows the performance of the “Omega” test system placed on the roof of building 640 at AFIT to validate the system operated as intended. A clear progression from daylight to night time can be seen for the Mono-Si panel attached, especially around the 145th time interval where there was a clean rise in power as the sun rose and a fall as it set. At this time interval, we can also see a reduction in humidity and an increase in temperature moving just ahead of the production of power. NOTE: This data excludes all time periods where power produced was less than 0.005W or the ambient temperature registered less than -20C or higher than 35C. Elimination of low power periods simply eliminated night hours for the sake of clarity on the chart. Elimination of the extreme temperatures removed statistical outliers caused by disturbances to the test system as the research team adjusted it or updated the code and continued data collection.

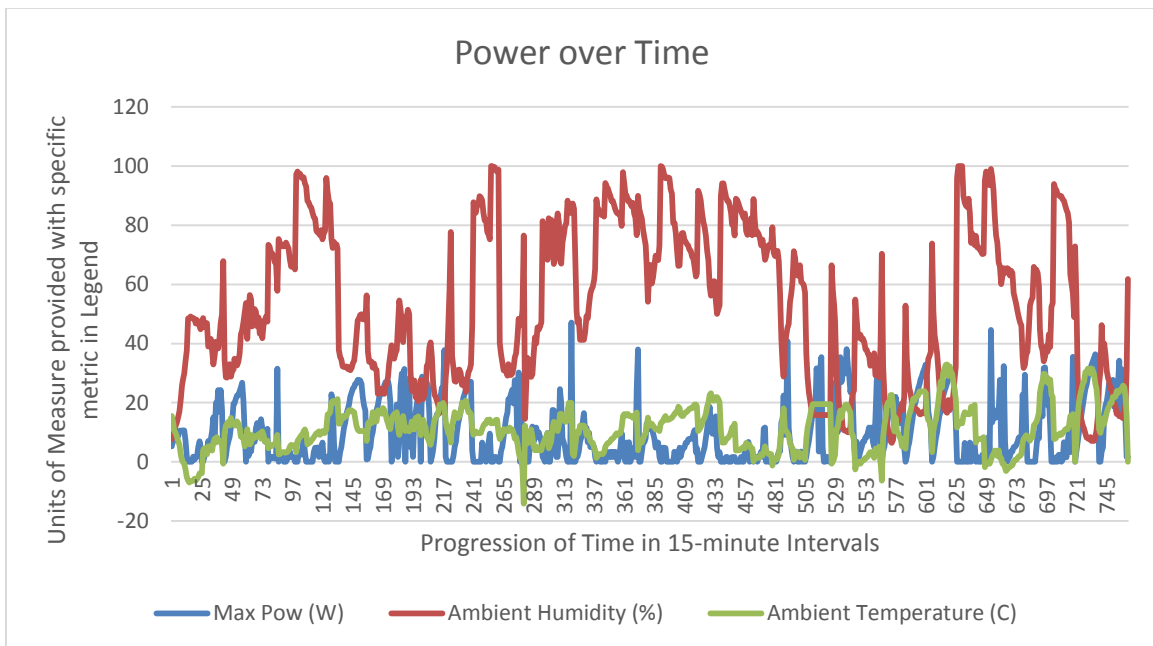


Figure 32. Power over Time from “Omega” test system

Figure 33 analyzes the same data as that shown in Figure 32 but rather than the x-axis being a progression of time, it represents the data sorted by highest power produced to lowest power produced. This enables the research team to identify a trend more clearly than attempting to analyze the data over the progression of time. There appears to be a clear positive correlation between Power and Temperature with a negative correlation between Power and Humidity. Linear fit lines are provided, though the R-squared values show that these may not be the most accurate way to model the data. This is evidence that, while a correlation may be apparent, there may be some sort of synergistic effect between temperature and humidity or that outside variables influence performance.

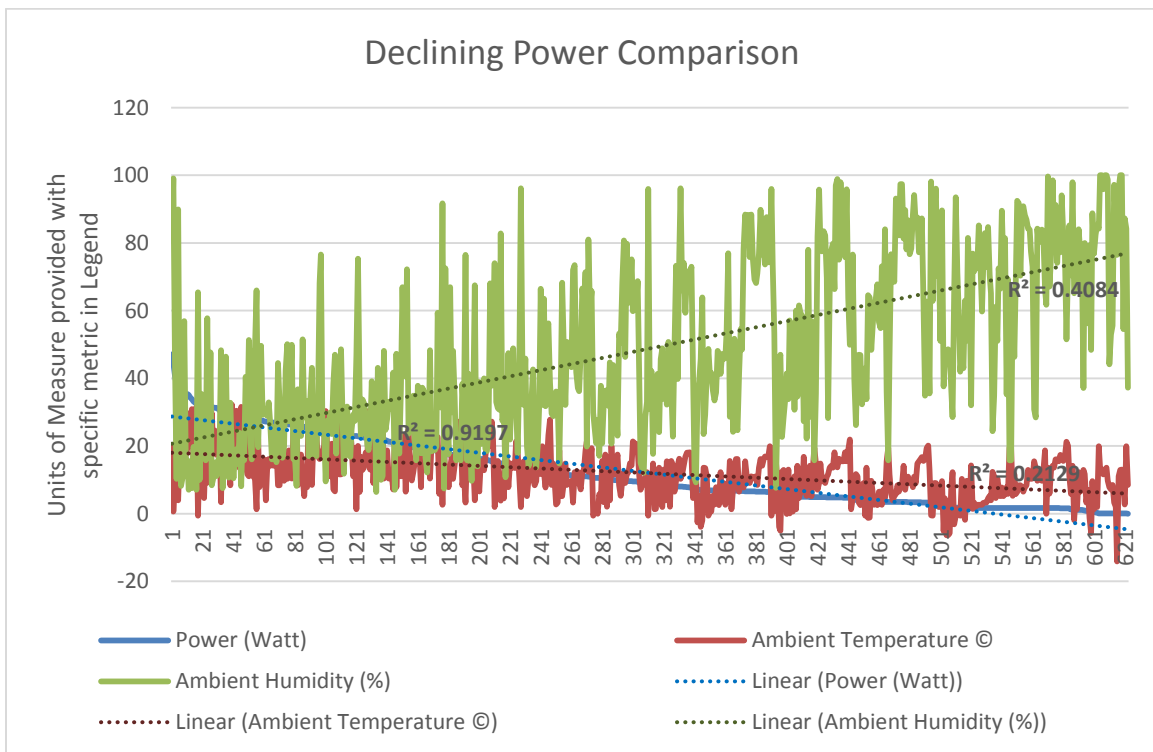


Figure 33. Declining Power Comparison to Ambient Humidity and Ambient Temperature

Using the data in Figure 32 and Figure 33, a basic Multivariate Correlation Analysis was conducted as well as a Fit Model using Ambient Temperature, Ambient Humidity, and their crossed values to form a regression to calculate Power. These are shown in Figure 34 and Figure 35. While the Multivariate Analysis is showing relatively low correlations, there are clear ovoid shapes showing a general trend in a specific direction for them. In initial data collected from the “Beta” test system, these correlations were lower and, so, a general upward trend in correlation is shown as more data is collected.

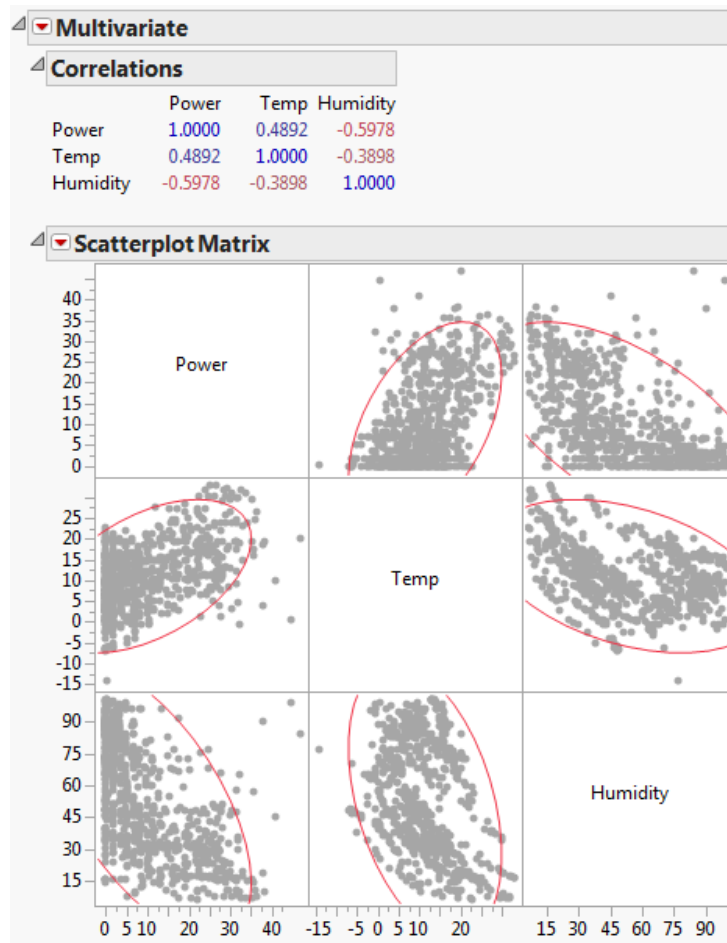


Figure 34. Multivariate Analysis of Cleaned Omega Test Data

Figure 35 shows an R-squared value of 0.45 when we analyze the data to form a linear regression using Ambient Humidity, Ambient Temperature, and their crossed values to calculate power produced. While this is low, it is an upward trend from the data original collected by the “Beta” test system. The volume of data in these preliminary results is very low, but it is showing general, observable trends and positive progression as more data is collected.

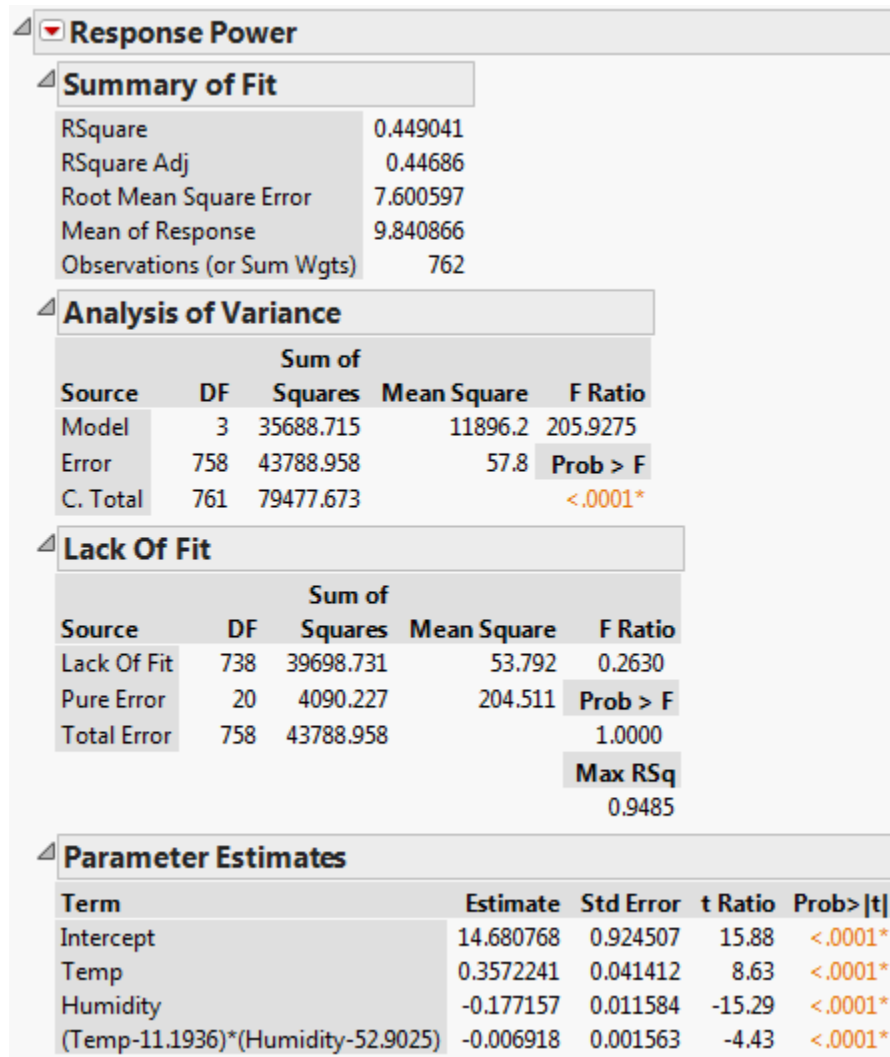


Figure 35. Fit Model of Cleaned Omega Test Data

Appendix E – Test Standard Heuristics

The test standards identified with each of the following heuristics is evidence that these materialistically unique products can be implemented as pavement systems without need for change to pavement design methodologies. Elaborated above, this is a significant concern, especially for DoD applications as modifying the design process represents a significant mission risk. The existing processes have been in development since the Romans first used concrete. To change the process represents a need for major testing and validation of the new design process. Instead, if we can implement a new material using the same process then liability, procedural, and organizational concerns are reduced. The primary concern becomes the performance of the material and if it meets the specifications of current pavements.

- 1) ASTM Test Standard D7264 for the flexural modulus:
 - a. It identifies the Modulus of Elasticity for “polymer matrix composite materials...[and] structures”
 - b. It uses the three-point loading apparatus in Figure 36

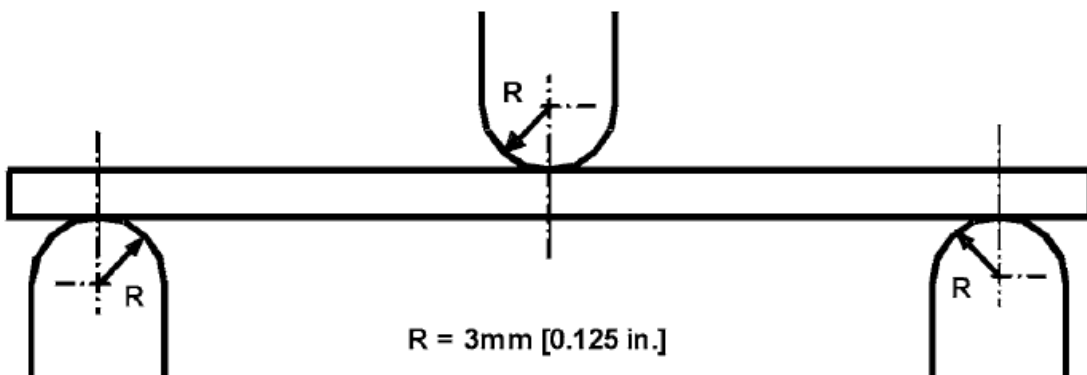


Figure 36. Three-Point Loading Fixture specified in C78 and D7264 [19] [18][18, 19]

- c. It allows for the complicated sandwich construction of the SR3 paver
- 2) ASTM Test Standard C1645-16 for freeze/thaw cycling:
- a. It allows for solutions with a chemical profile similar to that which occurs on pavements due to chemicals by calling for a saline solution of $3 \pm 0.1\%$ (by weight) NaCl
 - b. It is designed for interlocking paver units much like the SR3 paver
 - c. It evaluates the potential effects of moisture ingress on the electrical properties of the specimen
 - d. It accounts for the unique geometry of the SR3 Paver by exposing varying material surface areas in the fully constructed unit verses specimens of the materials
 - e. It uses a methodology similar to real-world conditions by fully submerging the paver under the solution for successive, 24-hour freeze/thaw cycles
- 3) ASTM Test Standard C272/C272M-16 for moisture conditioning:
- a. It is designed to evaluate water absorption of core materials in sandwich constructions
 - b. It evaluates the effects of moisture of a similar chemical profile as would exist in real world scenarios
 - c. It evaluates damage on an incremental scale similar to traditional pavement testing
 - d. It uses a methodology similar to the successive freeze/thaw cycling that could be expected be in real world conditions

4) ASTM Test Standard C273/273M-16 for shear properties of core materials in sandwich constructions:

- a. It identifies the “force-deflection behavior...when loaded in shear parallel to the plain of the facings” as shown in Figure 37

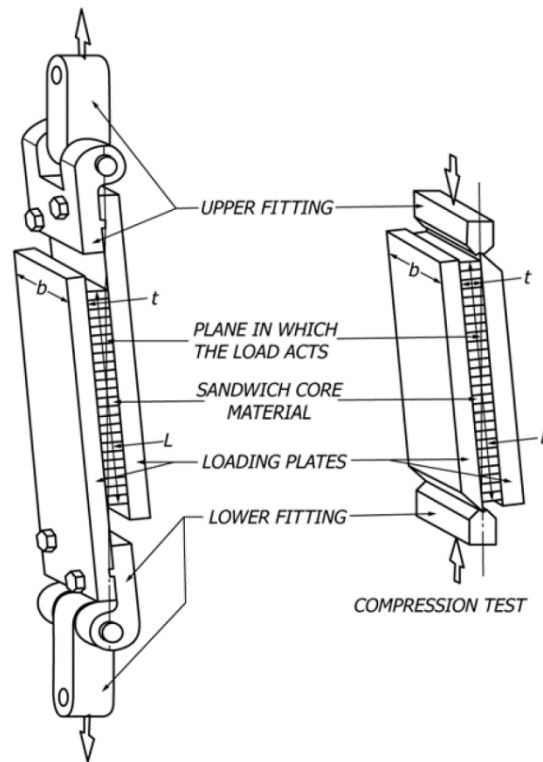


Figure 37. Specimen mounting and loading configuration for C273M-16 [40]

- b. It allows those core materials to be bonded directly to the glass adherends
- c. It analyzes the effects of a shear force on one surface of the product as it translates through the product like a tire starting, stopping, or turning on the top layer while the base layer is anchored in place
- d. It identifies the internal shear strength of the polymer composite layer of the SR3 product

5) ASTM Test Standard D4027-98(2011) for the structural adhesion of the polymer layer:

- a. It allows the polymer to be adhered to the glass adherends by loading the test specimen as shown by the large black arrow on the top right of

Figure 38

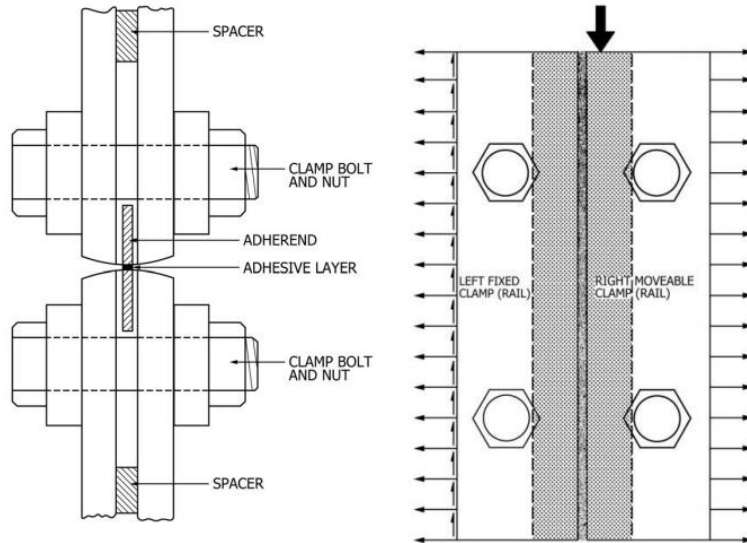
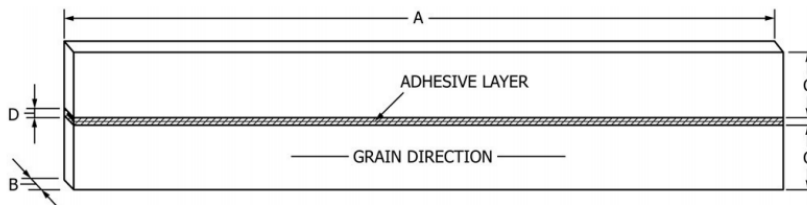


Figure 38. Specimen mounting and loading diagram from D4027-98(2011) [34]

- b. It identifies the specific bond strength of the polymer layer to the adherends for a specimen meeting the dimensions shown in Figure 39



DIMENSIONS		
	INCH	MM
A	8	203
B	0.125	3.18
C	0.75	19.0
D	0.031	0.79

Figure 39. Test specimen specifications for D4027-98(2011) [34]

Previously published research proposed specific test standards based on an initial analysis of the library of ASTM Active Test Standards [6]. The focus of this work was in reducing the time to market for emerging technologies with great potential. The library of test standards was found to have a significant number of test standards that all used nearly identical methodologies and analysis with the only significant difference between them being the material tested. For example, Table 22 shows the procedures and analysis portions of Test Standard C1026 and C1645. One of these is for interlocking concrete paver units as mentioned in the heuristics above and the other is for glass tiles designed for outdoor applications. Both involved successive cycles of freezing and thawing followed by visual and weight analysis to determine the damage of the cycles.

Table 22. Comparison of Procedures for ASTM Test Standard C1026 and C1645 [35][36][35, 36]

C1026 Procedures and Analysis	C1645 Procedures and Analysis
Freeze to 27°F over 3-6 hours	Freeze to 23°F for 16 hours
Thaw to 40°F over 3-6 hours	Thaw to 40°F 8 hours (24 hour cycle)
Evaluate after 300 cycles	Evaluate after 7, 28, and 49 cycles
Dry specimen in the oven for 24 hours, cool in a desiccator, record the dry weight of the specimen	Dry residue for 4+ hours and weigh, continue drying until successive weights change by less than 0.2%
Visually inspect specimens for damage	Describe the damage suffered

What is reflected in the comparisons of the standards is that the development of standards appears to be based on their need for specific applications rather than the application of specific stressors. Because of this, numerous standards have been developed to address specific products and their applications that are nearly identical to other standards [6]. Proposed in that research was a review of the library of standards alluded to above in order to identify the common stressors being analyzed across multiple standards and to create a general standard for the evaluation of that stressor [6]. Should

application specific appendices to a test standard be required, they can be added, but these should be extremely rare as there is a limited number of ways that a product can be frozen and thawed. The same goes for moisture conditioning as there are only so many ways a product can be submersed in water for an extended period of time.

Even amongst applied load tests, as opposed to environmental load tests mentioned above, there are a limited number of fixtures which can be used to apply loads to a specimen. The Three-Point Loading Apparatus shown in Figure 36 has numerous standards for specific materials and its use. However, the fixture is only used in one way across all of them. If the standards were written from the viewpoint of the stressor versus the material, a single standard would exist for the use of this fixture with potential appendices to provide notes on important nuances of specific materials.

By adjusting the architecture of the library of ASTM standards, product developers could more quickly test their products to a specific standard and product roll-out would be accelerated. Additionally, the variance in testing could be reduced greatly resulting in a more uniform performance of the standards. This concept applies to photovoltaic pavements as well. The materialistically unique products could be tested to the same standard as traditional pavement materials, accelerating the identification of their performance capabilities. This is done by establishing minimum performance characteristics for the various variables in concern (flexural modulus, shear strength, etc. for rigid pavements separate from flexible pavements due to their load transfer methods) and allowing any material that can meet those standards to be used in pavement design.

Furthermore, as heuristics are the foundation of determining acceptable standards, logic can also be applied directly to testing rather than filtering testing. One of the goals

of testing is to determine the shear strength of the SR3 paver. If the ability to test an entire paver as a unit is available, it may provide useful information. This will be dangerous as the pavers are large so the failure will likely be cataclysmic, but it could also provide interest information regarding how the geometry of the pavers influences the shear strength. For this reason, ASMT Test Standard D4255/D4255-15a, Procedure B uses the Three-Rail shear loading method, the apparatus for which and the mounting diagram is shown in Figure 40. This standard could be modified and applied directly to a full SR3 Paver as shown in Figure 41. Again, this is a non-standard testing methodology and is not guaranteed by any testing agency to provide accurate data. But the potential is apparent and it is a logical extrapolation of the expected loads on the final product. Should the testing identified in the heuristics above provide all the required data, though, non-standard testing such as this is unnecessary and, so, the risks both to researchers, equipment, and the validity of the information are unnecessary.

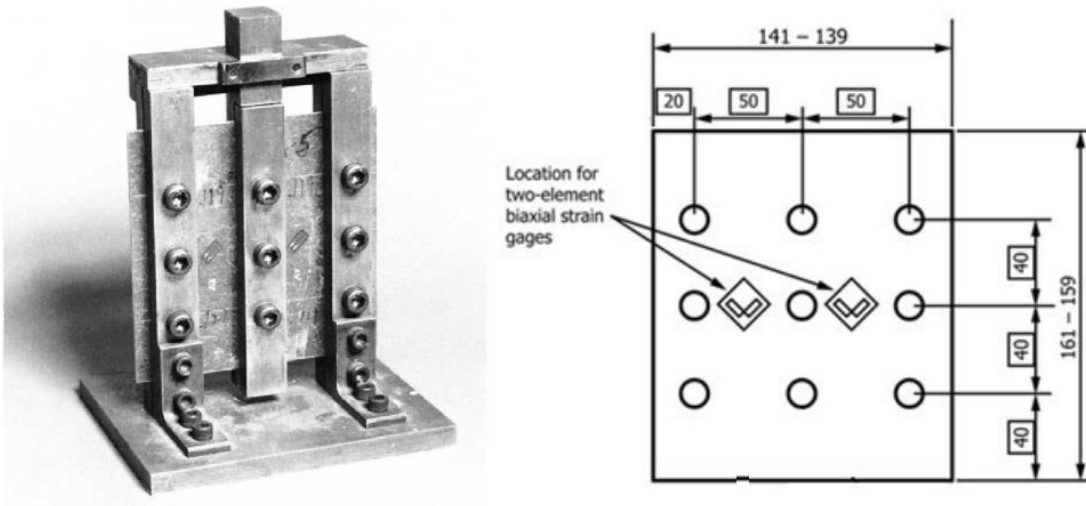


Figure 40. Three-Rail shear testing apparatus and mounting diagram for D4255-15a [37]

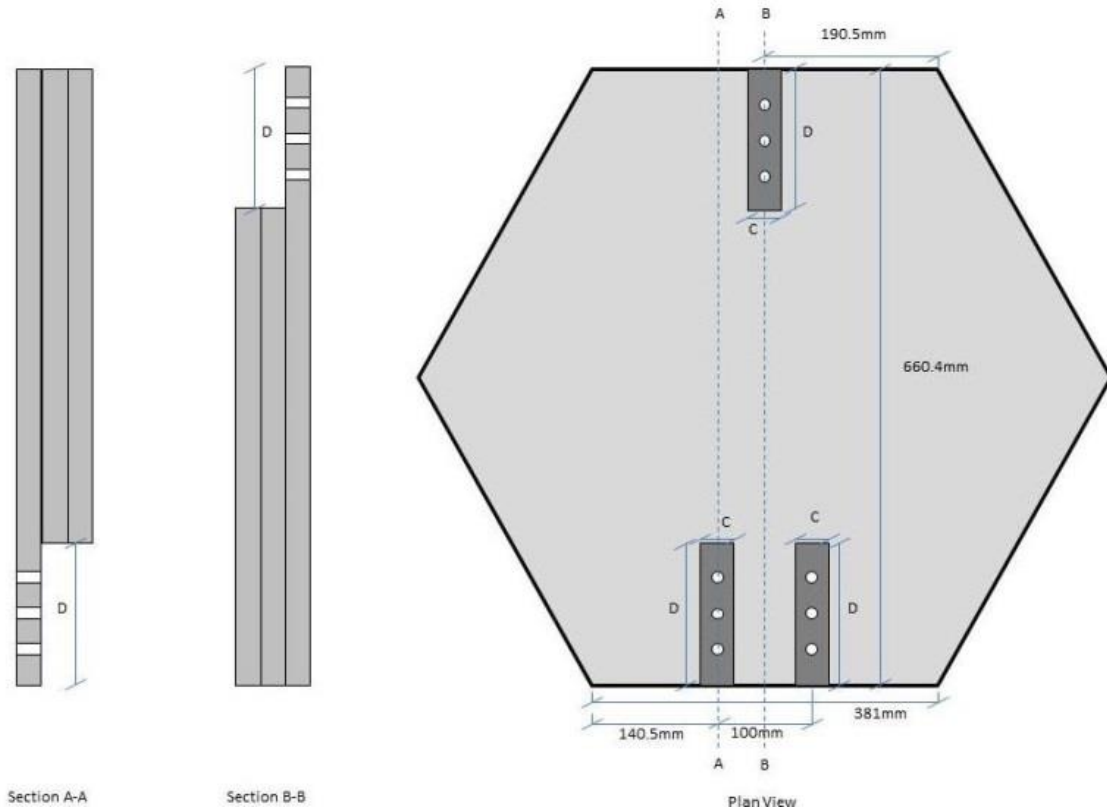


Figure 41. Modified SR3 paver for attachment of the Three-Rail Shear Test apparatus [37]

Of course, this does not absolve concerns regarding usability. A mirrored surface would make a poor road surface due to reflectivity. Reason and engineering judgment will play a role as well as objective product performance in accordance with established standards. This relies on the subjective, experience related portions of design and are the reason why Engineers must be licensed to approve designs. Liability will still remain on their shoulders should they certify a product as safe for implementation. Furthermore, governing agencies may set performance characteristics. The American Society of Civil Engineers, in conjunction with AASHTO, the FHWA, the FAA, State Governments, and the Federal Government may set specific performance metrics which can be evaluated by these stressor specific standards.

Equipment was found on Wright-Patterson Air Force Base with which all of these test standards could be performed. Based on this analysis, a funding proposal was prepared in April 2016 for AFIT to perform product testing for SRI based on the funding provided to them by the DoT SBIR Phase IIB program. The results of the testing, due to the highly competitive nature of this market of emerging technologies, was to be covered by a Cooperative Research and Development Agreement and would be considered sensitive in accordance to the legal restrictions of that agreement. Unfortunately, SRI chose to work with a different university based on their funding proposal.

References

- [1] T. S. Green, "Civil Engineer Flight Plan," Department of Defense, Washington, D.C., 2016.
- [2] "National Solar Radiation Database: 1991-2005 Update: Typical Meteorological Year 3," National Renewable Energy Laboratory, 2005. [Online]. Available: http://rredc.nrel.gov/solar/old_data/nsrdb/1991-2005/tmy3/by_state_and_city.html. [Accessed 2 February 2017].
- [3] Alliance Sustainable Energy, LLC., "PVWatts Calculator," National Renewable Energy Laboratory, 2017. [Online]. Available: <http://pvwatts.nrel.gov/>. [Accessed 2 February 2017].
- [4] Air Force Civil Engineer Center Energy Directorate, "Building the Air Force Renewable Energy Portfolio," Air Force Civil Engineer Center, San Antonio, 2014.
- [5] J. Meserve, "Mouse Click Could Plunch City into Darkness, Experts Say," 2007. [Online]. Available: <http://www.cnn.com/2007/US/09/27/power.at.risk/index.html#cnnSTCText>. [Accessed 1 February 2017].
- [6] J. H. Nussbaum, R. A. Coutu, Jr. and R. A. Lake, "Standardized Testing of Non-Standard Photovoltaic Pavement Surfaces," in *National Aerospace & Electronics Conference & Ohio Innovation Summit (NAECON-OIS)*, Dayton, 2016.
- [7] C. P. Cameron, W. E. Boyson and D. M. Riley, "Comparison of PV System Performance-Model Predictions with Measured PV System Performance," Sandia National Laboratories, Albuquerque, 2008.
- [8] F. MacDonald, "The solar road in the Netherlands is working even better than expected," Science Alert, 11 May 2015. [Online]. Available: <http://www.sciencealert.com/solar-roads-in-the-netherlands-are-working-even-better-than-expected>. [Accessed 8 February 2017].
- [9] S. Brusaw and J. Brusaw, "Research & Findings: Phase IIB Research," Solar Roadways, Incorporated, 2016. [Online]. Available:

<http://www.solarroadways.com/Research/Funding#>. [Accessed 1 February 2017].

- [10] American Association of State Highway and Transportation Officials, "Materials Testing: Internal Audit Practice Aid," American Association of State Highway and Transportation Officials, Washington, D.C., 2015.
- [11] Transportation Curriculum Coordination Council, "Training Resources: Courses," American Association of State Highway and Transportation Officials, 2017. [Online]. Available: <https://tc3.transportation.org/training-resources/matrices/materials/>. [Accessed 1 February 2017].
- [12] American Association of State Highway and Transportation Officials, AASHTO Guide for Design of Pavement Structures, Washington, D.C.: American Association of State Highway and Transportation Officials, 1998.
- [13] DictionaryofConstruction.com, "Rigid Pavement," WebFinance, Inc., 2017. [Online]. Available: <http://www.dictionaryofconstruction.com/definition/rigid-pavement.html>. [Accessed 5 October 2016].
- [14] DictionaryofConstruction.com, "Flexible Pavement," WebFinance, Inc., 2017. [Online]. Available: <http://www.dictionaryofconstruction.com/definition/flexible-pavement.html>. [Accessed 5 October 2016].
- [15] E. C. Aldridge, Jr., *Department of Defense Unified Facilities Criteria*, Washington D.C.: Department of Defense, 2002.
- [16] U.S. Army Corps of Engineers, "Unified Facilities Criteria (UFC) 3-250-01FA, Pavement Design for Roads, Streets, Walks, and Open Storage Areas," Department of Defense, 16 January 2004. [Online]. Available: http://www.wbdg.org/FFC/DOD/UFC/ARCHIVES/ufc_3_250_01fa_2004.pdf. [Accessed 26 July 2016].
- [17] U.S. Army Corps of Engineers, "Unified Facilities Criteria (UFC) 3-260-02, Pavement Design for Airfields," Department of Defense, 30 June 2001. [Online]. Available:

http://www.wbdg.org/FFC/DOD/UFC/ufc_3_260_02_2001.pdf. [Accessed 26 July 2016].

- [18] American Society for Testing and Materials International, *D7264/D7264M-07, Standard Test Method for Flexural Properties of Polymer Matrix Composite Materials*, ASTM International, 2007.
- [19] American Society for Testing and Materials International, *C78/C78M-15b, Standard Test Method for Flexural Strength of Concrete (Using Simple Beam with Third-Point Loading)*, ASTM International, 2015.
- [20] A. H. Fanney, B. P. Dougherty and M. W. Davis, "Comparison of Predicted to Measured Photovoltaic Module Performance," *Journal of Solar Energy Engineering*, vol. 131, 2009.
- [21] E. Skoplaki and J. A. Palyvos, "On the Temperature Dependence of Photovoltaic Module Electrical Performance: A Review of Efficiency/Power Correlations," *Solar Energy*, no. 83, pp. 614-624, 2008.
- [22] D. D. King, "Photovoltaic Module and Array Performance Characterization Methods for All System Operating Conditions," in *NREL/SNL Photovoltaics Program Review Meeting*, Lakewood, 1996.
- [23] A. Nagengast, C. Hendrickson and H. S. Matthew, "Variations in Photovoltaic Performance Due to Climate and Low-Slope Roof Choice," *Energy and Buildings*, no. 64, pp. 493-502, 2013.
- [24] M. Mani and R. Pillai, "Impact of Dust on Solar Photovoltaics (PV) Performance: Research Status, Challenges and Recommendations," *Renewable and Sustainable Energy Reviews*, no. 14, pp. 3124-3131, 2010.
- [25] S. Mekhilef, R. Saidur and M. Kamalisarvestani, "Effect of Dust, Humidity, and Air Velocity on Efficiency of Photovoltaic Cells," *Renewable and Sustainable Energy Reviews*, no. 16, pp. 2920-2925, 2012.
- [26] P. Faine, S. R. Kurtz, C. Riordan and J. M. Olson, "The Influence of Spectral Solar Irradiance Variations on the Performance of Selected Single-Junction and Multijunction Solar Cells," *Solar Cells*, vol. 31, pp. 259-278, 1991.

- [27] D. L. King, W. E. Boyson and J. A. Kratochvil, "Photovoltaic Array Performance Model," Sandia National Laboratories, Albuquerque, 2003.
- [28] C. Riordan and R. Hulstrom, "What is an Air Mass 1.5 Spectrum?," Solar Energy Research Institute, Golden, 1990.
- [29] J. Tovar, F. J. Olmo and L. Alados-Arboledas, "One-Minute Global Irradiance Probability Density Distributions Conditioned to the Optical Air Mass," *Solar Energy*, vol. 62, no. 6, pp. 387-393, 1998.
- [30] "Class 5- Spectroscopy of Atmospheres," [Online]. Available: <http://lasp.colorado.edu/~bagenal/3720/CLASS5/5Spectroscopy.html>. [Accessed 21 February 2017].
- [31] M. L. Lomax, "Real Property Policysite," GSA Office of Governmentwide Policy, Washington, D.C., 2003.
- [32] M. Kottek, J. Grieser, B. Rudolf, C. Beck and F. Rubel, "World Map of the Koppen-Geiger Climate Classification Updated," Institute for Veterinary Public Health, 2006.
- [33] J. Nussbaum, "Photovoltaic Pavements: New Technology May Answer Concerns About Energy Security," *Air Force Civil Engineer*, pp. 18-19, Summer 2016.
- [34] American Society for Testing and Materials International, *D4027-98(2011), Standard Test Method for Measuring Shear Properties of Structural Adhesives by the Modified-Rail Test*, ASTM International, 2011.
- [35] American Society for Testing and Materials International, *C1026-13, Standard Test Method for Measuring the Resistance of Ceramic and Glass Tile to Freeze-Thaw Cycling*, ASTM International, 2013.
- [36] American Society for Testing and Materials International, *C1645/C1645M-11, Standard Test Method for Freeze-Thaw and De-icing Salt Durability of Solid Concrete Interlocking Paving Units*, ASTM International, 2011.

- [37] American Society for Testing and Materials International, *D4255/D4255-15a, Standard Test Method for In-Plane Shear Properties of Polymer Matrix Composite Materials by the Rail Shear Method*, ASTM International, 2015.
- [38] Y. Sukamongkol, S. Chungpaibulpatana and W. Ongsakul, "A Simulation Model for Predicting the Performance of a Solar Photovoltaic System with Alternating Current Loads," *Renewable Energy*, no. 27, pp. 237-258, 2002.
- [39] W. De Soto, S. A. Klein and W. A. Beckman, "Improvement and Validation of a Model for Photovoltaic Array Performance," *Solar Energy*, no. 80, pp. 78-88, 2006.
- [40] American Society for Testing and Materials International, *C273/C273M-16, Standard Test Method for Shear Properties of Sandwich Core Materials*, ASTM International, 2016.
- [41] American Society for Testing and Materials International, *C272/C272M-16, Standard Test Method for Water Absorption of Core Materials for Sandwich Constructions*, ASTM International, 2016.
- [42] EPA/BGNES, "novinite," Sofia News Agency, 12 November 2014. [Online]. Available:
<http://www.novinite.com/inpictures/9678/A+cyclist+drives+on+the+SolaRoad,+the+first+road+in+the+world+made+of+solar+panels,+during+the+official+opening+in+Krommenie,+the+Netherlands.+The+solar+energy+that+will+be+generated+can+be+used+for+t&.> [Accessed 22 February 2017].
- [43] D. King, "autoblog," AOL Inc., 5 February 2016. [Online]. Available:
[http://www.autoblog.com/2016/02/05/wattway-install-600-miles-solar-roads-france/.](http://www.autoblog.com/2016/02/05/wattway-install-600-miles-solar-roads-france/) [Accessed 22 February 2017].
- [44] Federal Aviation Administration, "FAA Rigid and Flexible Iterative Elastic Layered Design (FAARFIELD)," Federal Aviation Administration, Washington DC, 2016.

Vitae

Captain John H. Nussbaum graduated valedictorian from Florida Air Academy in Melbourne, Florida in 2005. He immediately entered undergraduate studies at the United States Air Force Academy in Colorado Springs, Colorado where he graduated with a Bachelor of Science degree in Civil Engineering in May 2009. He was commissioned upon graduation as a Second Lieutenant in the Active Duty Air Force. He completed his first Masters of Science degree in Civil Engineering from Missouri University of Science and Technology in Rolla, Missouri.

His first assignment was at Altus AFB as a Project Programmer in the 97th Civil Engineer Squadron in June 2009. During his tenure there he also served as a Program Manager and the Chief of Program Development. He also deployed to Kabul, Afghanistan as a Contract Officer's Representative and Program Manager for the Air Force Center for Engineering and the Environment under the Combined Security Transition Command – Afghanistan, Combined Joint Engineering Directorate for six months. In June 2012, he was assigned to the 100th Civil Engineer Squadron on Royal Air Force Station Mildenhall, England. He was assigned as the Operations Engineering Section Chief but stepped up to serve as the Operations Flight Chief for a year due to leadership deployments. After a six month deployment as the Construction Management Officer for the Air Force Civil Engineer Center imbedded in the 376th Expeditionary Civil Engineer Squadron, he transitioned to take command of the 100th Readiness and Emergency Management Flight. In September 2015, he started studies in the Graduate School of Engineering and Management, Air Force Institute of Technology. Upon graduation, he will be assigned to the 7th Air Force, Osan AB, Korea.

REPORT DOCUMENTATION PAGE

Form Approved
OMB No. 074-0188

The public reporting burden for this collection of information is estimated to average 1 hour per response, including the time for reviewing instructions, searching existing data sources, gathering and maintaining the data needed, and completing and reviewing the collection of information. Send comments regarding this burden estimate or any other aspect of the collection of information, including suggestions for reducing this burden to Department of Defense, Washington Headquarters Services, Directorate for Information Operations and Reports (0704-0188), 1215 Jefferson Davis Highway, Suite 1204, Arlington, VA 22202-4302. Respondents should be aware that notwithstanding any other provision of law, no person shall be subject to any penalty for failing to comply with a collection of information if it does not display a currently valid OMB control number.

PLEASE DO NOT RETURN YOUR FORM TO THE ABOVE ADDRESS.

1. REPORT DATE (DD-MM-YYYY) 10-02-2017		2. REPORT TYPE Master's Thesis		3. DATES COVERED (From - To) Sep 2015 - Mar 2017	
4. TITLE AND SUBTITLE ANALYZING THE VIABILITY OF PHOTOVOLTAIC PAVEMENT SYSTEMS: QUANTIFYING CLIMATE IMPACTS ON POTENTIAL POWER AND THE RISKS OF IMPLEMENTATION				5a. CONTRACT NUMBER	
				5b. GRANT NUMBER	
				5c. PROGRAM ELEMENT NUMBER	
6. AUTHOR(S) Nussbaum, John H., Capt, USAF				5d. PROJECT NUMBER Funds were JV'ed	
				5e. TASK NUMBER	
				5f. WORK UNIT NUMBER	
7. PERFORMING ORGANIZATION NAMES(S) AND ADDRESS(S) Air Force Institute of Technology Graduate School of Engineering and Management (AFIT/ENV) 2950 Hobson Way, Building 640 WPAFB OH 45433-8865				8. PERFORMING ORGANIZATION REPORT NUMBER AFIT-ENV-MS-17-M-206	
9. SPONSORING/MONITORING AGENCY NAME(S) AND ADDRESS(ES) The Civil Engineer School 2950 Hobson Way WPAFB, OH 45433-7765 (937) 255-5654 x2156 (DSN 5654 x2156) cess@afit.edu				10. SPONSOR/MONITOR'S ACRONYM(S) CESS	
12. DISTRIBUTION/AVAILABILITY STATEMENT DISTRIBUTION UNLIMITED				11. SPONSOR/MONITOR'S REPORT NUMBER(S)	
13. SUPPLEMENTARY NOTES					
14. ABSTRACT Three global manufacturers of photovoltaic pavement systems have garnered both interest and ire of technical communities who see potential but are concerned about implementation. Solar Roadways, Incorporated out of Sandpoint, Idaho is the sole U.S. manufacturer. Consisting of hexagonal pavers with a sandwich construction of tempered glass and polymer fill, the paver units are self-heating and contain multi-colored light emitting diodes (LEDs) as well as an integrated drainage system in their final construction. Existing research has documented how qualitative analysis identified test standards required to find the implement this technology without changing airfield pavement design methodologies. Additionally, at over four times the space efficiency, concerns regarding the reduction in per-square-inch performance efficiency are absolved. In this research, statistical analysis is used to develop the Global Photovoltaic Power Potential Laboratory (GP3L). This study establishes a theoretical potential for photovoltaics across the United States Air Force (USAF) as well as enhances the understanding of the correlation with ambient temperature and quantifies a possible correlation between ambient humidity to the performance of photovoltaics. The GP3L system allows for logistical regressions, based on a modified Koppen-Geiger Climate Classification System, as well as linear regressions based on ambient conditions. Lastly, it proposes a methodology of quantifying subjectively established risk to the installation mission caused by implementing photovoltaic pavement systems. This methodology also identifies the quantity of various pavements which can be replaced based on the Mission Dependency Index (MDI) of 26 different Category Codes (CATCODE) of pavements while maintaining acceptable levels of risk.					
15. SUBJECT TERMS energy security, energy autonomy, renewable energy, photovoltaic, photovoltaic pavement, solar road, pavement, risk, test standard, material testing, design method, pavement design, solar roadways, solaroad, wattway					
16. SECURITY CLASSIFICATION OF:			17. LIMITATION OF ABSTRACT UU or SAR	18. NUMBER OF PAGES 158	19a. NAME OF RESPONSIBLE PERSON JOHN H. NUSSBAUM, Capt, USAF
a. REPORT U	b. ABSTRACT U	c. THIS PAGE U			19b. TELEPHONE NUMBER (Include area code) (937) 255-6565, x 7238 (john.nussbaum@afit.edu)